The exploration of phage-based therapeutics for multi-drug resistant bacterial pathogens

by

Carly Maddison Davis

A thesis submitted in partial fulfilment of the requirements for the degree of

Master of Science

in

Molecular Biology and Genetics

Department of Biological Sciences
University of Alberta

Abstract

Pathogenic bacteria have a plethora of mechanisms to survive within the human body, and the effectiveness of antibiotics to treat these infections is rapidly declining due to an increase in antimicrobial resistance (AMR) and a lack of new drug discovery. AMR is a significant global concern, and these infections are predicted to cause over 10 million deaths per year worldwide by 2050 if left unchecked. It is clear that alternative antibacterial strategies are desperately needed, and the therapeutic use of bacteriophages is a promising area of research. Phages are viruses that target and lyse bacterial cells via adsorption to cells using a cellular receptor, injecting their genetic material, and replicating themselves until the cell bursts. Phages use a different mechanism than antibiotics to kill bacteria, so many antibiotic resistance mechanisms carried by AMR bacteria provide no protection against phage infection. This means phages are an effective tool to kill drug-resistant bacteria, and unlike antibiotics, phages exclusively attack and lyse specific host bacteria, leaving beneficial bacterial flora unharmed. To explore the efficacy of phage as an alternative treatment option I examined the application of phages in combination with sub-inhibitory (non-lethal) levels of the antibiotic aztreonam lysine (AzLys) on *Pseudomonas aeruginosa*, a high priority member of the ESKAPE pathogens; a concerning group of pathogenic bacteria exhibiting multi-drug resistance and virulence, are responsible for the majority of nosocomial infections, and are associated with the highest risk of mortality. Activity of phages E79 and phiKZ were increased in the presence of aztreonam lysine, in part due to accelerated time to lysis. Sub-inhibitory AzLys negatively affected the function of surface virulence factors type 4 pili (T4P) and flagella, and the combined treatment of *P. aeruginosa* biofilms with E79 and non-lethal levels of AzLys was more effective than phage treatment alone. To continue investigating phage therapy, I assembled, annotated, and analyzed the complete

genomes of two novel phages JC1 and Carl1 that can infect the deadly opportunistic pathogen *Burkholderia cenocepacia*. I further characterized JC1 and showed it possesses an impressive host range, uses the inner core of the LPS as its cellular surface receptor, and has a high virulence index at 37˚C. I also identified the *attP* site and location of integration in its bacterial host genome when it takes the form of a prophage. Genetic engineering of this phage could result in a promising phage therapy candidate for the treatment of *B. cenocepacia* infections. Continued research on the isolation, characterization, and application of phages is necessary so the use of phage as a therapy can become an accessible treatment option for chronic and antibiotic resistant infections.

Acknowledgments

Firstly, I would like to thank Dr. Jonathan Dennis. Thank you for the years of guidance and support. Thank you for taking in a 2nd year undergraduate student with barely any lab experience and helping her grow into a skilled molecular and micro- biologist. Thank you for the countless reference letters and for believing in my potential as a scientist.

Thank you to my committee members Dr. Paul Stothard and Dr. Dominic Sauvageau for sharing your expertise with me. Your kind words and insights meant a lot.

Thank you to my family. Thank you for always being by my side, even when it was jokingly telling me to find the cure to cancer or asking me when I will finally get a job. Thank you for helping me peruse my education, thank you for believing in me, thank you for being proud of me, thank you for loving me unconditionally.

Thank you to the present and past lab members of the Dennis and Raivio labs. Thank you for the countless hours of feedback during lab meetings, practice presentations, and discussions in the office. Thank you for all the laughs, getting through this degree without all of you would be unimaginable. Thank you to Danielle Peters and Jaclyn McCutcheon for being exceptional mentors. Thank you for always answering my endless stream of questions and for all the brainstorming sessions.

Thank you to NSERC and Alberta Innovates for making the decision to pursue my education and discover new things less of a financial burden.

Finally, thank you to everyone who smiled and nodded when I explained my research because you had no idea what I was talking about. I hope my thesis can help you all understand a little bit more about the world of antimicrobial resistance and alternative therapeutic options.

Table of Contents

List of Tables

List of Figures

Symbols

Δ	Change in energy
::	Interruption of the genetic locus by insertion

List of Abbreviations

aa	amino acid
AMR	antimicrobial resistance
ATP	adenosine triphosphate
AzLys	aztreonam lysine
Bcc	*Burkholderia cepacia* complex
BLAST	Basic Local Alignment Search Tool
bp or kbp	base pair or kilobase pair
°C	degrees Celsius
CBCCRRR	Canadian *Burkholderia cepacia* complex Research and Referral Repository
CD-Search	conserved domain search
CDS	coding domain sequence
CF	cystic fibrosis
CFTR	cystic fibrosis transmembrane conductance regulator
CFU	colony forming units
CGD	chronic granulomatous disease
DNA	deoxyribonucleic acid
DUF	domain of unknown function
EOP	efficiency of plating
EPS	exopolysaccharide
ESKAPE	***E****nterococcus faecium,* ***S****taphylococcus aureus,* ***K****lebsiella pneumoniae,* ***A****cinetobacter baumannii,* ***P****seudomonas aeruginosa, and* ***E****nterobacter* spp

g or mg or µg	gram or milligram or microgram
gDNA	genomic DNA
gp	gene product
h	hour
ID	identity
IPATH	Innovative Phage Applications and Therapeutics
kV	kilovolt
L or mL or µL	liter or milliliter or microliter
LB	Lennox broth
LD_{50}	50% lethal dose
LPS	lipopolysaccharide
M or mM	molar or millimolar
MDR	multi-drug resistant
MIC	minimum inhibitory concentration
min	minute
mm or µm or nm	millimeter or micrometer or nanometer
MOI	multiplicity of infection
MUSCLE	Multiple Sequence Comparison by Log Expectation
N/A	not applicable
NCBI	National Center for Biotechnology Information
NSERC	National Sciences and Engineering Research Council
OD	optical density
ORF	open reading frame

PAPS	3′-Phosphoadenosine-5′-phosphosulfate
PAS	phage-antibiotic synergy
PCR	polymerase chain reaction
PFU	plaque forming units
RNA	ribonucleic acid
rRNA	ribosomal ribonucleic acid
SM	suspension media
Stm	streptomycin
Tc	tetracycline
TCS	two component system
Tp	trimethoprim
tRNA	transfer ribonucleic acid
T4P	type IV pilus
vol	volume
wt	weight
X-gal	5-Bromo-4-Chloro-3-Indolyl β-D-Galactopyranoside

Chapter 1

Introduction

Pseudomonas

Isolation and taxonomy

The genus *Pseudomonas* (*Pseudo* meaning false and *monas* meaning unit) was first described in 1894 by Botanist Walter Emil Friedrich August Migula [1] shortly after the "father of bacterial taxonomy" Ferdinand Cohn published his bacterial classification system based on the shape and general appearance of bacterial cells [2,3]. Migula described the cells as having polar organs of motility, and inaccurately described the rare formation of spores occurring in some species [1,4]. Shortly after, he proposed *P. pyocyanea* (now known as *P. aeruginosa*) as the type species [4,5]. The genus *Pseudomonas* is therefore a part of the early history of bacterial taxonomy [6].

Taxonomic classification of bacteria took quite a few years for microbiologists to master, as morphological and physiological experiments were not enough to separate phenotypically similar bacteria; it was not until the introduction of genomic comparison experiments that accurate classification of these species really began [2]. By the mid 1900s (and prior to DNA hybridization techniques) there were more than 800 species assigned to *Pseudomonas*. In the 1970's Palleroni et al (1973) was able to classify this bacterial group into five rRNA subgroups using DNA–DNA hybridisation and rRNA-DNA hybridisation results. The authors kept the name *Pseudomonas* for rRNA group I (*Pseudomonas sensu stricto*) and suggested that the other rRNA groups be assigned to other genera of the same or different families.

The genus *Pseudomonas* is a group of metabolically diverse Gram-negative, non-spore forming, aerobic, motile bacilli with one or more polar flagella that belong to the Gammaproteobacteria class [8,9]. *Pseudomonas* is a very well-studied, complex genus and currently houses the most species out of any other Gram-negative genera. In 2015, there were

144 validly published species, and in 2020 there were 240 [8,10]. The complexity is exhibited just by the sheer size of this genus, and to this day new genera and species transfers are being proposed as more in-depth taxonomic studies are completed [10].

Pseudomonas aeruginosa

Pseudomonas aeruginosa (*aeruginosa* or 'greenish-blue' from the latin verdigris meaning 'rusted copper') is 1–5 μm long and 0.5–1.0 μm wide, and is a facultative anaerobe that can grow in the presence of oxygen (aerobic respiration) or nitrate (anaerobic respiration) and also has limited anaerobic growth using arginine [9,11]. This bacterium cannot grow at 4˚C but is able to grow at temperatures up to 42˚C; the optimal growth temperature for this species is 37˚C and it can utilize a large array of carbon sources [9]. *P. aeruginosa* is a fluorescent pseudomonad, capable of producing fluorescent and phenazine (pyocyanin) pigments (often responsible for the greenish-blue colours), and characteristically produces single polar flagellum [9].

P. aeruginosa has been referred to by a variety of different names over the course of its early history, including *Pseudomonas polycolor, Bacteria aeruginosa, Bacillus pyocyaneus, Pseudomonas pyocyanea, and Pseudomonas aeruginosa* [12]. In 1951 Haynes defined the species more precisely, and standardized its nomenclature to *Pseudomonas aeruginosa* [13]. The neotype strain (a strain accepted by international agreement to replace a type strain that is no longer in existence) for *P. aeruginosa* is ATCC 10145 [14]. *P. aeruginosa* is an opportunistic pathogen that possesses extreme multi-drug resistance (MDR) and is commonly acquired in hospital settings [15]. However, this species is found ubiquitously in the environment, from soil (especially the rhizosphere), water, plants, animals, and humans, to more extreme settings such as soap and jet fuel [16–18]. *P. aeruginosa* can also be isolated from areas that commonly come into contact with water, including sinks, swimming pools, and medical devices/equipment that work with water [16].

Clinical significance

P. aeruginosa has been of clinical significance since at least the 1850s, where it was observed to discolour the dressings of surgical wounds and later described to cause blue-green pus in patient wounds [19]. However, this was before *P. aeruginosa* had been taxonomically classified, and the first reported case of infection was identified by Carle Gessard in the 1880s, under the name *Bacillus pyocyaneus,* derived from the words *Bacillus* (rod) *pyo* (pus) *cyaneus* (blue) [20]. In 1894 the bacterium was noted to be widely distributed, and that "epidemics of blue pus" were semi-regularly seen in hospitals [21]. A review in 1947 collected all published reports of *P. aeruginosa* bacteremia, and noted the species was responsible for 31.9% of bacteremia cases in adults [22]. Concern for these infections began to rise in the late 1950s and 60s because of its increased occurrence in burn patients and the absence of effective antibiotics [12]. During the Vietnam War, *P. aeruginosa* was one of the three most common and virulent wound pathogens [23] and between 1977 and 1984 *P. aeruginosa* was one of the four most frequently isolated pathogens from just over 10,000 multiple trauma patients admitted to the Shock Trauma Center Maryland Institute for Emergency Medical Services System [24].

Today, *P. aeruginosa* is a member of the ESKAPE pathogens (***E****nterococcus faecium,* ***S****taphylococcus aureus,* ***K****lebsiella pneumoniae,* ***A****cinetobacter baumannii,* ***P****seudomonas aeruginosa* and ***E****nterobacter* spp.); a concerning group of pathogenic bacteria exhibiting multi-drug resistance and virulence [25]. These pathogens are capable of "escaping" antimicrobial biocidal activity, are responsible for the majority of nosocomial infections, and are associated with the highest risk of mortality [26,27]. In 2017 the World Health Organization (WHO) listed *P. aeruginosa*, along with *Acinetobacter baumannii* and *Enterobacteriaceae*, as a critical priority antibiotic resistant-bacteria for research and development [28,29].

Common infections (and risk factors) associated with *P. aeruginosa* infections include soft tissue (burns, open wounds, post-surgery), urinary tract (urinary catheter use), bacteremia (immunocompromised), diabetic foot (diabetes, impaired microvascular circulation), respiratory/pneumonia (old age, chronic obstructive pulmonary disease, cystic fibrosis, mechanical ventilation), swimmer's ear (tissue injury, water blockage in ear canal), keratitis (extended contact lens wear, contaminated contact lens solution), and hot tub rash (improperly cleaned hot tubs) [30]. Of particular importance is this pathogen's ability to cause respiratory infections in hospitalized patients; these infections can be hospital- (common) or community- (uncommon) acquired and can be acute (typically caused by direct trauma) or chronic (most patients usually have an underlying medical condition affecting the immune response) [30].

Acute *P. aeruginosa* lung infections are common in the healthcare system; they are usually associated with poor patient health, presence of multidrug-resistant strains in hospitals, and previous use of broad spectrum antibiotics [30,31]. *P. aeruginosa* can cause a variety of nosocomial pneumonias, but ventilator associated pneumonia (VAP) is the most concerning, with a mortality rate up to 30% in some institutions [32]. These acute inflammatory infections are usually caused by free-living, planktonic cells, and if not eradicated during the acute infection, this species can adapt to the lung environment and grow as a biofilm, the characteristic definition of a chronic *P. aeruginosa* infection [30,33].

Individuals with Cystic Fibrosis (CF) are most commonly affected by chronic pseudomonal lung infections and many acquire the lung infection during adolescence and can live with the infection for over 20 years [30]. Individuals with CF have a recessively inherited disease that results in dehydrated and thickened airway surface liquid (ASL) that significantly affects the clearance of mucus from the airways [30,34]. CF patients are highly susceptible to lung

infections caused by a variety of bacteria, but *P. aeruginosa* is the most prevalent pathogen causing infection in adult CF patients and is one of the leading causes of morbidity and mortality in the CF community [35,36].

Transmission of *P. aeruginosa* infections can occur by a variety of different routes including patient-to-patient transmission and contact with contaminated environments, medical devices, and reservoirs [37–39]. A study done in 2018 found that 41.1% of *P. aeruginosa* outbreaks from 2000-2015 were from contaminated medical devices (eg, bronchoscopes, surgical instruments, or nursing equipment), 34.5% were from direct person-to-person transmission (i.e. contact through hands of patients, staff, and visitors) and 14.4% by contaminated water [39]. Another study examined 164 patients from the CF Centre of Florence and concluded the risk of patient-to-patient transmission was low, but found that despite isolation precautions a risk of cross-infection still existed in the CF centre and proposed it could be due to interaction with the same contaminated environments [38]. *P. aeruginosa* has incredible adaptive abilities, and it has been shown to be able to survive on dry inanimate surfaces of hospital environments from 6 h up to 16 months [40].

Environmental significance

Pseudomonads are an extremely versatile group of bacteria, and though some (predominantly *P. aeruginosa*) can cause infections in humans [41], many species have environmental significance. The rhizosphere is notably impacted by *Pseudomonas* species, a study of 150 fluorescent *Pseudomonas* strains showed 40% stimulated wheat seedling root growth, 40% inhibited root growth, and only 20% showed no effect [42]. Root colonization by these species can have a range of effects. They can cause disease if it is a plant pathogen, or they can protect against disease by producing antifungal metabolites (AFMs), they can promote plant

growth by producing phytohormones (phytostimulation), increase the availability of nutrients, such as nitrogen, phosphate and micronutrients (biofertilization), and a variety of species are capable of degrading environmental pollutants, making them significant in the field of bioremediation [43,44].

P. aeruginosa strain PAO1 has been shown to colonize well with wheat roots and protect wheat and cucumber from fungal pathogens [45]. *P. aeruginosa* has also been shown to play a role in biocontrol for pepper, tomato, cocoyam, and bean plants, protecting them from common plant pathogens [46]. This species can produce hydrogen cyanide (HCN) [47] which has been shown to protect several plants from root disease [48], and it has been shown to produce a large amount of indole acetic acid when grown with tryptophan, an important plant growth hormone [49]. *P. aeruginosa* has also been isolated from the rice rhizosphere and been shown to promote the growth of Basmati rice [50], exhibit plant growth-promoting traits including phosphate and zinc solubilization, ammonia production, and organic acid production [51], and has been shown to produce extracellular chitinase enzyme, which can degrade fungal cell walls [52].

A noteworthy characteristic of *P. aeruginosa* is its ability to produce rhamnose-containing glycolipid biosurfactants (rhamnolipids). Though rhamnolipids play a role in virulence, they also have a variety of industrial applications including the production of high purity chemicals and surface coatings, bioremediation additives, biocontrol agents, medical agents, and as food additives [53,54]. Synthetic surfactants, typically derived from petroleum products, are non-biodegradable and widely utilized as detergents, solubilizers or emulsifying agents [55]. Biosurfactants on the other hand are produced by microbial fermentation and are biodegradable; they can therefore be used to replace synthetic surfactants as an environmentally friendly option [55]. Unfortunately, the industrial applications and commercialization of

rhamnolipids is currently limited by the pathogenicity of *P. aeruginosa* and the relatively low level of production, as well its pathogenicity may cause safety and health concerns during large-scale production and applications [54,55].

***Burkholderia cepacia* complex**

Isolation and taxonomy

William Burkholder discovered *Burkholderia cepacia* (formerly *Pseudomonas cepacia*) in 1950, where he noted the phytopathogen's ability to cause sour skin onion rot [56]. He described the novel pathogen as a rod shaped Gram-negative, strictly aerobic, non-sporulating organism with one to three flagella. The novel genus *Burkholderia* was proposed by Yabuuchi et al (1992) and *Pseudomonas cepacia* was renamed *Burkholderia cepacia* after molecular and phenotypic analysis of the *Pseudomonas* rRNA homology group II bacteria. Further phenotypic and genotypic analysis of *B. cepacia* led to the identification of 5 phenotypically similar, but genotypically distinct species, now known as the *Burkholderia cepacia* complex (Bcc) [58]. The authors grouped these 5 species into genomovars I-V, a term that denotes phenotypically similar but genotypically distinct groups of strains [59]. Today these species are known as *B. cepacia* (genomovar I), *B. multivorans* (genomovar II), *B. cenocepacia* (genomovar III), *B. stabilis* (genomovar IV), and *B. vietnamiensis* (genomovar V) [57,58,60–62].

The Bcc is a group of Gram-negative, non-spore-forming, aerobic bacilli that belong to the β-proteobacteria class and are comprised of multiple chromosomes rich in insertion sequences with considerable genetic diversity, exceptional nutritional versatility, and an ability to colonize plant and animal tissues [63,64]. They are usually catalase- and oxidase-positive, have an optimal growth temperature between 30-35˚C, and can use a wide variety of carbon sources,

including penicillin, azelaic acid and tryptamine [65,66]. To date, there are at least 24 species in the Bcc [67,68]. Genomovars VI-IX were added a few years after the formation of the Bcc, representing species *B. dolosa, B. ambifaria, B. anthina, and B. pyrrocinia*, respectively [69–71]. *B. latens, B. diffusa, B. arboris, B. seminalis, B. metallica,* and *B. ubonensis* were added to the complex in 2008 and *B. contaminans* and *B. lata* were added in 2009 [72,73]. From 2013-2015 *B. pseudomultivorans, B. stagnalis* and *B. territorii* were added, bringing the total to 20 species [74]. Most recently *B. paludis, B. alpina*, *B. catarinensis, B. puraquae,* and *B. orbicola* have been identified as novel species in the Bcc [67,75–78], however *B. alpina* was recently reclassified as *Pararobbsia alpina* comb [79]. In 2014 there were 16 novel unnamed species in the Bcc (Other Bcc A-P) that needed formal naming and description [80], therefore it is likely the Bcc will continue to increase in members as time goes by.

Clinical significance

B. cepacia emerged as an opportunistic human pathogen in the 1970s where it was isolated from the lungs of 54 patients with CF [81]. The authors also noted that *B. cepacia* had been found in patients who had never been hospitalized or who rarely used aerosol therapy, raising the question of where they got the infection. Isles et al. (1984) described a steadily increasing rate of infection with *B. cepacia* in CF patients, the detrimental health effects associated with them, and just how challenging treatment was due to the multi-drug resistant (MDR) nature exhibited by *B. cepacia*.

In 1993 precautionary measures to separate hospitalized CF patients colonized by *B. cepacia* from non-colonized patients was recommended by Thomassen et al (1986). The results of their study showed the new infection control measures had an approximate 80% decrease in incidence rate for acquiring new *B. cepacia* colonization in the CF hospital community and led

the authors to suggest these results could be because of patient-to-patient transmission. This topic remained controversial for a few years with some suggesting patient-to-patient transmission was not commonly occurring [84,85]. The involvement of patient to patient transmission became generally accepted in the 90's when LiPuma et al (1990) shared a case study where they provided evidence that a patient acquired a *B. cepacia* infection after attending a summer camp with a patient who was colonized with the same *B. cepacia* strain, and after Govan et al (1993) provided multiple cases of patient-to-patient transmission of the same *B. cepacia* strains within and between CF centers and described social contacts before colonization. Both of the authors recommended contact between patients colonized with *B. cepacia* from those not colonized should be avoided. Govan et al (1993) further suggested that the guidelines should not be restricted to just CF patients in hospitals, as regular close contact is associated with a high risk of cross-infection.

The lack of predictability towards the rapid clinical decline in CF patients [82] is particularly concerning. Notably the authors first described the clinical patterns of *B. cepacia* infections as:

"(l) chronic asymptomatic carriage of *P. cepacia* (either alone or in combination with *P. aeruginosa*); (2) progressive deterioration over many months, with recurrent fever, progressive weight loss, and repeated hospital admissions; and (3) rapid, usually fatal deterioration in previously mildly affected patients. There is great variability in the course of the disease, and deterioration did not occur at the same rate in all patients."

The third pattern later became known as "cepacia syndrome", a fatal combination of necrotizing pneumonia, rapid respiratory decline, and bacteremia [88,89]. Cepacia syndrome fatality is very high, with only 9 reported cases of successful treatment [89–96].

Today, *B. cepacia* has expanded to include many species known as the Bcc as discussed above. Infections with the Bcc in the CF community remain difficult to accurately identify, and treat, and have the ability to spread between patients [97]. Though the CF community is impacted the most by these opportunistic pathogens, they also cause fatal disease in patients with chronic granulomatous disease (CGD), a disease caused by a genetic immunodeficiency and is characterized by chronic infections and inflammatory complications [98]. Immunocompetent individuals are not typically vulnerable to Bcc infection, though there is an increasing number of reported cases of Bcc infections for these individuals including but not limited to community-acquired pneumonia [99], skin infections [100], septic arthritis [101], endocarditis [102–105], infections resulting from exposure to contaminated medical solutions [106], frontal sinus infection [107], cepacia syndrome [89], systemic infection [108], bacteremia [109–111], sepsis [112], urinary tract infection and urosepsis [113,114], pyogenic spondylodiscitis (vertebrae infection) [115,116], and an abdominal abscess [117]. A number of Bcc species have been associated with infections in humans, but the two most predominant and problematic species are *B. cenocepacia* and *B. multivorans* [97].

Burkholderia cenocepacia

B. cenocepacia has been a human health concern since the late 80s [65,87,118] and remains to this day one of two most common Bcc species found in the lungs of cystic fibrosis (CF) patients [119]. As mentioned above, individuals with CF are compromised in their ability to clear mucous from their lungs (a primary innate defense mechanism in the human airways) [120]; the thick mucus accumulates and provides favorable conditions for colonization by bacteria [121]. In 2020 *B. cenocepacia* was the most common species isolated from the lungs of Canadian CF patients, responsible for 50% of the infections [119]. The formal naming of *B. cepacia* genomovar III to the binomial name *B. cenocepacia* took a few more years to achieve than genomovars I, II, IV and V

due to the lack of differential biochemical tests and PCR based identification procedures available at the time to distinguish genomovar III from *B. cepacia* (genomovar I) [62,122]. The prefix 'ceno-' means recent or new, and the type strain *B. cenocepacia* J2315 (LMG 16656/ CF5610) was responsible for massive spread of infection in CF patients in the late 80s to early 90s [65,87,118] and was the first sequenced Bcc genome [61,123]. *B. cenocepacia* is described as a motile Gram-negative rod 1.0 to 2.0 μm long and 0.6 to 0.9 μm wide [61].

B. cenocepacia is an opportunistic multi-drug resistance (MDR) gram-negative bacterium that is found ubiquitously in the environment, and in immunocompromised individuals it is associated with poorer prognosis, patient-to-patient transmission, and problematic treatment (Mahenthiralingam et al. 2005). Prior to July 2000, 80% of CF patients in Canada were infected with *B. cenocepacia* and only 9.3% were infected with *B. multivorans* [124]. However, a recent study by Zlosnik et al (2020) reviewed the epidemiology of *Burkholderia* infections in Canada for CF patients from 2000-2017 and observed a marked shift in the most common species from *B. cenocepacia* (30.3%) to *B. multivorans* (45%). This shift has also been observed in other parts of the world [126–128].

Shorter survival for CF patients has been observed for *B. cenocepacia* infections compared to *B. multivorans,* which could be a factor in the shift of infection prevalence from *B. cenocepacia* to *B. multivorans* (Jones et al. 2004; Zlosnik et al. 2015, Zlosnik et al., 2020). Additionally, 73% of *B. cenocepacia* infections before July 2000 were caused by the epidemic ET-12 strain (also known as J2315), but in the recent epidemiology study the authors noted that infection control practices have been successful in limiting the spread of epidemic strains, which is very likely playing another factor in the drop in *B. cenocepacia* infections, as this species is highly transmissible between patients [124,125]. Additionally, social contacts during summer camps

were very popular among CF patients until 1998 and were a likely cause of Bcc cross-infections [68,87]. Infection control measures to reduce the risk of patient-to-patient spread has resulted in a progressive decrease in Bcc prevalence, however despite the success in limiting the spread of infections, CF patients have continued to acquire novel Bcc infections at a consistent rate over the last 17 years [124,125]. A *B. cenocepacia* strain isolated from soil was indistinguishable from clinical isolates [131], and other known CF strains isolated from water [132,133] and raw meat [134] all provide evidence that new infections may be from an environmental source and that the prevalence of *B. multivorans* infections could reflect its prevalence in the environment [125].

Environmental significance

The Bcc have exceptional nutritional versatility, they are ubiquitous in nature, and have been isolated from water, soil, the rhizosphere, the hospital environment, animals, and humans [58]. Beyond being a problematic opportunistic pathogen, the Bcc have potential uses in biotechnological applications [64]. Bcc can fix atmospheric nitrogen, can produce the plant hormone indoleacetic acid (which aids in root and shoot development), and can produce a wide array of antimicrobial agents like cepacin, cepaciamide, cepacidines, altericidins, pyrrolnitrin, quinolones, phenazine, siderophores and bacteriocin-like agents that inhibit bacterial and fungal phytopathogens, protect against plant diseases, and promote plant growth [65,135]. Using the Bcc as a biopesticide could replace the use of toxic and highly persistent chemical pesticides [64]. Because the Bcc can use a variety of carbon sources they are extremely adept at bioremediation as they can break down man-made toxins like aromatic pollutants toluene and trichloroethylene, chlorinated aromatics found in pesticides and herbicides, and other soil and groundwater pollutants [63,64,135,136].

Although the beneficial aspects of the Bcc discussed here are promising, concerns have been rightfully raised towards the widespread commercial use of these bacteria because the risks of infection could increase for the vulnerable population as a result [64]. Moreover, since it is predicted that the most likely source of novel Bcc infections for CF patients are originating from the natural environment [125] introducing Bcc voluntarily into the ecosystem could have detrimental effects for the CF community and other vulnerable individuals. Regardless of whether the agricultural and industrial applications of Bcc are utilized, prevention measures may need to be recommended to limit the acquisition of infections from the environment [68].

Cystic Fibrosis

As mentioned above, members of the Bcc and *P. aeruginosa,* are commonly isolated from the lungs of CF patients [119]. CF is an autosomal recessive disease caused by mutations in the cystic fibrosis transmembrane conductance regulator (CFTR) gene [34]. The CFTR protein primarily functions as a chloride anion channel; impairment of its function causes a disruption in salt and water transport that generates thick, viscous secretions that can affect many different areas of the body including the lungs, pancreas, liver, intestine, reproductive tract and salt content in sweat gland secretions [34]. The disruption of salt and water transport in the lungs leads to a build-up of thick, sticky mucus, that is hard to clear, which compromises one of the primary innate defense mechanisms against bacterial infection in human airways [120]. This thick mucus provides an ideal environment for bacteria to adhere to and cause infection [137]. Persistent bacterial infection, inflammation, impaired mucus clearance, and further increased airway mucus viscosity leads to irreversible damage of the lungs, and progressive lung disease remains the main cause of CF patient morbidity and mortality [34,119].

Bacterial infections need to be prevented or cleared quickly in order to preserve the lung function and health of CF patients. In Canada, the total CF population has grown by 31% since 2001, which coincides with the increasing median age of survival; in 2000 the median age was around 35, and in 2020 it has risen to 55 [119]. While the expected lifespan of individuals with CF has continued to steadily increase over the past few decades, largely due to improved therapeutic regimens, progressive lung disease is still a prominent issue [68,119]. The development of better therapeutic alternatives to eliminate MDR bacteria from the lungs of individuals with CF is imperative. The preservation of lung function remains a top priority, so that CF patients might benefit from new therapies in the future, and hopefully one day cystic fibrosis can become a manageable disease [138].

Bacterial Virulence Mechanisms

Bacterial characteristics that negatively affect host health/survival or help the bacteria to survive and colonize within the host are known as virulence factors [139,140]. The Bcc, *P. aeruginosa*, and many other pathogenic bacteria utilize a variety of cellular structures, molecules, and regulatory systems to survive and cause disease within their hosts; this next section will briefly describe a variety of common virulence factors used by Gram-negative bacteria.

Endotoxins

The term endotoxin was coined in 1982 by Richard Pfeiffer [141], however not much was known beyond the fact that they could mimic deleterious effects of bacteria [142]. Bacterial endotoxins, or lipopolysaccharides (LPS), make up a significant proportion of the outer membrane of most Gram-negative bacteria [143]. The LPS is a well-known virulence factor that

plays a key role in host-pathogen interaction, allowing for evasion of host defences, persistent inflammation, and increased antimicrobial resistance [144]. Increased susceptibility to antibiotics and decreased *in vitro* fitness has been illustrated in truncated LPS bacterial mutants, with larger truncations resulting in a greater loss of resistance and fitness [145,146]. The outer core of the LPS offers bacteria resistance to complement-mediated killing, a significant component of the human innate immune system [143,147]. Endotoxins are also incredible inducers of cytokines and can cause a severe over-immune reaction known as a cytokine storm; this "storm" can result in sepsis or toxic shock syndrome, and eventually death [142].

Motility Systems

Structural features like flagella and pili are virulence factors that facilitate movement, adhesion/attachment, biofilm formation and colonization of host tissues [139,140,148]. Flagella are composed of a motor and base controlled by signal transduction, and can be attracted or repulsed by chemical gradients by changing the direction of rotation of the flagella [149]. Additionally, the flagella elicits a strong host immune response, can export substances associated with virulence, and allow for penetration of host barriers and establishment of systemic infections [139,150]. Pili are hair-like filaments composed of pilin subunits that extend from the cell membrane into the external environment [151]. Type IV pili can cause twitching or gliding in a variety of species by retracting their pili attached to surfaces in a "pulling" type fashion, and disruption of pilus assembly or function results in reduced virulence for many Gram-negative bacteria [152]. Cable pili are another type of pili used for adherence by certain strains of *B. cenocepacia* and are thought to play a role in colonizing the respiratory tract of their host [153]. Motility allows organisms to survive within their host environment, and mutations that impair motility often reduce or attenuate virulence [139].

Secreted Toxins and Enzymes

Secreted products like toxins and enzymes play a key role in tipping the outcome of bacterial-host infections to favour the pathogen [139,154]. Toxins are generally enzymes that can inhibit or activate host cell physiology by modifying targets in the host via posttranslational modifications (PTMs) or noncovalent interactions, and injection of small amounts of purified toxin can cause the same fatal symptoms seen with infection [151,154]. Toxins can be classified into four groups: (i) toxins that bind to host cell plasma membrane receptors and corrupt intracellular signalling; (ii) toxins that disrupt the plasma membrane via pore formation or phospholipase activity; (iii) AB toxins (two-component protein complexes) that utilize receptor-mediated endocytosis to inject toxic enzymatic components into host cells; and (iv) toxins delivered directly into host cells by the bacterium using an injection needle apparatus [154]. Other enzymes that are considered virulence factors typically damage host tissues, some examples of these enzymes include hyaluronidases (cleaves proteoglycans in connective tissue), streptokinases and staphylokinases (breaks down fibrin clots), lipases (degrades accumulated host oils), haemolysins (punch holes in host cells), and nucleases (digests released RNA and DNA) [139,151]. Other enzymes, like urease, can help bacteria survive intracellularly [155].

Siderophores

Siderophores were first discovered in the 1950s [156]. Siderophores are high affinity iron chelating molecules that deliver iron to bacteria, and are essential virulence factors in many Gram-negative pathogens [157]. Bacteria that can overproduce siderophores have been described as hypervirulent, whereas decreased virulence and fitness during infection and colonization is seen with bacteria unable to produce or secrete siderophores [157]. Siderophores are unique, abundant, and all perform one redundant task, and growing evidence supports the idea that structural

diversity with functional redundancy may allow evasion of host immune factors [157]. Furthermore, iron is required in all life forms, and its chelation by siderophores can affect host cellular homeostasis, resulting in siderophores acting like toxins causing cell death, and may even be a potential cancer treatment [157].

Biofilms

The term 'biofilm' was first coined in 1978 by Costerton and collogues [158] and is used to define organized communities of microbes embedded in a self-produced extracellular polymeric substance (EPS) matrix; this formation allows for the socialisation and shared living of microbial cells and often increases resistance to many environmental stresses [139,151,159]. Biofilm formation is associated with virulence in many bacterial species, and they are seen as an adaptive lifestyle allowing bacteria to resist the harshness of many environments. In the clinical setting they pose a significant challenge and can be nearly impossible to eradicate [159,160]. This is largely due to the fact that biofilms have increased resistance to antibiotics, biocides, and the host immune system compared to planktonic bacteria, though the mechanism for this phenomenon is not completely understood [159,161,162]. Furthermore, antibiotics have been shown to induce biofilm formation, supporting the idea that biofilm formation is a response to harsh environments, and highlights possible complications of these effects in healthcare [163,164].

Secretion Systems

Secretion systems play a vital role in exporting other virulence factors from the cytosol of the bacteria into the host environment, or directly into host cells [165]. Extracellular protein secretion in Gram-negative bacteria can be challenging because the proteins must cross two (and, sometimes three) phospholipid membranes. To date, there are currently 11 different secretion systems, with the type X and XI secretion systems only being described within the last two years,

and the Type VII system is only found in Gram-positive bacteria [166–169]. Secretion systems play a variety of roles in virulence including but not limited to: secreting, injecting, or delivering toxins, enzymes, and effector proteins to bacteria, host cells, or the environment, drug efflux, bacterial communication, and even bacterial motility [139,165,169]. The innate host immune system has also been observed to detect and respond to the presence of secretion systems and their secreted substrates during infection [165], and is likely a strategy developed by the host to distinguish pathogenic organisms from commensals [165,170].

Quorum Sensing

Quorum sensing is a process of cell-to-cell communication using small molecules which allows bacteria to share information about their population density, and regulate gene expression accordingly [139,171]. The process includes the production, detection, and response to autoinducers (extracellular signaling molecules), and allows bacteria to synchronize gene expression and act together in unison [171,172]. Quorum sensing plays a role in many microbial traits associated with virulence including cell maintenance, biofilm formation, toxin production, horizontal gene transfer, antibiotic production, natural competence, sporulation, and the expression of secretion systems (SS) [139,173]. Quorum-sensing also interacts with the host, with some molecules influencing the immune response and immunoglobulin production, or promoting the apoptosis of macrophages and neutrophils [174,175] . Conversely, human airway epithelial cells have been shown to target quorum sensing by inactivating quorum-sensing molecules [176]. Quorum Sensing Inhibitory (QSI) treatments may therefore be a potential option to combat pathogenic bacterial infections [177].

Two-component Systems

Two-component systems (TCS) are a widely used signal transduction system that respond to changing environments and control a multitude of gene regulatory systems [178]. The ability of bacterial cells to efficiently adapt to different environments is frequently mediated by TCSs, and the relationship between quorum sensing and the response to TCSs is often closely linked [139,178]. TCSs consist of a sensor histidine kinase (HK) and a response regulator (RR); when stimulated, the HK will autophosphorylate and transfer the phosphoryl group to a conserved aspartate residue on the RR [139,179]. There is a variety of different types of TCSs and the role they play in the pathogenicity and virulence of bacteria is not well understood, however it has been shown that mutant strains lacking certain TCSs display attenuated virulence and activate an immune response in animal models, and some TCSs regulate gene clusters that promote cell growth, biofilm formation and virulence in pathogenic bacteria [179].

Antibiotic Resistance

Preventing disease with the use of antibiotic-producing microbes can be traced back to 1550 BC where mouldy bread and medicinal soil are listed amongst other remedies [180]. Salvarsan, a synthetic arsenic based drug, was introduced for the clinical treatment of syphilis in 1910 [181] and the methods used to identify a drug to treat a specific disease marked the beginning of systematic screens for drug discovery [182]. The first broad spectrum antimicrobial in clinical use was sulfonamide drug Prontosil, and shortly after that the clinical use of beta-lactam drug penicillin [182]. Less than a decade after the clinical introduction of penicillin, the first bout of antibiotic resistance began, however this was combated with the discovery of new beta-lactam antibiotics. Today, there are over 30 different classes of antibiotics, but the antibiotic resistance

crisis continues to rise due to the overuse and misuse of these medications, and the significant decline in new drug discovery to counter resistance [182,183].

Antimicrobial resistance (AMR) is a significant global concern, and it is predicted that AMR bacterial infections could cause over 10 million deaths per year worldwide by 2050 if left unchecked, outpacing many other deadly diseases and infections [184]. Alternative antibacterial strategies are desperately needed. In Canada there were just under 1 million bacterial infections in 2018, with a quarter having resistance to first line antimicrobials (antimicrobials known to work the best with the least amount of side effects) [185]. Of these infections, 14000 people died and 40% of these deaths would not have occurred if these infections had been susceptible to first line antimicrobials [185]. A study done in 2019 looking at 204 countries and territories estimated that around 4.95 million deaths associated with bacterial AMR occurred in 2019, with 1.27 million of these deaths attributed to bacterial AMR [186]. The following sections will discuss common mechanisms of antibiotic resistance for Gram-negative bacteria.

Efflux Pumps

Efflux pumps were first identified in 1980 by McMurry and colleagues where they described the energy-dependant efflux of tetracycline [187]. Efflux pumps actively remove antibiotics from the cell using energy in the form of ATP hydrolysis or proton motive force [188]. They can also remove a variety of other compounds including heavy metals, organic pollutants, plant-produced compounds, quorum sensing signals, bacterial metabolites and neurotransmitters [188]. The role of efflux pumps in antibiotic resistance is likely a secondary role, as efflux pumps are ancient, present in all living organisms, and are well conserved among species, suggesting they have undergone evolutionary selection long before the use of antibiotics in therapy, and do not necessarily need to be acquired by horizontal gene transfer [188,189]. In addition to providing

resistance against antibacterial compounds, efflux pumps have been shown to play a role in bacterial virulence. For example, knock-out mutants have been shown to have impaired invasiveness and virulence in epithelial cells and mice, respectively, and overexpression of an efflux pump was shown to accumulate lower quantities a quorum sensing signal, and consequently displayed reduced virulence [190,191]. Together with the role they play in regulating quorum-sensing, inhibition of efflux pumps may increase antibiotic susceptibility and reduce virulence in bacterial pathogens [188].

Permeability Barriers

The fluidity of the cytoplasmic bilipid membrane in bacteria directly impacts permeability [192]. Gram-negative bacteria are intrinsically resistant to many antibacterial agents because of the reduced permeability due to an outer membrane (OM) and thin peptidoglycan layer that lies between the two bilipid layers [193]. The Gram-negative OM also contains lipopolysaccharides (LPS) which are lipid molecules (typically lipid A) covalently bonded to polysaccharide units, and contribute to reducing membrane fluidity and increase the permeability threshold due to their tightly packed nature [192,194]. To deal with the decreased permeability of their membrane structure, Gram-negative bacteria also have a variety of proteins known as porins, and though they aid in the essential uptake of nutrients, they also restrict the influx of many antibiotics [192]. Porins have been shown to slow the influx of drugs by a number of mechanisms including size limitations [195], hydrophobicity [196] and charge repulsion [196,197].

Modification of Drug Targets

Another mechanism of antibiotic resistance occurs through the modification of antibiotic targets by genetic mutation or post-translational modification [198]. Drug targets can be genetically altered by point mutations, homologous recombination, and occasionally deletion of the gene all

together, or targets can be enzymatically modified, for example via methylation [199]. Many antibiotics specifically bind to their targets with high affinity, effectively preventing normal function of the target, so any mutation or modification that blocks antibiotic activity but does not affect normal function of the target can confer antibiotic resistance to the cell [198]. There are a variety of genes identified that can methylate ribosomal subunits, effectively altering or blocking the target-binding site, and providing resistance to a variety of antibiotics [198]. The charge of the LPS can also be modified by the addition of phosphoethanolamine, which results in reducing the binding activity of polymyxin antibiotic colistin, and is typically caused by mutations that affect the expression of regulators affecting LPS production [198,200]. Another closely related mechanism of target modification is target protection, in which target protection proteins (TPPs) interact with the antibiotic targets and confer resistance through steric hindrance, conformational changes, or restoring functionality despite the presence of the bound antibiotic [201]. For example, genes have been shown to encode pentapeptide repeat proteins (PRPs), which protect topoisomerase IV and DNA gyrase proteins from quinolone antibiotics [202–204].

Drug Inactivation

In addition to preventing antibiotics from entering the cell, actively removing them, or altering their targets, bacteria can destroy or modify antibiotics as another means of resistance [198]. Drug inactivation can be accomplished by a variety of mechanisms including enzymatic degradation or cleavage, chemical modification, and sequestration [198,199]. Enzymatic inactivation of antibiotics not only provides resistance to the bacterial cell, but can help sensitive cells in the environment to survive by lowering the environmental antibiotic concentration; a well-known example of this is the inactivation of beta-lactam antibiotics by hydrolyzing enzymes known as beta lactamases, and has been observed to protect sensitive cells in natural microbial

communities [205,206]. Chemical modifications (i.e., acetylation, adenylation, glucosylation and phosphorylation) provide protection against a variety of antibiotic classes by preventing the antibiotic from binding to its target protein via steric hindrance; some of these antibiotics include aminoglycosides (i.e., kanamycin, gentamycin, and streptomycin), chloramphenicol, and beta lactams. [199,206]. Antibiotic sequestration prevents the antibiotic from reaching its target with proteins that bind the antibiotic and block their function, these proteins may be similar the target molecules, mimicking them, or there may be no obvious similarity to the target [206,207]. Some bacteria then have mechanisms to remove the antibiotics bound by these sequestering proteins [206].

Alternative Therapeutic Options

The discovery and approval of new antibiotics has substantially declined over the years, and is no longer enough to outpace antibiotic resistance; the potential of a "post-antibiotic era" is upon us, and common infections may once again have no cure [208,209]. Colistin, a bacterial natural product, is considered the last line of defence against a number of Gram-negative pathogens, and plasmid-mediated resistance against colistin has already been identified [210–212]. Some researchers still have hopeful views towards the discovery of new antibiotics to combat the war against AMR [182], however many support the opinion that antibiotics alone are no longer sufficient, and alternative treatment options are necessary [209,213–215].

The amount of research dedicated to finding alternative treatment options for AMR bacteria is substantial, and there are at least 19 alternatives-to-antibiotics that have been studied [216]. Antibodies are a promising alternative treatment, as they can bind to and inactivate pathogens, virulence factors, and toxins [216]. Lysins, phage encoded enzymes that can destroy the

cell wall of a target bacteria, are a potential replacement for antibiotics because of their direct antibacterial action [217]. Wildtype and engineered bacteriophage are another promising alternative as they can infect and kill bacteria and replicate at the site of infection [216,218,219]. Immune stimulation in conjunction with antibiotic treatment has also been proposed because successful treatment requires an adequate immune response [216]. Furthermore, the development of vaccines to substantially reduce infections with problematic bacteria and, consequently, the need for antibiotics, is a very promising avenue [216,220]. The remainder of this chapter will briefly discuss two promising alternative treatment options for AMR bacterial infections.

Phage Therapy

An alternative treatment option for AMR bacteria is the therapeutic use of bacteriophages. Their use as a therapy in North America declined after the discovery of antibiotics, but the increase in antimicrobial resistance has renewed phage therapy as a promising alternative treatment option [221]. Phages are viruses that specifically target and lyse bacterial cells via adsorption to cells using a cellular receptor, injecting their genetic material, and replicating themselves until the cell bursts [221]. Phages exclusively attack and lyse specific host bacteria, leaving beneficial bacterial flora unharmed [219]. As discussed above, the misuse of antibiotics has led to an increase in antibiotic resistance, with the prediction that AMR could be more deadly than cancer by 2050 [184]. Because of this threat, acceptance of phage therapy as a potential treatment option is growing, and the first North American phage therapy center, the Center for Innovative Phage Applications and Therapeutics (iPATH), opened at the University of California San Diego in June 2018.

In addition to host specificity, phages are advantageous for therapy because they use different mechanisms to kill bacteria than antibiotics, meaning they are effective at killing drug-

resistant bacterial infections [218]. Some phages also possess the ability to penetrate and/or break down bacterial biofilms, where antibiotics often show decreased effectiveness due to the increased antibiotic resistance exhibited by cells within these communities [159,218]. While phages hold many answers to the issue of AMR infections, selection and characterization of bacteriophages for therapy must be done carefully, as some phages can increase bacterial virulence through lysogenic conversion and be maintained through cell division as a prophage [222]. Additionally, bacteria can develop resistance to phage infection through numerous mechanisms including the mutation of the phage receptor on their cell surface, leaving phages unable to adsorb to and kill the bacterial cell [219]. The use of phage cocktails, a combination of phages that target different cell surface receptors, is a proposed solution to overcome this problem [219]. Alternatively, phage can display antivirulence activity if mutation of the receptor leaves the cell with a significant fitness disadvantage [223]. For example, if the phage receptor is LPS, pili, flagella, or an efflux pump, then when a bacteria mutates to evade infection by the phage it will also be losing a major virulence factor, affecting its ability to survive and cause disease in its host.

Phage-Antibiotic Synergy

An extension of phage therapy is phage-antibiotic combination therapy. It has been shown by a variety of studies that some antibiotics can induce increased phage activity at sub-inhibitory concentrations, a phenomenon termed "phage–antibiotic synergy" (PAS) [224–229]. This natural phenomenon was described following the discovery that some phage titers and plaque sizes increase in the presence of sub-inhibitory (non-lethal) levels of antibiotics [224]. Lytic phage activity was shown to increase in the presence of four different classes of antibiotics against *Burkholderia cenocepacia*, even with cells possessing elevated antibiotic resistance, suggesting

that PAS could still be used as an alternative treatment option for AMR bacterial infections [225]. The well-studied bacteriophage T4 has been shown to have increased activity in the presence of cefotaxime, and cause increased susceptibility to the antibiotic by the host *Escherichia coli* [226]. Additionally, it has been shown that the combined application of phage and antibiotic treatments is significantly more effective at eradicating *P. aeruginosa* biofilms than either treatment alone [227].

It has been speculated that phages and antibiotics likely evolved synergistic interactions because together they can reduce the chances that bacterial populations will develop resistance to either killing agent [230]. With many pharmaceutical companies reducing the research and development of new antibiotics because of a lack of return on investment [231], combined antibiotic and phage treatment may be one way of increasing the efficacy of antibiotics that are ineffective on their own.

Chapter 2

Aztreonam lysine increases the activity of phages E79 and phiKZ against *Pseudomonas aeruginosa* PA01

A version of this chapter has been published as:

Davis, C. M., McCutcheon, J. G., Dennis, J. J. 2021. Aztreonam lysine increases the activity of phages E79 and phiKZ against *Pseudomonas aeruginosa* PA01. Microorganisms, **9**(1): 152.

Objectives

The objectives of this study were to a) determine whether a synergistic effect exists between the virulent phage E79 and the antibiotic aztreonam lysine (AzLys) on *P. aeruginosa* strain PA01 in vitro, b) if an effect exists, to study how the increased activity is occurring, c) to determine if AzLys has any effects on the function of the polarly expressed structures flagella and type 4 pili (T4P), and d) to examine the effects of AzLys on phage phiKZ, which requires a functional T4P to infect its host. Trend et al. (2018) showed that phage E79 does not induce apoptosis or the production of inflammatory cytokines on airway epithelial cells isolated from children with or without CF. They also consider the potential of E79 as a phage therapy agent due to its wide host range against *P. aeruginosa* clinical isolates, stable high-titer stocks, and no known presence of bacterial pathogenicity islands.

Materials and Methods

Bacteria, Phage, and Growth Conditions

P. aeruginosa strain PA01 [233] was used in all experimental analyses. Bacteriophage E79 is a lytic phage that belongs to the previous phage family *Myoviridae* and infects many *P. aeruginosa* strains [234,235]. E79 was obtained from the Félix d'Herelle Reference Center for Bacterial Viruses (Laval University, Quebec, Canada). PhiKZ is a jumbo lytic phage that also belongs to the previous *Myoviridae* family and infects many *P. aeruginosa* strains [236] and was gifted to us by Joe Bondy-Denomy (University of California, San Francisco, USA). Propagation of E79 and phiKZ phage stocks and determination of titer were performed on PA01 using the double agar overlay method as previously described [237,238]. Phage titers used in each experiment are described in the relevant sections. Bacteria were grown aerobically overnight at 37 °C on half-strength Lennox (½ LB) solid medium or in ½ LB broth with shaking at 225 rpm. PA01

overnight cultures were subcultured 1:100 and grown to an optical density at 600 nm (OD_{600}) of 0.1 to obtain exponential-phase growth cultures. In all experiments, AzLys was added to media in the commercially available soluble form of Cayston (Gilead Inc., Foster City, CA, USA), which is an aztreonam derivative that improves respiratory symptoms of CF patients caused by chronic *P. aeruginosa* infections [239]. Statistical analysis for all experiments was conducted using GraphPad Prism 8 (Graph-Pad Software Inc., San Diego, CA, USA).

Minimum Inhibitory Concentration (MIC)

MIC protocol was followed according to Wiegand et al. (2008) using ½ LB broth and the antibiotics were prepared either in 0.17% saline (AzLys) or in 100% ethanol (aztreonam) and diluted to the desired concentrations in ½ LB broth. The OD_{600} was measured after 24 h using a Victor X3 spectrophotometric plate reader (PerkinElmer, Woodbridge, ON, Canada). The experiment was repeated in biological triplicate, with three replicates each.

Transmission Electron Microscopy (TEM)

P. aeruginosa PA01 cells were prepared for electron microscopy as follows. A volume of 100 µL of a 0.2475 mg/mL AzLys stock, or 0.17% NaCl for the control, was mixed with 3 mL of 0.7% ½ LB top agarose and poured onto a ½ LB agar plate to obtain a final concentration of 1.06 µg/mL, assuming AzLys fully diffuses. Once solidified, 100 µL of exponential-phase PA01 culture was spread gently across the top agarose and incubated at 37 °C overnight. Cells were collected from control and AzLys plates, standardized by weight, suspended in 1 mL 1 × phosphate-buffered saline (PBS), pH 7.2, washed twice with 1 mL of 1 × PBS, resuspended in 200 µL of EM fixative (2.5% glutaraldehyde, 2% paraformaldehyde, 0.1 M phosphate buffer, pH 7.2) and incubated at room temperature for 30 min. The fixed cells were pelleted at 8000× g for 1 min and resuspended in 1 mL of 1 × PBS. For visualization of bacterial samples, 10 µL of

sample was incubated on a carbon-coated copper grid for 2 min and stained with 2% phosphotungstic acid (PTA) for 10 s. To visualize phage interaction with PA01, E79 was propagated as described above, substituting ½ LB agarose for overlays. Bacterial samples were mixed in a 1:2 ratio with high-titer 10^9 PFU/mL E79 stock for 2 min and 10 µL of this mixture was loaded on a carbon-coated copper grid as described above. Transmission electron micrographs were captured using a Philips/FEI (Morgagni) transmission electron microscope with charge-coupled device camera at 80 kV (University of Alberta Department of Biological Sciences Advanced Microscopy Facility, Edmonton, AB, Canada). The average length and width measurements ± standard deviation for PA01 were calculated using Microsoft Excel from 10 individual bacteria measured using ImageJ software [241] (NIH, Bethesda, MD, USA).

Phage–Antibiotic Synergy Modified Double Agar Overlay

Double agar overlay plaque assays were used to determine the effect of AzLys on plaque size [237] with modifications [225]. Briefly, 100 µL of exponential-phase PA01 culture was incubated with 100 µL of phage stock at 10^3 PFU/mL for 7 min, mixed with 100 µL of AzLys and 3 mL of 0.4% ½ LB top agar, and overlaid onto 1.5% agar ½ LB solid media. Plates were incubated at 37 °C overnight until plaques formed. For controls, 100 µL of modified suspension medium (SM) (50 mM Tris-HCl pH 7.5, 100 mM NaCl, 10 mM MgSO4) was added in place of each AzLys concentration or phage suspension to account for agar dilution effects. AzLys concentrations used were calculated as 1.875, 3.75, 7.5 and 10 µg/mL within the 3 ml layer of top agar. Expecting the AzLys to diffuse evenly throughout the 20 mL agar plate, the final experimental concentrations are 0.27, 0.53, 1.06 and 1.41 µg/mL, respectively. Phage plaques were backlit and viewed under the magnifying glass of a New Brunswick Scientific colony counter (model C110), and plaque diameter was measured using digital calipers manufactured by Tresna (Guilin,

China). Ten plaques were measured at random per treatment group. Experiments were repeated in biological and technical triplicate and average plaque diameter was calculated from the 90 plaque measurements. Data were compared using an unpaired one-way ANOVA with Dunnett's post-test.

Phage Plaquing Assays

Phage plaquing ability was determined as described previously [238], with slight modifications. Briefly, 100 µL of overnight culture was mixed with either 200 µL ½ LB or 100 µL AzLys and 100 µL ½ LB for a desired concentration of 1.06 µg/mL AzLys. This concentration was used because it is in the middle of the three concentrations that showed PAS activity for E79. A volume of 3 mL of 0.7% ½ LB top agar was added to this and overlaid onto ½ LB plates and allowed to dry at room temperature for 1 h. Phage stocks were 10-fold serially diluted in SM. A volume of 5 µL of each dilution was spotted onto the plates and incubated overnight at 37 °C.

One-Step Phage Growth Curve

The bacteriophage growth curves were performed as previously described [242] with some modifications. Briefly, two 1:100 subcultures were grown in the absence or presence of 1.06 µg/mL AzLys to an OD_{600} of 0.1, equal to approximately 2.0×10^8 CFU/mL. This concentration of AzLys was used because it is in the middle of the three concentrations that showed PAS activity for E79. Phages were added to 10 mL of each exponential-phase culture to obtain a multiplicity of infection (MOI) of three and incubated at 37 °C with aeration at 225 rpm. A volume of 10 µL was removed in triplicate from each culture at desired time points, and serially diluted in 90 µL of chilled 1 × PBS. A volume of 5 µL of each dilution was spotted on ½ LB double agar overlays containing PA01 culture to assess phage titer. This process was repeated in

triplicate, and the rate of phage adsorption was calculated as the change in PFU/mL over time during the latent period. Burst size was calculated using the formula "burst size = P – x/I – x" where P is the maximum number of phages after lysis, I is the number of phages initially added to the culture, and x is unadsorbed phage. Statistical analysis was performed using a paired t-test.

Twitching Motility Assay

P. aeruginosa PA01 twitching motility in the presence of AzLys was assessed as previously described [243], with some modification. A single colony was suspended in 100 µL of ½ LB broth and stab inoculated with a sterile toothpick through a 3 mm thick ½ LB 1% agar layer containing 0, 0.27, 0.53, 1.06, or 1.41 µg/mL of AzLys. Plates were incubated with humidity at 37 °C for 24 h. Twitching zones beneath the agar were stained using 3 mL of TM developer solution (40% water, 10% glacial acetic acid, 50% methanol) for 30 min and measured using ImageJ software [241] (NIH, Bethesda, MD, USA). Experiments were repeated in biological and technical triplicate and average twitching diameter was calculated from the nine twitching zones. Statistical analyses were performed using an unpaired one-way ANOVA and Dunnett's post-test.

Swimming Motility Assay

Swimming motility of PA01 in the presence of AzLys was assessed as previously described [244] with some modifications. Briefly, 100 mL/plate ½ LB 0.3% agar containing 0, 0.27, 0.53, 1.06, or 1.41 µg/mL of AzLys was poured 7 mm thick in 15 mm petri dishes and allowed to solidify for 2 h at room temperature. A volume of 2 µL of overnight PA01 liquid culture standardized to an OD_{600} of 1.0 was injected halfway through the agar. The plates were incubated for 24 h at 37 °C and swimming zones were measured using ImageJ software [241] (NIH, Bethesda, MD, USA). Experiments were repeated in biological and technical triplicate and

average swimming diameter was calculated from the nine swimming zones. Statistical analyses were performed using an unpaired one-way ANOVA and Dunnett's post-test.

PAS Killing Assay

In a 96-well microtiter plate, 100 µL of exponential-phase PA01 culture at 2×10^8 CFU/mL was added to 50 µL of phiKZ phage stock for the desired MOI and 50 µL of AzLys or ½ LB to test PAS effects. For controls, 100 µL of SM was added in place of phage suspension, and ½ LB was added in place of AzLys. The plates were incubated for 24 h at 37 °C and 225 rpm. The OD_{600} was measured using a Victor X3 spectrophotometric plate reader (PerkinElmer, Woodbridge, ON, Canada). Each treatment was repeated in biological triplicate, with three replicates each. Statistical analyses were performed using unpaired t-tests.

PA01 Biofilm Formation and PAS Treatment

Biofilms were formed on polystyrene pegs of the MBEC™ biofilm inoculator with a 96-well base (Innovotech Inc., Edmonton, AB, Canada) following established protocols (MBEC™ Assay Procedural Manual, Version 1.1., 2015), with some modifications. *P. aeruginosa* PA01 overnight cultures were grown at 37 °C in ½ LB broth for 18 h, standardized, then diluted 1:100 in tryptic soy broth (TSB) to obtain a starting inoculum of approximately 10^7 CFU/mL. The 60 central wells of the microtiter plate were filled with 200 µL of starting inoculum and the outside wells were filled with 200 µL of TSB broth as aseptic controls and to prevent edge effects due to evaporation. The plates were covered with 96-peg polystyrene lids and incubated for 24 h at 37 °C and 120 rpm with humidity. The developed PA01 biofilms were washed in 200 µL of 0.9% saline for 5 min to remove non-adherent cells and the lid was transferred to a treatment plate containing 0, 1.41, 1.6, 1.8, or 2.0 µg/mL of AzLys with and without 10^4 PFU E79 in 200 µL volume total. The biofilms were incubated for 4 h at 37 °C and 120 rpm with humidity followed

by washing in 200 µL of 0.9% saline for 5 min. To quantify the biofilm biomass, the lid was transferred to a 96-well plate containing 200 µL of 0.9% saline and biofilms were dislodged from the pegs using a water bath sonicator (Branson Ultrasonic Cleaner Model B-32) for 30 min. The OD600 was measured using a Victor X3 spectrophotometric plate reader (PerkinElmer, Woodbridge, ON, Canada). Each treatment was repeated in biological triplicate, with six replicates each.

Scanning Electron Microscopy (SEM) of Biofilms

To visualize the morphology of *P. aeruginosa* PA01 biofilms, MBEC™ pegs carrying biofilms grown for 24 h and treated with 0 or 1.6 µg/mL of AzLys for 4 h were broken off the lid using sterile flat nose pliers and prepared as follows. Biofilm pegs were suspended in EM fixative overnight at room temperature, then washed three times in 1 × PBS for 10 min each. The fixed samples were dehydrated using a series of ethanol washes for 10 min each (50, 70, 90, 100, 100%) followed by ethanol:hexamethyldisilazane (HMDS) washes (75:25, 50:50, 25:75) for 10 min each. Finally, the biofilms were washed with 100% HMDS for 20 min, and then left in HMDS overnight with the lid slightly ajar to air dry. HMDS was used in place of critical point drying [245]. Once dried, the samples were mounted onto SEM stubs, sputter coated with gold and viewed in a Zeiss Sigma Field Emission SEM (University of Alberta Department of Earth and Atmospheric Sciences Scanning Electron Microscope Laboratory, Edmonton, AB, Canada).

Results and Discussion

Effects of Sub-Inhibitory AzLys on PA01 Morphology

AzLys belongs to the monobactam class of antibiotics that inhibit cell wall biosynthesis, and many antibiotics that disrupt cell division have been observed to cause morphological changes at sub-inhibitory concentrations [224,225,246–248]. To investigate whether AzLys changes the

morphology of *P. aeruginosa* PA01, we observed PA01 grown in the presence or absence of a sub-inhibitory concentration of AzLys using transmission electron microscopy (TEM). The MIC of AzLys for the PA01 strain tested is 8 μg/mL and the sub-inhibitory concentration is <2 μg/mL (Figure 2-1). To show that *P. aeruginosa* strain PA01 is not unusual in its resistance profile to AzLys, its MIC was compared to other *P. aeruginosa* strains (Figure 2-1; Table 2-1). The sub-inhibitory concentration is defined as the point where no bacteria are killed by the antibiotic concentration present. In the presence of AzLys, the morphology of PA01 is filamentous, a dramatic change from its wild-type single-cell rod structure (Figure 2-3A and B). These bacteria appear unable to form a septum between cells to complete cell division, forming significantly larger cells in both diameter and length under the stress of AzLys. Under normal growth conditions, single PA01 cells are on average 1.15 ± 0.18 μm in length and 0.51 ± 0.05 μm in width. These dimensions increase significantly in the presence of AzLys, with single PA01 cells (i.e., cells that have not undergone filamentation) measuring 1.8 ± 0.18 μm in length ($p < 0.0001$) by 0.55 ± 0.03 μm in width ($p < 0.05$). This morphological change could aid phage activity by a number of potential mechanisms. It has been suggested that an aberrant filamentous cell structure may cause increased bacterial membrane sensitivity to phage lysis proteins, such as lysozymes and holins, as well as allow for an increased rate of phage production [224]. This increased rate of phage production is correlated with cell size and is proportional to the amount of protein-synthesizing machinery within a cell at the time of infection, leading to increased phage burst sizes [249]. An increased burst size would allow low numbers of initial phages to self-propagate faster than normal under the same conditions. Additionally, it was observed that phage adsorption is directly proportional to cellular surface area [249]; therefore, increased cell surface

area upon AzLys-induced filamentation may result in an increased rate of phage adsorption and allow phages to infect and spread through a bacterial population more quickly.

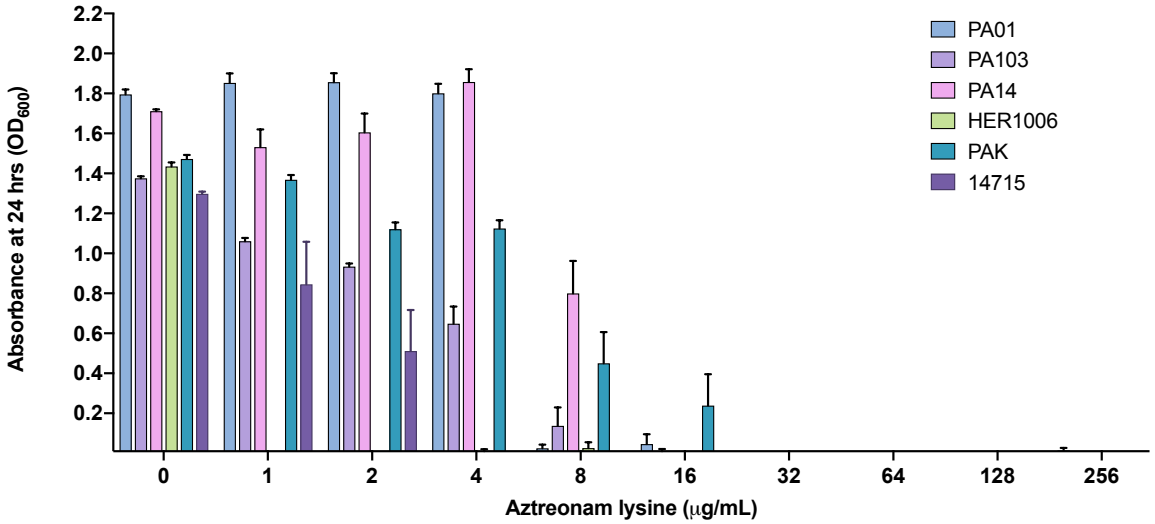

Figure 2-1: MIC of aztreonam lysine (AzLys) on different *P. aeruginosa* strains. Each strain was grown to exponential phase and diluted 1:100 to approximately 10^5 CFU/mL and grown for 24 h at 37 °C in the presence of AzLys at varying concentrations. Optical density at 600 nm (OD_{600}) was measured to obtain culture growth. Error bars represent standard error of the mean (SEM).

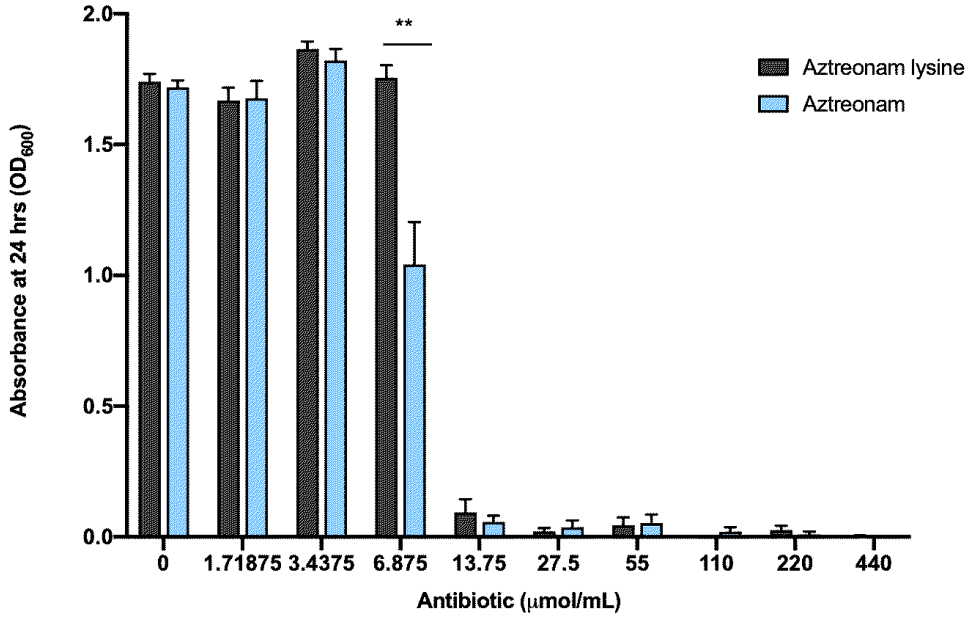

Figure 2-2: MIC of aztreonam lysine (AzLys) versus aztreonam on *P. aeruginosa* PA01. Exponential phase PA01 was diluted 1:100 to approximately 10^5 CFU/mL and grown for 24 h at 37 °C in the presence of either AzLys or Aztreonam antibiotic at varying concentrations. Optical density at 600 nm (OD_{600}) was measured to obtain culture growth. Statistical analysis was performed using an unpaired t-test (**; $p < 0.01$). Error bars represent standard error of the mean (SEM).

Table 2-1: Aztreonam Lysine minimal inhibitory concentrations for *P. aeruginosa* strains.

	P. aeruginosa strain					
	PA01	PA103	PA14	HER1006	PAK	14715
MIC (µg/mL)	8	16	16	<1	32	4

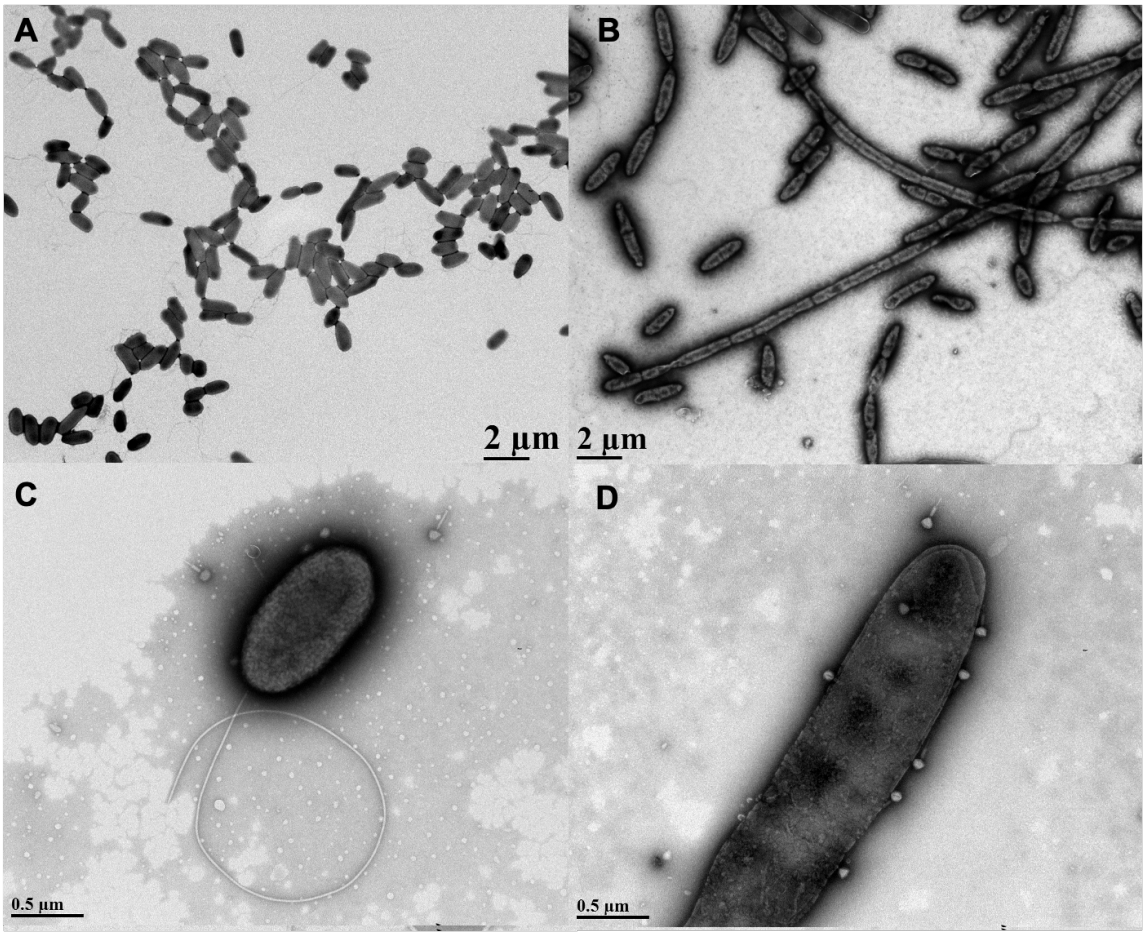

Figure 2-3: Effects of sub-inhibitory aztreonam lysine (AzLys) on *P. aeruginosa* PA01 morphology and phage E79 recognition. Electron micrographs showing PA01 grown under normal conditions (A) without or (C) with E79, and PA01 grown in the presence of 1.06 µg/mL AzLys (B) without or (D) with E79. Bacteria and phages were stained with 2% PTA and visualized by transmission electron microscopy at 4,400-fold (A and B) and 28,000-fold (C and D) magnification. Images are representative of at least 10 different bacterial cells per sample.

The lytic phage E79 uses LPS as a receptor to bind to its bacterial host for infection [250] and any increase in cell membrane will likely result in an increase in LPS, as it is a major

component of the outer membrane of Gram-negative bacteria. To observe whether there may be an increased association of E79 with filamentous cell surfaces, a high-titer E79 stock was incubated with PA01 bacterial samples grown in the presence or absence of sub-inhibitory concentrations of AzLys and viewed by TEM. An increase in the number of phages congregated on the surface of filamentous PA01 bacterial cells grown in the presence of AzLys was observed compared to the number of E79 adhered to normal PA01 bacterial cells (Figure 2-3C and D). Based on 10 different TEM pictures, there was an average of 2 ± 1 phage per cell under normal growth conditions, and 5 ± 2 phage per cell in the presence of AzLys (data not shown). These results show that filamentous cells are larger and can attract more phage per cell than normal growing PA01 cells. These observations are consistent with reported findings that elongated or filamentous cells may provide phages with increased access to their receptors on the cell surface, therefore promoting increased phage production and/or accelerated time to lysis [225,249].

Effects of Different Sub-Inhibitory AzLys Concentrations on E79 Activity

To determine whether the presence of sub-inhibitory concentrations of AzLys could increase the activity of E79 on *P. aeruginosa* PA01, plaque sizes were compared in a double agar overlay assay in the presence or absence of sub-inhibitory AzLys concentrations (Figure 2-4A, and C). Because plaque size is largely determined by burst size and time to cell lysis [224], increased plaque size is representative of increased phage lytic activity. Our results show a significant increase in the average plaque diameter of E79, producing plaques 1.7-fold larger in the presence of 1.41 μg/mL and 1.6-fold larger for 1.06 μg/mL AzLys as compared to the control ($p < 0.0001$). No significant increase in plaque size was observed for the two lower AzLys concentration of 0.27 and 0.53 μg/mL. Previous studies show that antibiotics affect bacterial morphology and/or growth rate, allowing the lytic activity of phages to increase [224,225,246–249]. Our

results therefore suggest that there is a minimum concentration of antibiotic necessary to cause a physiological change in the bacterium and induce increased phage activity. Phage production was affected minimally, with a small decrease in titer observed at 0.53 ($p < 0.01$), 1.06 and1.41 μg/mL ($p < 0.001$) of AzLys (Figure 2-4B).

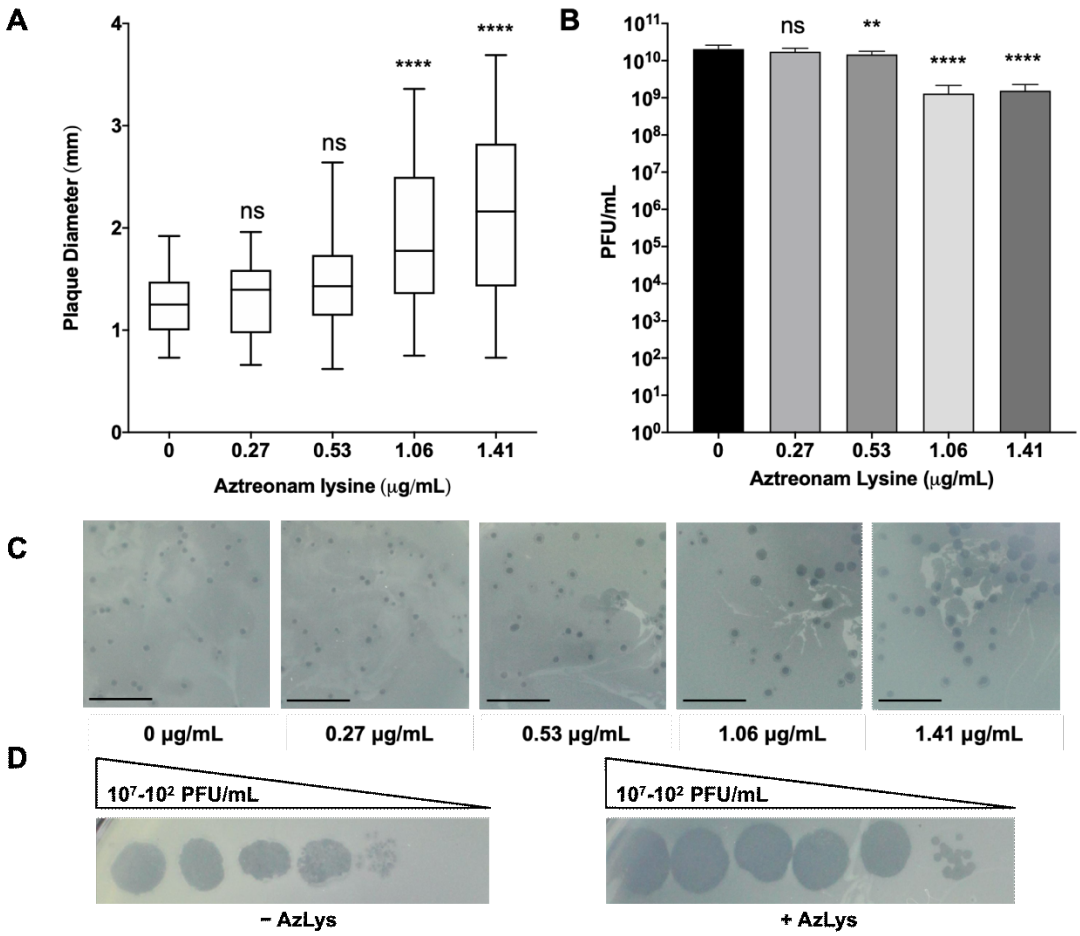

Figure 2-4: E79 and aztreonam lysine (AzLys) exhibit phage–antibiotic synergy (PAS) on *P. aeruginosa* PA01. (A) Box plot of plaque diameter, and (B), bar chart of average phage titer, of phage E79 in the presence of different concentrations of sub-inhibitory AzLys determined by a modified double agar overlay assay. Results are from three separate trials, with error bars representing the (A) largest and smallest plaque diameter and (B) standard deviation. Statistical analysis was performed using a one-way ANOVA with Dunnett's post-test compared to the control (**, $p < 0.01$; ****, $p < 0.0001$; ns, not significant). (C) Visual representation of E79 plaque morphology at increasing AzLys concentrations. All images were photographed at identical magnifications. Scale bars equal 20 mm. (D) Infection efficiency of E79 in the absence (-) or presence (+) of 1.06 μg/mL AzLys. Images are representative of three biological replicates, each with three technical replicates.

A plausible explanation for the small reduction in titer is discussed below. These results show that AzLys has a concentration-dependent effect on E79 activity; plaque sizes increase in diameter as sub-inhibitory AzLys concentrations increase (Figure 2-4A and C). Similar results

have been observed in *B. cenocepacia*, *Staphylococcus aureus*, and *E. coli*, which show an increase in phage plaque sizes as the sub-inhibitory concentration of various antibiotics is increased [225,226,251]. However, it has been demonstrated that cell size was not the only determinant of plaque size when comparing the effects of different antibiotics at sub-inhibitory concentrations [247] . The observed effects of AzLys may be due to more than one mechanism indirectly linked to increased cell size as described above. In addition to plaque size and phage titer, infection efficiency of E79 on PA01 changes in the presence of AzLys (Figure 2-4D). Efficiency of infection is increased by around 10-fold in the presence of 1.06 μg/mL of AzLys, the zone of lysis appears to be larger at all dilutions compared to the control, and plaque size is increased at the lowest dilution. The results suggest that E79 is able to infect PA01 cells better in the presence of AzLys. These results support our hypothesis that a one-way synergistic relationship exists between E79 and AzLys; the presence of sub-inhibitory concentrations of AzLys induces an increase in E79 activity as observed by the increase in E79 plaque size and infection efficiency on PA01.

Effects of AzLys on E79 Phage Growth Curve

To determine what aspects of the E79 infection cycle are being affected, we performed a one-step phage growth curve for E79 on PA01 in the presence or absence of 1.06 μg/mL AzLys. The phage growth curves are similar at certain time points of the infection cycle but differ in a number of ways when its host is grown in the presence of sub-inhibitory AzLys (Figure 2-5A and B). Firstly, there is a reduction in the latency period from approximately nine to six min (Figure 2-5A). This is shown again in Figure 2-5B, where phage growth rate has been calculated for each time range and is increasing at time interval 6–9 in the presence of AzLys, while still decreasing under normal conditions. Though this is a short time frame, it should be noted that a

consistent decline in phage titer is observed every 3 min prior to these measurements (intervals 0–3 and 3–6) and is still declining in the absence of AzLys (interval 6–9) (Figure 2-5A and B). Secondly, the decreased latent period is followed by moderate accelerated time to lysis between 9 and 45 min, though the rates of growth are not substantially different (Figure 2-5B). Despite the initial acceleration, lysis begins to slow, and the remainder of the time points do not differ between the two curves. The E79 + AzLys cycle is not completed earlier, and the total phage production following a single cycle of phage growth is not different between the two treatments. Given how similar many of the time points are between the two curves, the differences between the two curves are noteworthy. Using a paired t-test, the two curves compared to each other are statistically different from one another ($p < 0.05$), but there is no statistically significant difference in titer seen at individual time points. Lastly, the average rate of phage adsorption increases from 5.8×10^5 to 1.2×10^6 PFU mL−1 sec−1 in the presence of AzLys ($p = 0.0035$), supporting our hypothesis that E79 has increased association with the cellular surface in the presence of AzLys.

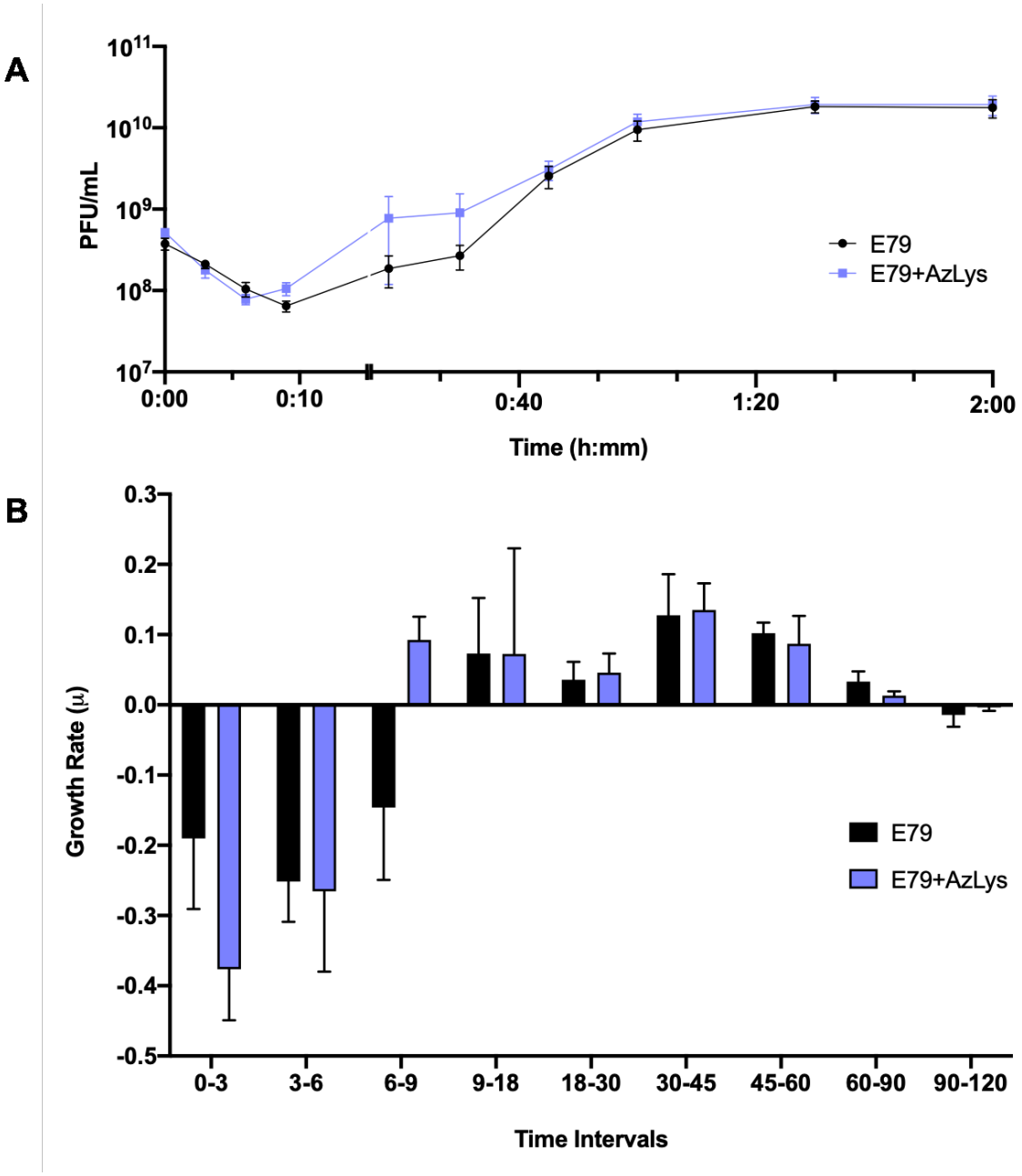

Figure 2-5: Aztreonam lysine (AzLys) shortens the latent period of the E79 one-step growth curve. Phage E79 was mixed with *P. aeruginosa* PA01 grown with or without 1.06 μg/mL AzLys at a MOI of approximately three. Phage titer was determined periodically over a 2 h incubation. (A) The one-step growth curve of E79, with each point representing the average of nine samples from three separate trials. Statistical analysis was performed using a paired t-test. (B) Growth rate of graph in (A) determined using the averages from each trial and calculated using growth rate equation $\log10N - \log10N_0 = (\mu/2.303)(t - t_0)$. All error bars represent the standard error of the mean (SEM).

In addition to providing information about phage adsorption and latency period, burst size can also be calculated from phage growth curves [251]. E79 burst size decreases from 58 to 44 phage per cell in the presence of AzLys, possibly explaining the slight reduction seen in phage titer in Figure 2-4B. A decrease in latency period shortens the amount of time for phage maturation, which can result in reduced burst size, but can also increase the phages' rate of exponential growth [252]. Though most PAS studies that examine phage production typically see an increase in burst size or final phage titer [224–226,246,248,253–256], it is important to note that PAS has still been shown to occur in the absence of increased phage production [225,247]. This discrepancy in phage production highlights that PAS may be generated by many different aspects of the phage infection cycle, and as proposed previously [225], it is possible that many different molecular mechanisms are responsible for the total PAS effects observed for every different phage and antibiotic combination. A study by Kim et al. (2018) reported that increased T4 phage production in *E. coli* with the addition of ciprofloxacin is a result of delayed time to lysis caused by an insufficiency of holins in the larger filamented bacteria. In the present study, the observed PAS in the presence of AzLys, with unchanging final phage production after one phage infection cycle, may be explained by the observed accelerated time to lysis rather than a delayed time to lysis. Our growth curve results support the conclusion that the increased PAS lytic activity of E79 in the presence of AzLys may be caused by a combination of increased phage adsorption, potentially due to cell filamentation, and accelerated time to lysis.

PAS Treatment of PA01 Biofilms In Vitro

Recently, a number of papers have been published that examine different aspects of PAS on *P. aeruginosa* biofilms [227,257–265]. We were particularly interested to discover whether pragmatic PAS with a lytic phage and AzLys was more effective at eradicating PA01 biofilms

than phage treatment alone. To test this hypothesis, we used the MBEC™ biofilm inoculator with 96-well base plates (Innovotech Inc., Edmonton, AB, Canada) to create identical biofilms growing on plastic pegs. Because biofilms are different from planktonic cells on transcriptomic, proteomic and physiological levels [266], we first sought to determine whether AzLys affects PA01 biofilms similarly to the effects observed on planktonic PA01 cells. Consistent with observations that biofilms exhibit increased resistance to antibiotics, we were able to increase the maximum sub-inhibitory concentration from 1.41 μg/mL to 2 μg/mL AzLys without inhibiting cell growth (data not shown). PA01 biofilms grown for 24 h and treated for 4 h in the presence or absence of 1.6 μg/mL AzLys were imaged using scanning electron microscopy (SEM) (Figure 2-6). Similar to planktonic PA01, AzLys causes aberrant division of biofilm cells and results in long filamentous structures, suggesting that PAS effects could also be observed with biofilm-grown cells.

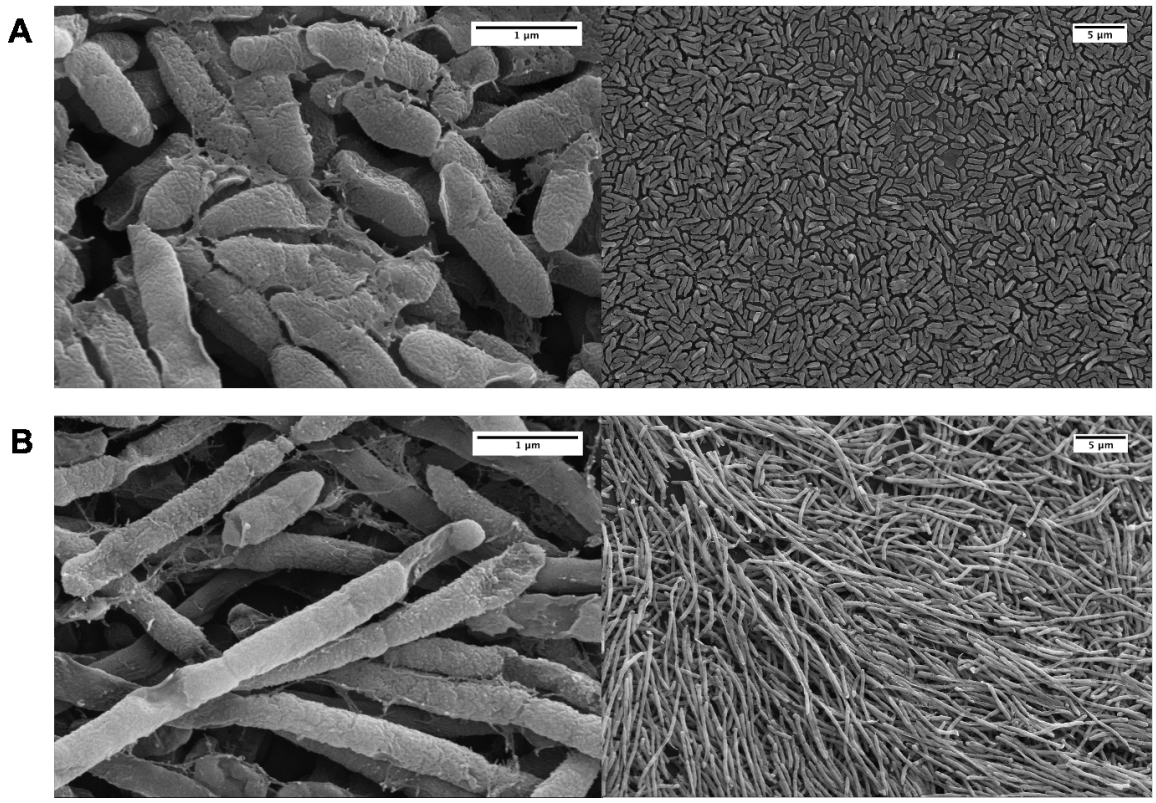

Figure 2-6: Effect of sub-inhibitory aztreonam lysine (AzLys) on *P. aeruginosa* PA01 biofilm morphology. Electron micrographs show PA01 biofilm under (A) normal conditions or (B) in the presence of 1.6 µg/mL AzLys. Biofilm pegs were mounted onto stubs, sputter coated with gold, and visualized using a Zeiss Sigma Field Emission SEM at 20,000-fold (left panels) and 2000-fold (right panels) magnification.

To test whether AzLys causes E79 to be more effective at eradicating PA01 biofilms than treatment with E79 alone, 60 identical PA01 biofilms were grown for 24 h and treated for 4 h with or without varying concentrations of AzLys (1.4; 1.6; 1.8; 2 µg/mL) and E79 (10^4 PFU/well). The average PA01 biofilm mass (OD_{600}) plus or minus the standard deviation for the 10 different treatment groups is shown in Figure 2-7. No statistically significant difference was observed between biofilm mass with or without AzLys treatment, confirming that the levels of AzLys used are not inhibiting growth. The lowest AzLys concentration used in combination with E79 decreased biofilm mass 1.7-fold as compared to E79 alone ($p < 0.01$), while the highest AzLys PAS concentration showed a 3.1-fold decrease as compared to phage treatment alone ($p <$

0.0001). No statistically significant difference between the biofilm mass for the four PAS treatment groups was observed. These results show that AzLys increases the biofilm reduction activity of E79 phage, with combination of the two treatments resulting in a significant reduction in biofilm mass compared to phage treatment alone.

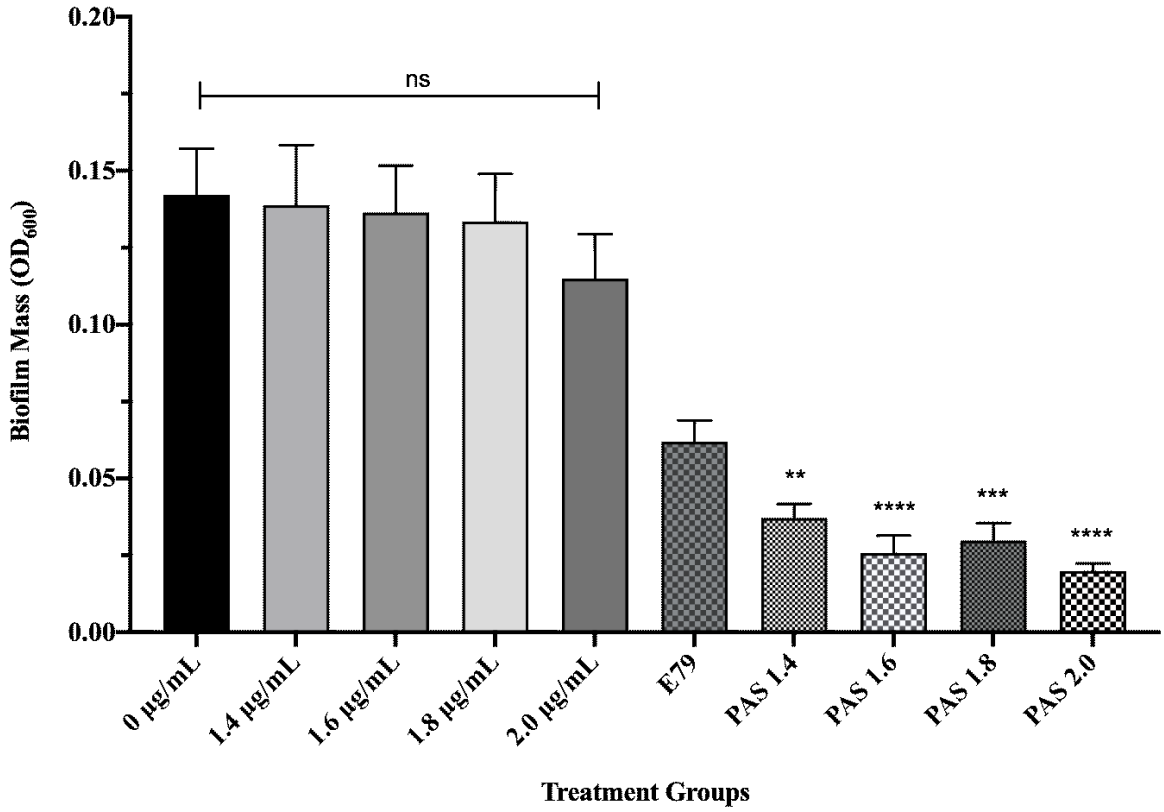

Figure 2-7: E79 and aztreonam lysine (AzLys) exhibit phage–antibiotic synergy (PAS) on *P. aeruginosa* PA01 biofilms. Biofilms were grown for 24 h followed by treatment for four hours in TSB media at 37 °C with shaking at 120 rpm with added sub-inhibitory AzLys, E79 phage (10^4 PFU/well), or a combination of both. Biofilms were disrupted back into a planktonic culture using a water bath sonicator, and optical density at 600 nm (OD_{600}) was measured to obtain biofilm mass. Statistical analysis was performed using ANOVA and Dunnett's post-test compared to the control (**, $p < 0.01$; ***, $p < 0.001$; ****, $p < 0.0001$). Error bars represent the standard error of the mean (SEM).

Effects of Sub-Inhibitory AzLys on PA01 Surface Structures

Though AzLys can increase the activity of a phage that uses LPS as its receptor, it seems unlikely that it would be able to increase the activity of a phage that uses a receptor whose

expression might decrease due to filamentation, rather than increase like LPS. Numerous studies suggest that sub-inhibitory concentrations of cell wall-disrupting antibiotics may negatively affect bacterial virulence factors [267–272]. Due to the changed cellular morphology of PA01 caused by the presence of sub-inhibitory AzLys, we were interested to determine whether polar motility structures on the cell surface such as pili and flagella were also affected [273]. Type IV pili (T4P) are cell surface structures involved in cell motility, virulence, and adhesion [274], and are a common receptor for many *P. aeruginosa* specific phages [238]. Based on the observation that PA01 undergoes aberrant cell division in the presence of AzLys, resulting in linked, filamentous cells and a reduced number of poles, it is likely that T4P expression or function may be decreased under these conditions. Assessment of T4P function via twitching motility for PA01 bacteria grown in the presence of four different sub-inhibitory AzLys concentrations revealed that sub-inhibitory levels of AzLys significantly decreases twitching motility in a concentration-dependent manner (Figure 2-8A). All four AzLys concentrations tested show a significant decrease in twitching motility compared to the twitching diameter of 19.5 ± 2.0 mm when PA01 is grown in the absence of AzLys. Twitching motility was eliminated at the highest sub-inhibitory AzLys concentration of 1.41 μg/mL. These results show that sub-inhibitory levels of AzLys have a concentration-dependent negative effect on T4P function in PA01.

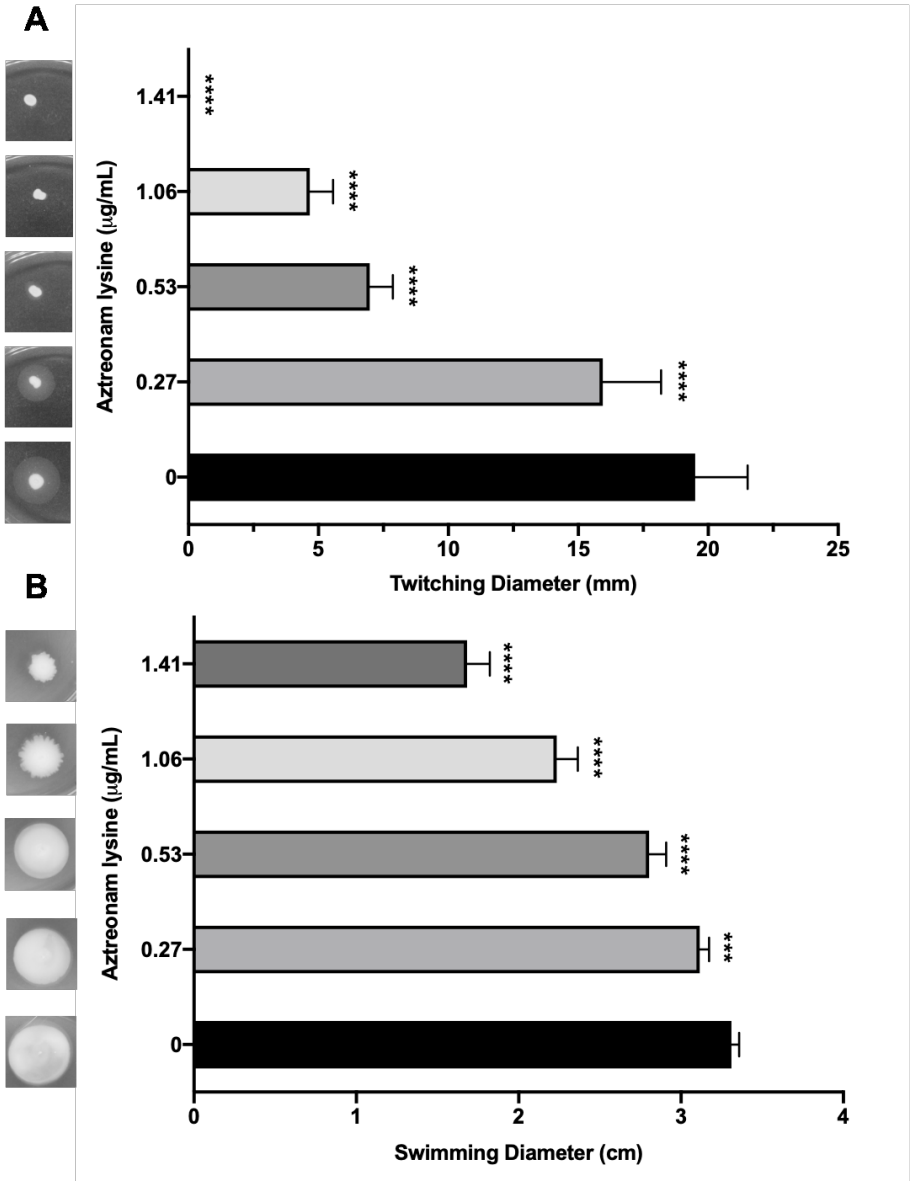

Figure 2-8: Effect of sub-inhibitory concentrations of aztreonam lysine (AzLys) on the motility of *P. aeruginosa* PA01. (A) PA01 grown in the presence or absence of sub-inhibitory AzLys concentrations were stab inoculated through 1% agar and incubated for 24 h at 37 °C. Twitching zones below the agar were visualized with TM developer solution and the diameter was measured using ImageJ [241]. (B) PA01 grown in the presence or absence of sub-inhibitory AzLys concentrations were stab inoculated midway through 0.3% ½ LB agar and incubated for 24 h at 37 °C. Diameter of swimming zone was measured using ImageJ. Representative twitching or swimming zones are shown on the left and the average diameter of each from nine replicates is shown on the right, including error bars showing standard deviation. Statistical analyses were performed using ANOVA and Dunnett's post-test compared to the controls (***, $p < 0.001$; ****, $p < 0.0001$).

In addition to T4P, we investigated whether AzLys also negatively affects the function of other polar motility structures. *P. aeruginosa* has a single polar flagellum [275] that is responsible for mediating bacterial movement through liquid or low-viscosity conditions, known as swimming motility [244]. If aberrantly divided filamentous cells express fewer flagella based on cell mass than normal, the addition of AzLys may result in decreased swimming ability. Assessment of swimming motility in the presence of sub-inhibitory concentrations of AzLys shows a decrease in swimming zone diameter (Figure 2-8B). This negative effect is concentration dependent, with the highest concentration of 1.41 μg/mL reducing flagellar function by approximately 49.3% compared to cells grown without AzLys. While this concentration-dependent effect is similar to the observed reduction in twitching motility, 1.41 μg/mL AzLys did not eliminate swimming motility as it did for twitching motility (Figure 2-8). Fonseca et al. (2004) similarly observed a decrease in both twitching and swimming motility following the exposure of eight different strains of *P. aeruginosa* to 0.5 MIC piperacillin/tazobactam. However, antibiotics can also have the opposite effect on motility; an increase in swimming motility was observed for *Chromobacterium violaceum* when exposed to sub-inhibitory concentrations of kanamycin [276]. How an antibiotic affects motility and other virulence factors is likely determined by the way the cell responds to the environmental stressor. Therefore, it may be important to pair a cell's response to an antibiotic with the requirements of the phage infection cycle when searching for synergistic activity between an antibiotic and a phage. It is plausible that *P. aeruginosa* phages using the T4P or flagella as a receptor may not exhibit a significant increase in phage adsorption or infection efficiency in the presence of antibiotics that cause filamentation, and PAS effects may not be observed.

Effects of AzLys on T4P-Specific Phage phiKZ

To test the hypothesis that filamentation may not increase the activity of phages that use receptors found at the poles of *P. aeruginosa*, we examined the plaque diameter and phage titer of phiKZ in the presence of varying sub-inhibitory concentrations of AzLys. The virulent phage phiKZ requires a functional T4P to infect *P. aeruginosa* [277]. Our results show that AzLys did not cause a significant increase in phiKZ plaque diameter or phage titer compared to the control (Figure 2-9A and B), and a decrease in plaque size at the two lowest sub-inhibitory concentrations is observed ($p < 0.001$, $p < 0.01$). A possible explanation for this decrease in plaque size could be reduced phage adsorption rates due to reduced access to cellular receptors caused by filamentation. It is unknown why the plaques returned to average size as AzLys is increased, but it is possible that phiKZ exhibits a decreased latency period and/or accelerated time to lysis, as seen with E79, allowing the plaques to return average size as the effects of the antibiotics are increased.

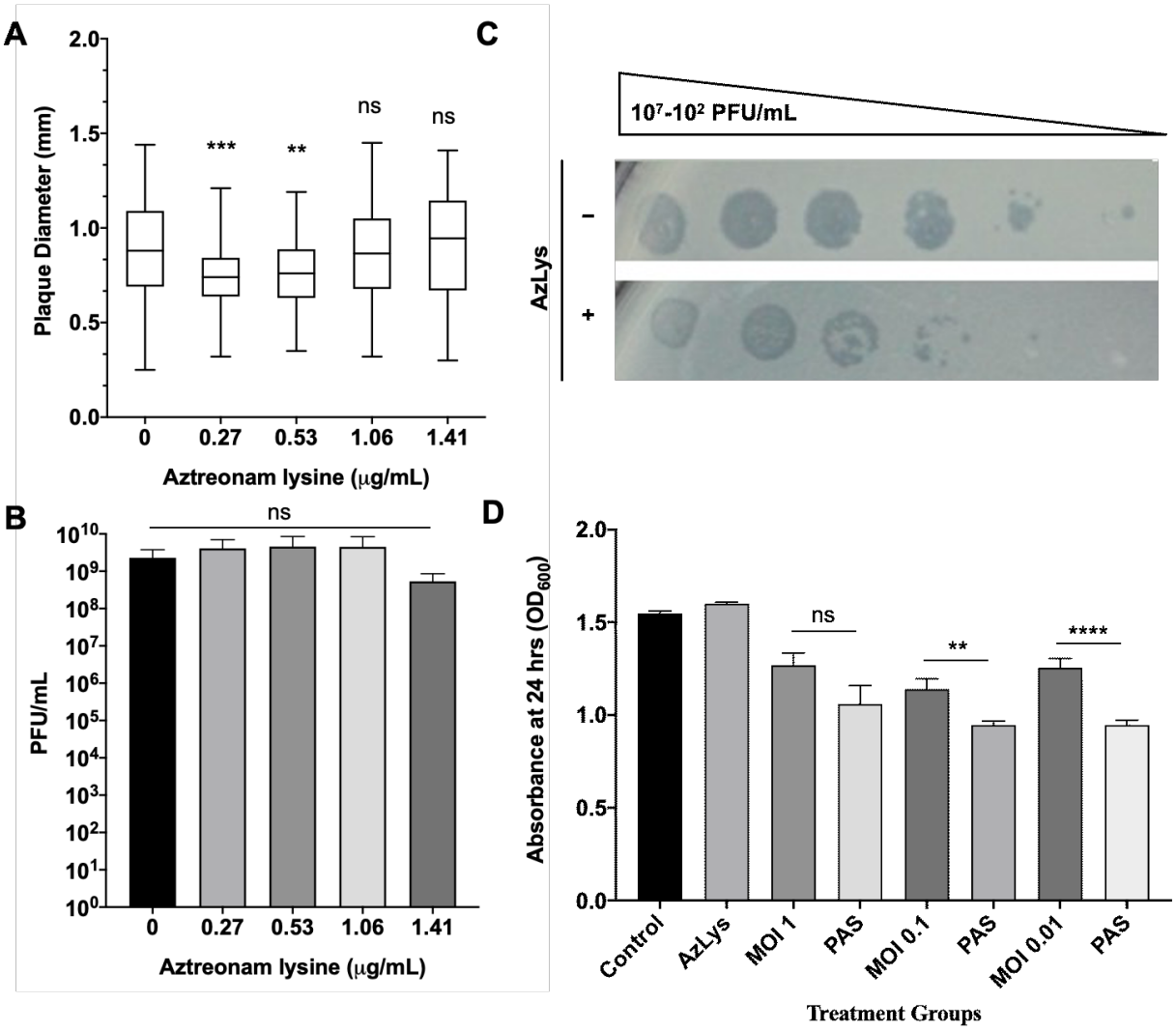

Figure 2-9: Effects of aztreonam lysine (AzLys) on *P. aeruginosa* phage phiKZ that uses the T4P as its receptor. (A) Box plot of plaque diameter, and (B) bar chart of average phage titer, of phage phiKZ in the presence of different concentrations of sub-inhibitory AzLys determined by a modified double agar overlay assay. Results are from three separate trials, with error bars representing the (A) largest and smallest plaque diameter and (B) standard deviation. Statistical analysis was performed using a one-way ANOVA with Dunnett's post-test compared to the control (** $p < 0.01$; *** $p < 0.001$; ns, not significant). (C) Infection efficiency of phiKZ in the absence (-) or presence (+) of 1.06 μg/mL AzLys. Images are representative of three biological replicates, each with three technical replicates. (D) Killing effect of phage phiKZ was examined with or without the addition of 1.06 μg/mL AzLys. Values are averages from three trials, with error bars representing the standard error of the mean (SEM). Statistical analysis was performed using unpaired t-tests (** $p < 0.01$, **** $p < 0.0001$; ns, not significant).

To examine whether phiKZ efficiency of infection is affected by AzLys, phiKZ was spotted in 10-fold dilutions on double agar overlays with and without 1.06 μg/mL AzLys (Figure

2-9C). PhiKZ efficiency of infection is decreased by approximately 10-fold, and zones of clearing look more diffuse in the presence of AzLys. To further investigate how cell exposure to AzLys affects the activity of phages that use T4P as their receptor, we assessed whether phiKZ exhibits a change in killing activity in the presence of 1.06 μg/mL AzLys (Figure 2-9D). PhiKZ was added at MOIs of 1, 0.1, and 0.01 to exponential-phase cells and optical density (OD_{600}) was measured at 24 h. Unexpectedly, PA01 exhibited a greater reduction in growth with combination treatment as compared to phiKZ treatment alone, at all MOIs, two of which were statistically significant (MOI 0.1, $p < 0.01$; MOI 0.01, $p < 0.0001$). These results indicate that although there was no observed increase in phiKZ plaque size, phage production, or infection efficiency, we were still able to observe PAS with AzLys on PA01.

Effects of AzLys on PhiKZ Phage Growth Curve

Due to the increase in killing action observed by combination treatment with phiKZ and AzLys, we sought to determine how AzLys might affect the growth curve of phiKZ. We performed a one-step phage growth curve for phiKZ on PA01 in the presence or absence of 1.06 μg/mL AzLys. Similar to the trend seen in the E79 growth curves, the phiKZ curves differ from each other in a number of ways, but some time points remain remarkably similar between the two groups (Figure 2-10A). In both curves, the phiKZ titer rises slightly at 9 min, and no obvious decrease in titer is observed (Figure 2-10A and B). Thus, we were unable to calculate phage adsorption rates. Though this is unfortunate, it is not uncommon for some one-step growth curves to lack an obvious adsorption phase [224,228,252]. Moderate accelerated time to lysis in the presence of AzLys occurs from 30 to 60 min, where phiKZ is being released both earlier and at a faster rate, as compared to the control (Figure 2-10A and B). Similar to the E79 growth curves, after the accelerated lysis, phage production begins to slow down, and phiKZ in the presence of

AzLys completes its cycle at the same time as the control, with no obvious increase in final phage production (Figure 2-10A,B). We also see a small decrease in burst size from 14 to 9 in the presence of AzLys. However, no significant decrease in phage titer after overnight infection was observed for phiKZ (Figure 2-9B). The phenomenon of accelerated time to lysis has been observed before with penicillin, another cell wall inhibiting antibiotic, and was shown to accelerate time to lysis for a staphylococcus phage [253]. As discussed previously, Kim et al. [228] showed contrasting results with other antibiotics that cause filamentation of *E. coli*, resulting in a delayed time to lysis and increased phage production. A plausible explanation for how accelerated time to lysis paired with a slight reduction in burst size causes increased activity is that accelerated phage maturation allows for phage to be released and infect new cells faster, accelerating the overall rate of killing. These results together suggest that the phenomenon of PAS is more complex than just a change in cell morphology that causes a consistent change in phage activity, and likely depends on a variety of factors including the type of bacteria, phage, and antibiotic being used.

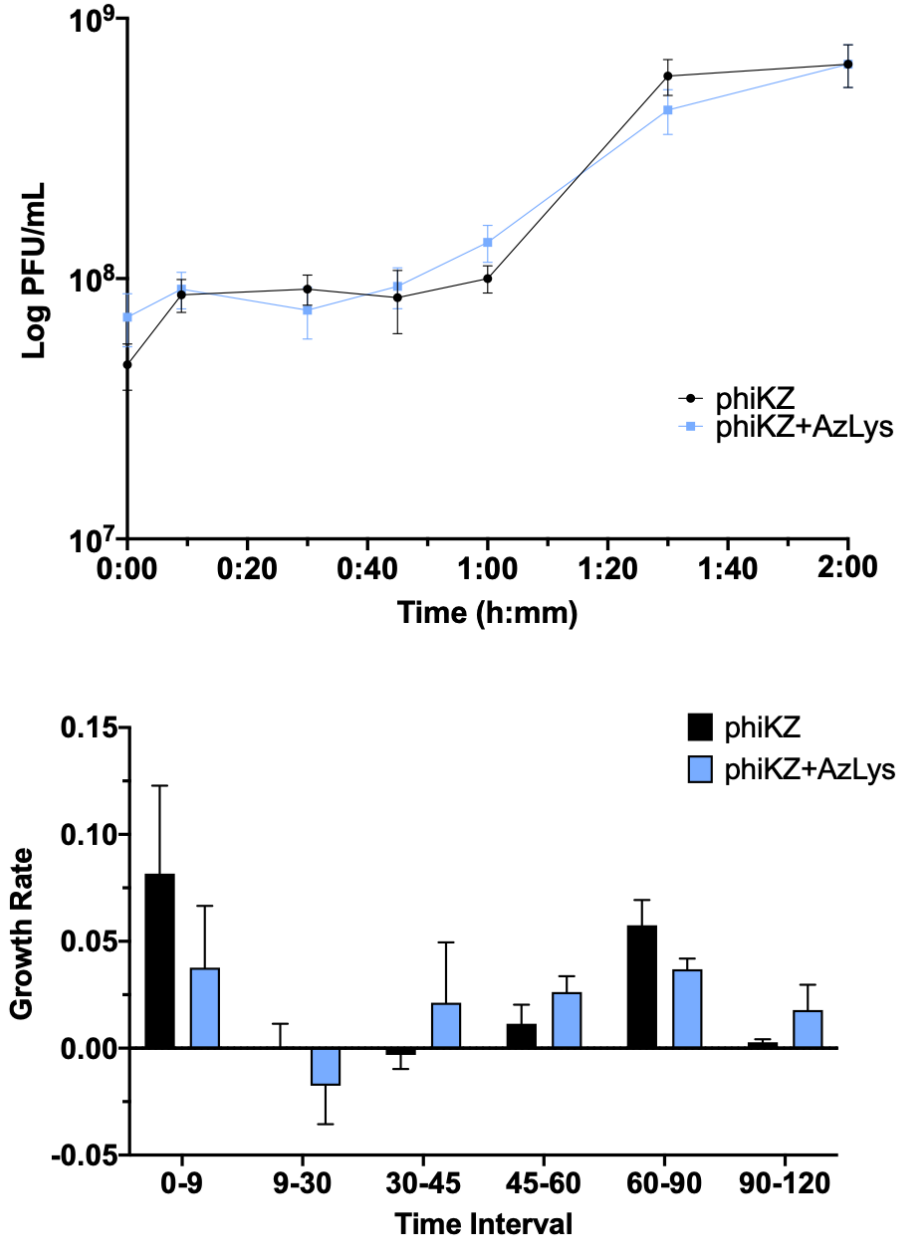

Figure 2-10: Aztreonam lysine (AzLys) shortens the latent period of the phiKZ one-step growth curve. Phage phiKZ was mixed with *P. aeruginosa* PA01 grown with or without 1.06 µg/mL AzLys at a MOI of approximately three and phage titer was determined periodically over a 2 h incubation. (A) The one-step growth curve of phiKZ, with each point representing the average of nine samples from three separate trials. Statistical analysis was performed using a paired t-test. (B) Growth rate of graph in (A) determined using the averages from each trial and calculated using growth rate equation log10N-log10N0 = (µ/2.303) (t-t0). All error bars represent the standard error of the mean (SEM).

Conclusions

It is estimated that 60–80% of CF adults will develop a chronic *P. aeruginosa* lung infection [35]. Once *P. aeruginosa* progresses to a chronic infection in individuals with CF, eradication of these infections is nearly impossible [278]. In addition, re-colonization is common due to *P. aeruginosa* persistence in the upper airways [278]. However, PAS has the potential to improve treatment for chronic infections with the combined action of antibiotics and select phages increasing killing activity against pathogens [224,225,227,248,249,253,257–265,279–287], and a variety of studies have shown that the combined use of antibiotics and phages reduces the emergence of resistance to one or both killing agents [227,280–282,286–289]. In this study, we show that AzLys increases the activity of phiKZ against planktonic culture, and increases the activity of E79 against biofilms. Phage E79 has previously been shown to be a promising candidate for use in phage therapy [232] and its activity appears to be increased by a combination of increased adsorption to the host, increased infection efficiency, and accelerated time to lysis. This study also shows that although AzLys negatively affects the expression of the T4P virulence factor, an increased killing activity of T4P-dependent phiKZ was observed that may be caused by accelerated time to lysis. This finding highlights the hypothesis that PAS is complex and occurs through a variety of different mechanisms. It further shows that standard methods for identifying PAS, such as plaque size and phage titer, are not always sufficient to determine whether synergy exists. Overall, this study demonstrates the efficacy of PAS against *P. aeruginosa* PA01 in vitro and helps to establish PAS with AzLys as a promising treatment expansion for the CF community.

Acknowledgements

The authors thank Arlene Oatway from the University of Alberta Department of Biological Sciences Advanced Microscopy Facility for assistance with TEM, and Nathan Gerein at the University of Alberta Department of Earth and Atmospheric Sciences Scanning Electron Microscope Laboratory for help with SEM. The authors thank members of the Dennis and Tracy Raivio's labs for thoughtful and helpful discussions. The authors also thank Joe Bondy-Denomy from the University of California, San Francisco for gifting phage phiKZ.

Chapter 3

The isolation and characterization of a broad host range Bcep22-like podovirus JC1

A version of this chapter has been published as:

Davis, C. M., Ruest M. K., Cole, J.H., Dennis J. J. 2022. The isolation and characterization of novel broad host range Bcep22-like Podovirus. Viruses, **14**(5): 938.

Objectives

The objectives of this research were to a) assemble and annotate the genome of bacteriophage JC1, and b) to characterize JC1 by analysing its host range, morphology, growth curve, receptor, virion-associated proteins, lifestyle, and virulence index.

Materials and Methods

Bacterial Strains and Growth Conditions

Bacterial strains used in this study are listed in Table 3-1. *B. cenocepacia* clinical isolate from Vancouver was named Van1 and used for isolation of phages from soil samples. Van1 and the JC1 lysogen were grown aerobically overnight at 37 °C on full-strength Lennox (LB; 10 g/L tryptone, 5 g/L yeast extract, 5 g/L NaCl) solid medium or in LB broth with shaking at 225 RPM unless stated otherwise. All other strains were grown at 30 °C on half-strength LB. Media was supplemented with 50–150 µg/mL tetracycline (Tc) antibiotic for plasmid maintenance when necessary. Suspension media (SM; 50 mM Tris-HCl [pH 7.5], 100 mM NaCl, 10 mM $MgSC_4$) was used for all phage work. Any statistical analysis was conducted using GraphPad Prism 9 (Graph-Pad Software Inc., San Diego, CA, USA).

Phage Isolation, Propagation, Host Range Analysis, and Electron Microscopy

Phage JC1 (vB_BceP_JC1) was isolated by Jamie Cole from potting soil in Edmonton, AB, Canada as previously described [290] with *B. cenocepacia* clinical isolate Van1. Briefly, soil was mixed with 1/2 LB broth, SM, and *B. cenocepacia* Van1 liquid culture and incubated at 30 °C overnight with aeration. The soil slurry was then pelleted by centrifugation and the supernatant was filter sterilized using a Millex-HA 0.45 µM syringe-driven filter unit (Millipore, Billerica, MA, USA). A double agar overlay with Van1 and the supernatant was incubated

overnight at 30 °C. A single plaque was isolated using a sterile Pasteur pipette and suspended in 500 µL of SM with 20 µL chloroform to generate a JC1 stock.

Propagation of JC1 was performed at 30 °C using double agar overlays as previously described [237,290], or in liquid. For liquid propagation, 150 µL of a Van1 overnight culture was mixed with 150 µL of JC1 lysate (10^{10} PFU/mL) and incubated for 30 min. After the brief incubation 1.5 mL of SM and 15 mL of LB broth was added to the mixture and incubated overnight with aeration at 225 RPM. Bacterial cells were pelleted by centrifugation at 18,514× *g* for 3 min. The supernatant was collected, and filter sterilized using a Millex-HA 0.45 µM or 0.22 µM syringe-driven filter unit (Millipore, Billerica, MA, USA). JC1 phage stocks were serially diluted into SM and spotted onto soft agar overlays of Van1 to determine stock titer. Plaques were backlit and viewed under magnification using a New Brunswick Scientific colony counter (model C110). Average plaque size was determined from 10 plaques ± standard deviation measured using a digital caliper (Tresna, Guilin, China).

Table 3-1: Host range analysis of JC1 on 85 *Burkholderia* strains.

Burkholderia species	Strain	Efficiency of Plating (EOP)	Source / Reference
B. cepacia	ATCC 25416^T	ND	Onion / [291–293]
	ATCC 17759	ND	Soil, Trinidad / [9,291–293]
	CEP509 / LMG 18821	6.7 x 10^{-7}	CF patient, Australia / [291]
	CEP521	7.3 x 10^{-7}	CF patient, Canada / CBCCRRR*
B. multivorans	ATCC 17616	+++	Soil, USA / [9,58,291,294,295]
	C3430	ND	CF patient, Canada / [296]
	C1576, LMG 16660	ND	CF-e patient, UK / [58,297]
	C5274	8.0 x 10^{-6}	CF patient, Canada / [296]
	C5393	ND	CF patient, Canada / [298]
	C5568	++	CF patient, Canada / [296]
	JC1	++	CF patient, Canada / [296]
	LMG 13010^T	++	CF patient, Belgium / [58,299]
	M1512	ND	CF patient, Canada / [300]

	M1865	ND	CF patient, Canada / [300]
	R810	ND	CF patient, Canada / [300]
	R1159	ND	CF patient, Canada / [300]
B. cenocepacia	AU1054	0.93	CF patient / [295]
	715j	ND	CF patient, USA / [301]
	BS1	++	CF patient, Canada / This study
	BS2	++	CF patient, Canada / This study
	BS3	++	CF patient, Canada / This study
	C1257	++	CF-e patient, USA / [296]
	C4455	++	CF-e patient, Canada / [296]
	C5424	0.25	CF-e patient, Canada / [291,298]
	C6433	ND	CF-e patient, Canada / [298,302]
	C8963	0.3	CF patient, Canada / [303]
	C9343	ND	CF patient, Canada / [303]
	CEP511	++	CF-e patient, Australia / [298]
	CEP0868	0.002	CF patient, Argentina / [300]
	D1	ND	Soil, USA / [300]
	HI2424	ND	Soil, USA / [300]
	J2315	0.14	CF-e patient, UK / [87,304]
	K56-2	+++	CF-e patient, Canada / [305]
	K63-3	ND	CF-e patient, Canada / [305]
	LMG 19240	ND	Wheat soil, Australia /[306]
	MCO-3	ND	Maize soil, USA / [131]
	PC184	0.19	CF-e patient, USA / [307]
	R161	+	CF patient, Canada / [300]
	R452	+	CF patient, Canada / [300]
	R750	0.9	CF patient, Canada / [300]
	R1284	0.022	CF patient, Canada / [300]
	R1285	0.6	CF patient, Canada / [300]
	R1314	++	CF patient, Canada / [300]
	R1434	0.86	CF patient, Canada / [300]
	R1619	++	CF patient, Canada / [300]
	R1882	0.53	CF patient, Canada / [300]
	R1883	0.47	CF patient, Canada / [300]
	R1884	1	CF patient, Canada / [300]
	R2314	0.73	CF patient, Canada / [300]
	RK1b	0.31	CF patient, Canada / [300]
	S11528	0.8	CF patient, Canada / [300]
	Van1	1	CF patient, Canada/This study
B. stabilis	LMG 14294	+	CF patient, Belgium / [299]
	C7322 / LMG 18870	6.0×10^{-4}	CF patient, Canada / [298]
	R450	ND	CF patient, Canada / [300]
	R2140	+	CF patient, Canada / [300]
	R2339	ND	CF patient, Canada / [300]
B. vietnamiensis	DBO1	ND	Soil, USA / [308]

	LMG 10929^{T}	ND	Rice, Vietnam / [58,60]
	PC259 / LMG 18835	+	CF patient, USA / [309,310]
	G4	ND	Soil, USA / [311]
B. dolosa	AU0158	++	CF patient, USA / [312]
	CEP021	+	CF patient, USA / [312]
	E12	8.6×10^{-5}	CF patient, UK / [312]
	STM1441	ND	Soil, Senegal / [312]
B. ambifaria	AMMD^{T}	ND	Soil, USA / [312]
	ATCC 53266	2.3×10^{-5}	Soil, USA / [312]
	CEP996	0.31	CF patient, Australia / [312]
	M53	ND	Soil, USA / [300]
B. anthina	AU1293	0.8	CF patient, USA / [312]
	C1765	4.3×10^{-3}	CF patient, UK / [312]
	J2552	ND	Soil, UK / [312]
	W92^{T}	ND	Soil, USA / [312]
B. pyrrocinia	ATCC 15958	ND	Soil, Japan / [312]
	ATCC 39277	ND	Soil, USA / [312]
	BC011	ND	Water, USA / [312]
	C1469	ND	CF patient, UK / [312]
Bcc Group K	CEP0964	ND	CF patient, Canada / [300]
	CEP1056	++	CF patient, Canada / [300]
	R445	3.1×10^{-5}	CF patient, Canada / [300]
B. lata	383	ND	Soil, Trinidad / [313]
Burkholderia sp.	JS150	1	Soil, USA / [300]
Pandoraea sp.	R1717	ND	CF patient, Canada / [21]
Ralstonia pickettii	ATCC 27511	0.7	Patient isolate, USA / [314]
	YH105	ND	Soil, USA / [315]

ND, Not detected; +, clearing at 10^{10} PFU/mL; ++, clearing at 10^{9} PFU/mL; +++, clearing at 10^{8} PFU/mL. EOP calculated by dividing PFU/mL on each strain by actual PFU/mL determined on strain Van1. Abbreviations: ^{T}, type strain; CF, cystic fibrosis isolate; CF-e, cystic fibrosis epidemic isolate. * Canadian Burkholderia cepacia complex Research and Referral Repository.

Host range analysis was performed using a collection of 85 phenotypically distinct clinical and environmental isolates listed in Table 3-1. A high titer JC1 phage stock (1×10^{10} PFU/mL) was serially diluted in SM and 5 µL of each dilution was spotted onto double agar overlays of each strain and incubated at 37 °C overnight. Efficiency of plating (EOP) was calculated by dividing the PFU/mL of JC1 on each strain by the actual PFU/mL determined on host Van1. EOP was only calculated for strains that JC1 could produce plaques on. Strains that

showed lysis, but no plaques, were included in the host range but were scored using a range of 1 to 3 "+" signs instead of an EOP score.

For electron microscopy, phages were purified by cesium chloride density gradient ultracentrifugation and dialysis. CsCl was dissolved in high titer JC1 lysate to a density of 1.45 g/mL followed by ultracentrifugation at 35,000 RPM in a 50.2 Ti rotor for 20 h at 4 °C. The phage band was extracted into 12 kDa molecular weight cut off dialysis tubing and dialyzed at 4 °C in 1.5 L SM for 4 days, with the SM buffer changed every 24 h. Ten µL purified phage lysate was loaded onto a carbon-coated copper grid for 2 min and stained with 4% uranyl acetate for 20 s, as previously described [238]. Transmission electron micrographs were captured using a Philips/FEI Morgagni transmission electron microscope with charge-coupled device camera at 80 kV (U. Alberta Dept. of Biological Sciences Advanced Microscopy Facility). The average capsid and tail dimensions ± standard deviation was calculated using Microsoft Excel based on measurements from 10 individual virions taken using ImageJ software (NIH, Bethesda, MD, USA).

Phage DNA Isolation and Sequencing

JC1 genomic DNA (gDNA) was isolated by Jamie Cole from a high titer phage stock using the Wizard Lambda DNA purification system (Promega Corp., Madison, WI, USA) with some modifications. A 1 mL aliquot of JC1 was incubated with 1 µL of 10 mg/mL DNase I (Thermo Scientific, Waltham, MA, USA), 10 µL DNase I buffer (1 M Tris-HCl, 0.25 M $MgCl_2$, 10 mM $CaCl_2$), and 0.6 µL of 10 mg/mL RNase A (Thermo Scientific) for 1 h at 37 °C. After incubation, 40 µL of 0.5 M EDTA (pH 8.5) was added to inactivate DNase I and 3.125 µL of 25 mg/mL proteinase K (Applied Biosystems, Carlsbad, CA, USA) and incubated at 55 °C for 1 h to degrade proteins and release phage DNA. The treated lysate was allowed to cool to room

temperature and added to 0.84 g of guanidine thiocyanate and 1 mL of pre-warmed (37 °C) resuspended Wizard DNA Clean-Up Resin (Promega Corporation, Madison, WI, USA). This mixture was rocked at room temperature for 20 min, then transferred into a syringe attached to a Wizard Minicolumn (Promega Corporation) and pushed though the column. The column was then washed with 3 mL 80 % isopropanol and dried by centrifugation for 2 min at 10,000× *g*. JC1 phage DNA was then incubated for 1 min with 100 µL of 80 °C sterile milli-Q water (Integrated DNA Technologies, Coralville, IA, USA) and eluted from the column by centrifugation for 1 min at 10,000× *g*. A NanoDrop ND-1000 spectrophotometer (Thermo Scientific, Waltham, MA, USA) was used to determine purity and concentration of eluted DNA. JC1 gDNA was sent for sequencing at The Applied Genomics Core at the University of Alberta. A Nextera XT library prep kit was used to generate the DNA genomic library followed by paired-end sequencing on a MiSeq (Illumina, San Diego, CA, USA) platform using a MiSeq v3 reagent kit. 4.8.

Bioinformatic Analysis of JC1

Read quality was assessed using FastQC v0.11.9 (http://www.bioinformatics.babraham.ac.uk/projects/fastqc/ accessed on 19 January 2022) and trimmed using Trimmomatic v.0.39 [316] with the following parameters: a four-base sliding window that cuts when the average quality per base drops below 20, removes leading and trailing low quality or N bases (below quality 3), and a minimum read length of 35 bp. Of 1,000,666 reads, 92.58% of both read pairs survived trimming and were assembled using SPAdes v3.13.0 [317], resulting in a final contig length of 61,191 bp contig with 1,711,139 reads mapping to 100% of the contig to give an average fold coverage of 3657. PCR and Sanger sequencing was used to confirm the assembly by amplifying 13 different regions spanning areas of lower coverage and

the "ends" of the contig. The product spanning the ends of the contig lacked a 9 bp repeat sequence, confirming a complete genome length of 61,182 bp. The JC1 genome was determined to be circularly permuted based on read coverage and assembly outputs.

Annotation of the contig was performed using three different annotation software: GLIMMER using the Bacteria and Archaea setting [318], Prodigal [319], and GeneMarkS for phage [320]. BLASTn was used to find related phages and BLASTp was used to identify predicted protein-coding genes and putative functions. Protein-protein BLAST was set to the Bacteria database (taxid:2) when no significant hits were found using the Viruses database (taxid:10239). NCBI non-redundant protein sequence and nucleotide collection databases (update date: 22 January 2022) were used. Hits with an E-value of 1×10^{-3} or greater were not considered significant, and annotations were recorded as hypothetical. Conserved domains were identified using Batch CD-Search against the CDD v3.19 58235 PSSMs database with default settings [321]. TMHMM 2.0 [322], and SignalP 6.0 [323], were used for lysis protein analysis and prediction of lipoproteins, respectively. Aragorn (Galaxy Version 0.6) [324] was used to identify potential tRNA genes. Protein alignments were created using MUSCLE [325]. Whole genome alignments and comparisons were done using MAFFT multiple aligner v1.4.0 [326] and Mauve v1.1.1 [327] plugins for Geneious and clinker v1.32 [328]. The complete genome sequence of JC1 was deposited in GenBank with the accession number OM283127.

Mass Spectrometry Analysis of JC1

JC1 was purified for proteomic analysis using a CsCl density gradient centrifugation. A 150 mL volume of JC1 lysate (10^{10} PFU/mL) was concentrated using ultracentrifugation at 28,700 RPM in a 50.2Ti rotor at 4 °C for 1.2 h. The JC1 pellets were resuspended with SM to a final volume of 16 mL and prepared for CsCl purification according to the manufacturer

recommendations (Beckman Coulter 2008). The CsCl gradient was centrifuged at 30,000 RPM in a 50.2Ti rotor at 4 °C for 20 h. JC1 ghost band was removed and dialyzed thoroughly with SM. Phage were prepared for mass spectrometry analysis by boiling purified lysate for 5 min in Laemmli sample buffer (62.5 mM Tris-HCl [pH 6.8], 2% SDS, 10% glycerol, 5% β-mercaptoethanol, 0.001% bromophenol blue), and running on a 10% SDS-PAGE gel. PageRuler Plus Prestained Protein Ladder (Thermo Scientific) was used as a molecular weight standard and 30 µL of JC1 CsCl purified lysate (10^{10} PFU/mL) in 1× sample buffer was loaded into an adjacent well. The lane was excised for whole-lane mass spectrometry analysis at the Alberta Proteomics and Mass Spectrometry (APM) facility located at the University of Alberta. Proteins were considered virion associated if they were identified by two or more unique medium to high quality peptides.

One-Step Growth Curve

One-step growth curve of JC1 on *B. cenocepacia* Van1 was conducted as previously described [229,242] with minor modifications. Overnight liquid cultures of Van1 were subcultured 1:100 and grown for approximately 2 h and 45 min to a CFU/mL of ~3×10^7. JC1 lysate was added at an MOI of approximately 2 and incubated at 37 °C with aeration at 225 RPM. A volume of 10 µL was removed in triplicate every 30 min and immediately serially diluted in 1× PBS. Phage titers were determined by spotting 5 µL of each dilution on soft agar overlays containing Van1 culture. Burst size was calculated using the formula "burst size = P/I" where P is the maximum number of phages after lysis and I is the number of phages initially added to the culture. The experiment was performed in technical and biological triplicate.

Complementation of LPS Mutants

Plasmids used in this study are listed in Table 3-2. The LPS genes for each of the seven mutants were amplified from *B. cenocepacia* K56-2 gDNA using primer pairs listed in Table 3-3. Resulting PCR products were digested with XbaI and KpnI Fast Digest restriction endonucleases (Thermo Scientific), ligated with T4 DNA ligase (NEB) into the vector pSCrhaB2-Tc, and transformed into *Escherichia coli* DH5α. Each resulting construct was verified with Sanger sequencing and transformed into the desired electrocompetent K56-2 LPS mutant strain.

Table 3-2: Plasmids used in this study

Plasmids	Description	Source
pSCrhaB2-Tc	*Burkholderia cenocepacia* rhamnose-inducible expression vector, Tc^R	(Juárez-Lara, unpublished)
pK56-2*hldAhldD*	pSCrhaB2 carrying K56-2 *hldA* and *hldD,* Tc^R	This study
pK56-2*waaC*	pSCrhaB2 carrying K56-2 *waaC,* Tc^R	This study
pK56-2*wabO*	pSCrhaB2 carrying K56-2 *wabO,* Tc^R	This study
pK56-2*waaL*	pSCrhaB2 carrying K56-2 *waaL,* Tc^R	This study
pK56-2*wabR*	pSCrhaB2 carrying K56-2 *wabR,* Tc^R	This study
pK56-2*wabS*	pSCrhaB2 carrying K56-2 *wabS,* Tc^R	This study
pK56-2*wbxE*	pSCrhaB2 carrying K56-2 *wbxE,* Tc^R	This study

Table 3-3: Primers used in this study

Primer name	Sequence (5'-3')	Function
2F	CTGCTTCTTCGATAGTGGTG	Anneals at 14,813 bp to 14,832 bp of JC1 genome, used to detect presence of JC1 genome in bacteria survivors of JC1 infection
2R	TCGGATTCCTCCTTCTCG	Anneals at 15,729 bp to 15,746 bp of JC1 genome, used to detect presence of JC1 genome in bacteria survivors of JC1 infection
attp_F	TCACGAGCAGGCTATACACG	Anneals at 1237 bp to 1256 bp. Flanks the predicted *attP* site upstream of gp1 serine recombinase.

attp_R	TGCAGCGTACAGACAGTTCC	Anneals at 1850 bp to 1869 bp. Flanks the predicted *attP* site upstream of gp1 serine recombinase.
rimO_F	ATCCCCCAAAGTAGGGTTCG	Anneals at 9 bp to 28 bp of Van1 *rimO gene*. Used to confirm integration site of JC1 with attP_R primer.
rimO_R	CACGGCCTGCATCACTTC	Anneals at 9 bp to 28 bp of Van1 *rimO gene*. Used to confirm integration site of JC1 with attP_F primer.
XOA8_kpnI_F	TAATGGTACCGAACAAAACGGCAAGAATCG	Anneals upstream of K56-2 *wabO* gene. KpnI site underlined.
XOA8_xbaI_R	TTTATCTAGAACCGTCATCTGGAAAGCTG	Anneals downstream of K56-2 *wabO* gene. XbaI site underlined.
CCB1_ kpnI_F	TTTTGGTACCGCCGGGTTTATCTTGAAAAG	Anneals upstream of K56-2 *waaC* gene. KpnI site underlined
CCB1_ xbaI_R	TTTTTCTAGAGACGGGACTTCGATGATCTG	Anneals downstream of K56-2 *waaC* gene. XbaI site underlined.
SAL1_ kpnI_F	TTATGGTACCGATGCACTCGTGATCGTGAC	Anneals upstream of K56-2 *hldA* gene. KpnI site underlined
SAL1_ xbaI_R	TTATTCTAGACTGGATCTCCGAAGAAAACG	Anneals downstream of K56-2 *hldD* gene. XbaI site underlined.
kpnI_F_XOA7	TAATGGTACCTACGTGGCGCACTGAAACAC	Anneals upstream of K56-2 *waaL* gene. KpnI site underlined
xbaI_R_XOA7	TAAATCTAGACGATATGGAACAGCAATCGC	Anneals downstream of K56-2 *waaL* gene. XbaI site underlined.
kpnI_F_RSF19	TAAAGGTACCACAGGTTGTATCGGCGTCTC	Anneals upstream of K56-2 *wbxE* gene. KpnI site underlined
xbaI_R_RSF19	TAAATCTAGAACTGCGCCTGGTTGTAACAC	Anneals downstream of K56-2 *wbxE* gene. XbaI site underlined.
kpnI_F_XOA15	TAAAGGTACCCGATTTCGCTAAAATGGCCC	Anneals upstream of K56-2 *wabR* gene. KpnI site underlined
xbaI_R_XOA15	TAAATCTAGAAGACGGTGTACTACCGCTTC	Anneals downstream of K56-2 *wabR* gene. XbaI site underlined.
kpnI_F_XOA17	TAAAGGTACCATCGGATTCAGTTCCAGCAG	Anneals upstream of K56-2 *wabS* gene. KpnI site underlined
xbaI_R_XOA17	TAAATCTAGAAGCCGTCTGACAGATTGCC	Anneals downstream of K56-2 *wabS* gene. XbaI site underlined.

Identification of Phage Receptor

High titer JC1 (10^{10} PFU/mL) was spotted onto double agar overlays of wt K56-2 or LPS mutants carrying either an empty vector control or the complementation plasmid and observed

for lysis. Receptor analysis was examined further as previously described [329]. Phage adsorption assays were performed with *B. cenocepacia* Van1 culture treated with either periodate or proteinase K to destroy either LPS or cell surface proteins, respectively. For proteinase K treatment, 2 mL of culture was treated with 0.2 mg/mL proteinase K (Applied Biosystems, Carlsbad, CA, USA), incubated at 37 °C for 3 h, and washed 2× with LB. For periodate treatment, 2 mL of culture was centrifuged at 6000× *g* for 3 min, and the bacterial pellet was resuspended in 1.5 mL sodium acetate (50 mM; pH 5.2) or sodium acetate with 10 or 100 mM IO_4^- and incubated for 2 h (protected from light). The cells were then washed 2× with LB. Bacterial suspensions were standardized using OD_{600}. A 100 µL volume of JC1 (1×10^6 PFU/mL) was incubated with a 500 µL sample of each treated bacteria, as well as an LB negative control and an untreated bacterial control for 30 min at room temperature. These samples were then centrifuged at 13,523× *g* for 3 min and tittered to determine the PFU/mL. The phage titer in the negative control supernatants were set to 100%. Each assay was performed in technical and biological triplicate.

Determination of JC1 Lifestyle and Integration Site

A liquid propagation of JC1 and Van1 was set up as described above. Surviving cells were collected by centrifugation at 6000× *g* for 5 min, and the supernatant was discarded. Cells were washed 3 times with LB broth to remove any extracellular phage and then resuspended in 5 mL LB broth. The washed cells were incubated again overnight at 37 °C with aeration at 225 RPM. The culture was then streaked onto LB solid media to obtain single colony isolates. Single colonies were then tested for superinfection resistance using overnight cultures of every isolate in a top agar overlay assay with Van1 spotted on top. Plates were incubated overnight at 37 °C and observed for zones of lysis. Colony PCR was also performed on each single colony to detect

the presence or absence of the JC1 genome. Single colonies with no zone of lysis and a positive PCR result were retained for further analysis.

Stability was analyzed by streaking out 4 different JC1 lysogen isolates on to LB agar plates and incubating for 2 days at 37 °C. A single colony was picked from these plates and struck out onto a new plate to obtain a second streak out. This was then done a third time to obtain a third streak out. One colony from each streaked plate for each lysogen was tested for superinfection resistance to JC1 and the presence of the JC1 genome using PCR as described above.

Determination of JC1 integration site was conducted as previously described [330] with some modifications. Primers were made that flanked the 133 bp intergenic region upstream of the predicted serine recombinase (gp1) (Table 3-3). Genomic DNA from a confirmed lysogen and pUCP22 were digested with SalI and ligated overnight with T4 DNA ligase (New England Biolabs) at 4 °C. 2.5 µL of the ligation mix was then used as a template in PCR using combinations of the primers that flank the upstream region of gp1 and M13 primers that flank the MCS of pUCP22. PCR products were sent for Sanger sequencing and analyzed using BLAST (https://blast.ncbi.nlm.nih.gov/Blast.cgi). The integration site was further confirmed with PCR using primer pairs that anneal to the Van1 genome flanking the identified integration site (Table 3-3).

Growth Analysis of Van1 vs. JC1 Lysogen and JC1 Virulence Index

Potential growth differences between *B. cenocepacia* Van1 and JC1 lysogen were assessed in 3 complete medias: LB broth, Mueller Hinton (MH) broth, and tryptic soy broth (TSB). Overnight cultures of each strain were subcultured 1:100 in LB broth and incubated at 37 °C for 2 h and 45 min. Subcultures were further diluted 1:100 into their desired media to a final

CFU/mL of 1×10^6. A volume of 200 µL was added to each well of a 96-well plate and placed in an Epoch™ 2 Microplate Spectrophotometer (BioTek) at 37 °C with orbital shaking at 237 cpm. OD_{600} was measured every hour for 48 h. Growth rate was calculated for exponential growth with the averages from each trial using growth rate equation (1):

$$\log_{10}N - \log_{10}N_0 = (\mu/2.303) \cdot (t - t_0) \quad (1)$$

The JC1 kill curves were performed similarly as described above with modifications. Van1 was prepared in LB as described above and 100 µL was mixed with 100 µL of JC1 diluted in LB to reach each desired multiplicity of infection (MOI). The 96 well plate was measured in an Epoch™ 2 Microplate Spectrophotometer (BioTek) at 30 °C or 37 °C with orbital shaking at 237 cpm. OD_{600} was measured every hour for 48 h. Local virulence was calculated by dividing the area under the curve for each MOI by the area under the curve of the bacterial control and subtracting that from 1. Global virulence index was calculated by taking the area under the curve generated from plotting the local virulence at each MOI tested against $\log_{10}$ MOI and diving it by 6 (all the MOIs tested-1). It is important to emphasize that global virulence indexes can only be compared if MOIs tested in the experiment are the same. Results for growth and kill curves were collected in technical and biological triplicate and analyzed using GraphPad Prism 9 (GraphPad Software Inc., San Diego, CA, USA).

Results and Discussion

Isolation, Morphology, and Host Range

Burkholderia phage JC1 (vB_BceP_JC1) was isolated by Jamie Cole from potting soil containing geranium (*Geranium dissectum*) and petunia (*Petunia exserta*) annual flowers using cystic fibrosis clinical isolate Van1. JC1 produces clear plaques with a diameter of 1 to 2 mm with overnight incubation at 37 °C and forms slightly turbid plaques of the same size at 30 °C

after a 2-day incubation. Transmission electron microscopy (TEM) was used to visualize JC1 and classify it as a *Podoviridae* phage with a C1 morphotype [331], having an average capsid diameter of 71 nm ± 1.24 nm and a short non-contractile tail with a length of 20 nm ± 0.91 nm and a width of 13 nm ± 0.67 nm. (Figure 3-1).

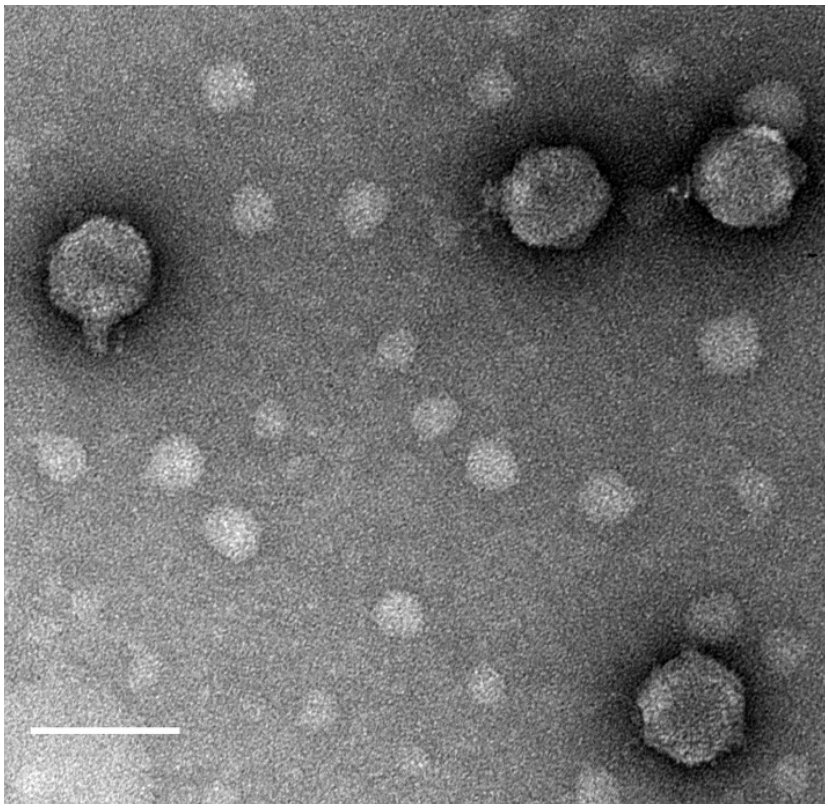

Figure 3-1: Transmission electron micrograph of JC1. High titer CsCl gradient purified JC1 virions were stained with 4% uranyl acetate on a copper grid and viewed at 140,000× magnification with a transmission electron microscope. Measurements of 10 phage particles have an average capsid diameter of 71 nm ± 1.24 nm and a short, noncontractile tail measuring 20 nm ± 0.91 nm in length and 13 nm ± 0.67 nm in width. Scale bar represents 100 nm.

Tail fibers were not observable in the TEM images. JC1 morphology is similar to Bcep22, BcepIL01, and DC1 [332,333], suggesting it may be a member of the Bcep22-like phage group. A one-step growth curve of JC1 on host strain Van1 shows a latent period of 1.5 h and a burst size of 296 virions at 6 h (Figure 3-2).

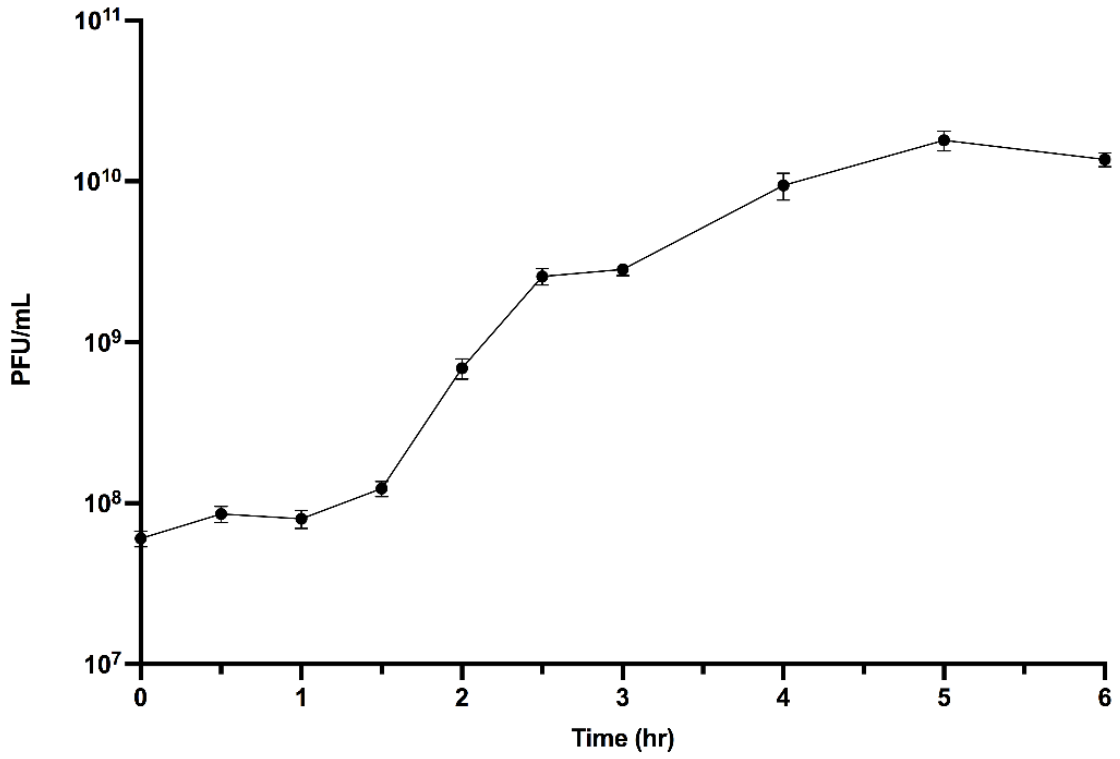

Figure 3-2: JC1 one-step growth curve on *B. cenocepacia* strain Van1. Subcultured Van1 was grown to approximately 3 × 10^7 CFU/mL at 37 °C. JC1 lysate was added at an MOI of ~2 and incubated at 37 °C with aeration at 225 RPM. Samples were taken every 30 min for 3 h, followed by every hour for 3 h, and serially diluted in 1× PBS. A total of 5 µL of each dilution was spotted on soft agar overlays containing Van1. Error bars represent the standard error of the mean (SEM). Data from three biological replicates is shown. Phage JC1 exhibits a latent period of 1 h and 30 min and a burst size of 296 virions per cell at 6 h.

The host range of JC1 was performed on a large panel of 85 Bcc clinical and environmental isolates revealing a very broad host range. JC1 is capable of infecting an impressive range of *Burkholderia* species including *B. cepacia*, *B. multivorans*, *B. cenocepacia*, *B. stabilis*, *B. vietnamiensis*, *B. dolsa*, *B. ambifaria*, *B. anthina*, Bcc Group K, *Burkholderia* sp, and *Ralstonia pickettii*, which possesses high similarity to Bcc [334]. JC1 showed lytic activity against 50 of the 85 strains, successfully forming plaques on 29 of the 50 (Table 3-1).

Receptor Binding

A significant number of *Burkholderia* phages likely use the LPS as their primary receptor for infection [335]. A collection of *B. cenocepacia* K56-2 LPS mutants have been previously constructed and characterized [145,146]. Plasmids complementing each LPS mutant were constructed and transformed into their designated strain. The collection of 7 LPS truncation mutants and their complemented strains were screened to determine if JC1 uses the LPS as its receptor. JC1 can infect K56-2 lacking an O-antigen and the outer core but is unable to infect mutants lacking varying degrees of the inner core (Table 3-4) [145,146]. Complementation of the three LPS truncation mutants restores JC1 infection. Since LPS make up a significant proportion of the outer membrane of Gram-negative bacteria, extreme truncations of the LPS may affect the organization of the membrane and may be indirectly affecting the ability of JC1 to infect mutant strains SAL1, CCB1, and XOA8 [145]. To further investigate if the LPS is the primary receptor of JC1, we examined phage adsorption against Van1 treated with either proteinase K or periodate, which destroy surface proteins or carbohydrates, respectively. JC1 was able to adsorb to untreated and proteinase K treated cells, but JC1 was unable to adsorb to cells treated with periodate (Figure 3-3). These results paired with the screening of the LPS mutants confirm that LPS is the primary receptor for JC1.

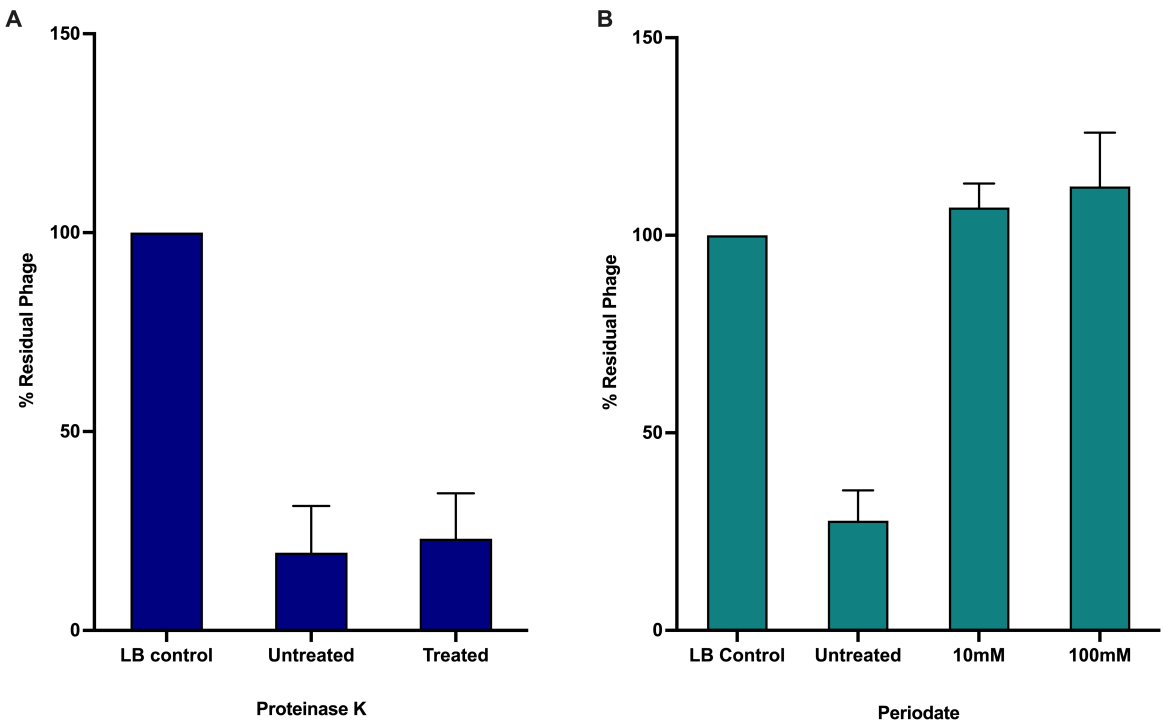

Figure 3-3: Effects of proteinase K and periodate treatment on JC1 adsorption to *B. cenocepacia* Van1. Bacterial overnights were incubated with either (**A**) proteinase K or (**B**) or periodate to observe if JC1 can adsorb to bacteria without surface proteins or carbohydrates, respectively. Error bars represent the standard error of the mean (SEM). Data from three biological replicates is shown.

Table 3-4. JC1 receptor identification on *B. cenocepacia* K56-2 LPS mutants.

Bacterial strain	Phenotype	pSCRhaB2	pSCRhaB2-complement
K56-2	Wildtype LPS	+	+
SAL1	K56-2 *hldA*:: pSL5, Lacks inner and outer core	–	+
CCB1	K56-2 *waaC*::pGPΩTp, Lacks inner and outer core	–	+
XOA8	K56-2 *wabO*::pGPΩTp, Lacks inner and outer core	–	+
XOA7	K56-2 *waaL*::pGPΩTp, Lacks outer core	+	+
XOA15	K56-2 *wabR*::pGPΩTp, Lacks outer core	+	+
XOA17	K56-2 *wabS*::pGPΩTp, Lacks outer core	+	+
RSF19	K56-2 *wbxE*:: pRF201, Lacks O-antigen	+	+

Truncation of the LPS to evade infection by JC1, or other phages that require the inner core for infection, should increase sensitivity to antimicrobial peptides such as polymyxin B, melittin, and human neutrophil peptide 1 (HNP-1) and possibly affect survival in vivo as seen in previous work characterizing strains lacking a complete LPS core oligosaccharide [145,146]. Combination therapy with these antimicrobials and phage could therefore prove very effective at reducing resistance and increasing sensitivity to both killing agents.

Genomic Characterization

The genome of JC1 is 61,182 bp in length (Figure 3-4) with a 65.4% G + C content and a coding density of approximately 95%. BLASTn analysis of the JC1 genome shows it is related to the Bcep22-like *Podoviridae* phages and belongs to the *Lessievirus* genus. JC1 is most similar to DC1 with 90.88% identity over 61% of the genome. Interestingly, JC1 also has similarity to a number of *Ralstonia* phages, which likely explains why JC1 is able to infect *R. picketti*. Using MAFFT alignment, JC1 is the most divergent of the Bcep22-like phages, with 54.3%, 57%, 59.1%, and 60% identity across the whole genome to Bcep22, BcepMigl, BcepIL02, and DC1, respectively (Figure 3-5).

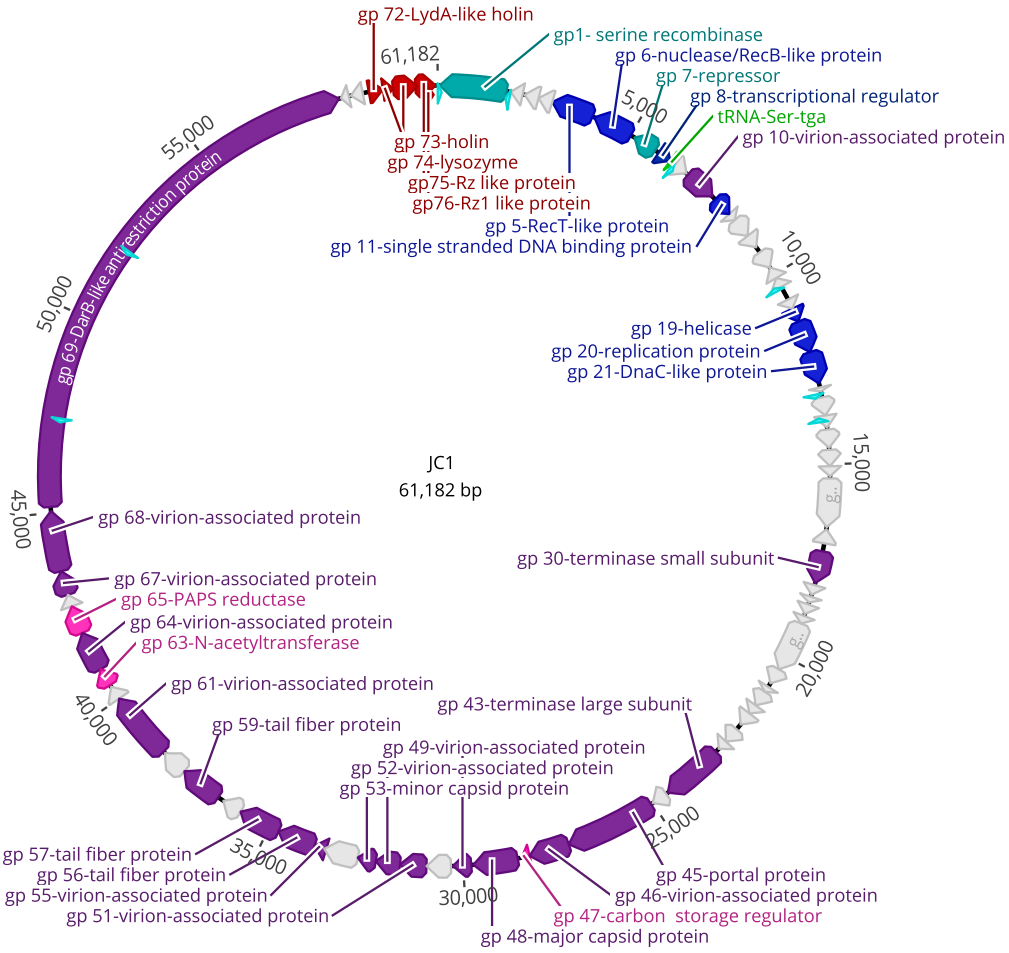

Figure 3-4: Circularized genomic map of JC1. Scale (in bp) is shown on the outer periphery. Assigned putative functions for each of the 76 predicted open reading frames are as follows: lysis (red), DNA replication, repair, and regulation (blue), lysogeny (teal), virion morphogenesis (purple), hypothetical (grey), tRNA (green), moron (pink), Rho-independent terminator (light blue). JC1 has a GC content of 65%. Image created using Geneious Prime.

	JC1	Bcep22	BcepMigl	BcepIL02	DC1	Gervaise
JC1		54.3%	57.0%	59.1%	60.0%	44.5%
Bcep22	54.3%		71.4%	63.2%	61.3%	44.3%
BcepMigl	57.0%	71.4%		70.8%	67.3%	45.6%
BcepIL02	59.1%	63.2%	70.8%		78.2%	45.0%
DC1	60.0%	61.3%	67.3%	78.2%		45.1%
Gervaise	44.5%	44.3%	45.6%	45.0%	45.1%	

Figure 3-5: Percent identity of Bcep22-like podoviruses and *Ralstonia* phage. Multiple sequence alignment was performed using MAFFT. Identical nucleotides between each genome are represented in greyscale and percent.

Though ~40% of the JC1 genome is dissimilar to the other Bcep22-like phages, and ~55% of the *Ralstonia* phage Gervaise differs from each Bcep22-like podovirus, the retained synteny between the phage genomes is apparent (Figure 3-6). Each phage encodes a putative serine or tyrosine recombinase on the reverse strand, a repressor-like gene, as well as a serine tRNA. Their entire, or almost entire, virion morphogenesis and lysis modules are encoded on the positive strands. Each phage encodes 3–4 tail fiber proteins followed by a conserved protein annotated as the head closure protein in *Ralstonia* phages. Additionally, all 6 of the genomes encode a massive DarB-like protein on the positive strand followed by two hypothetical proteins on the negative strand and the lysis module. Bcep22 and DC1 have the highest G + C content of the *Lessieviruses* at 66.2% while BcepIL02, BcepMigl, and JC1 have a lower G + C content around 65%, below that of *B. cenocepacia,* which possesses a 66.9% G + C content [123]. Noticeably, JC1, Bcep22, and BcepMigl all lack the presence of the PagP-like virulence factor found in BcepIL02 and DC1 [332,333]. Similarly to Bcep22 and BcepIL02, JC1 appears to be a circularly permuted phage, and the genome was set to begin after the predicted lysis module [332].

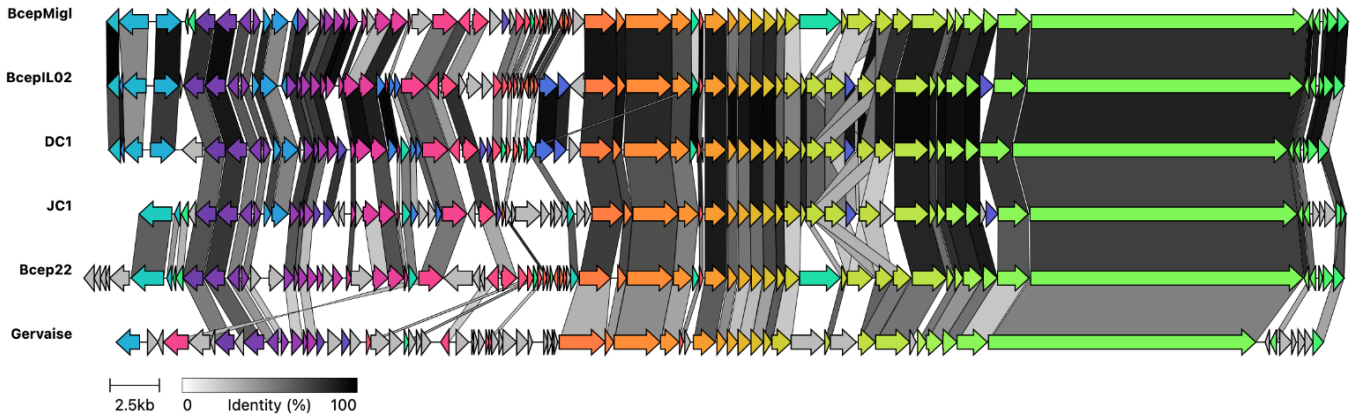

Figure 3-6: Clinker gene cluster comparison of Bcep22-like phages and Ralstonia phage Gervaise. Comparison of whole genomes for *Burkholderia* phage JC1 against the four other Lessievirus phages DC1, BcepIL02, Bcep22, and BcepMigl and related *Ralstonia* phage Gervaise. Percent amino acid identity is represented by greyscale links between genomes. Homologous proteins are assigned a unique color.

There are 76 predicted protein-coding genes and one predicted serine tRNA gene (Table 3-5, Figure 3-4). The predicted gene products have 12 GTG start codons and 64 ATG start codons. There are 50 TGA stop codons, with the remainder being 21 TAA codons and 5 TAG codons. BLASTp analysis of the 76 predicted proteins identified significant matches for every predicted gene product in the genome (Table 3-5, Figure 3-4). Predicted proteins gp4, gp16, gp17, gp33, gp34, gp37, gp39, gp42, and gp66 had no significant hits to the viruses database, but had hits to the bacterial database, all of which had very high percent identity to *B. multivorans* strains AU34603 (JAHPNN010000013.1), AU36904 (JAHPNA010000002.1), AU9032 (JAHPOS010000011.1), and AU11550 (JAHPOP010000012.1). Upon further analysis of these incomplete genomes, it appears that a potential 6th member of this podovirus group exists stably integrated into all four of these strains, though functionality of the prophage is unknown. It is important to note some base pair differences exist between the 4 lysogens that likely arose over time from integration in different strains. This prophage harbours around 96.4% similarity to JC1 and has all the genomic similarities discussed above with the other Bcep22-like phages.

Table 3-5: Bacteriophage genome annotations for JC1 obtained from BLASTp data.

Gene	Start	End	Strand	Length (aa)	Putative Function	BLASTp Hit	Species	Coverage (%)	E-Value	Identity (%)	Accession
1	1660	5	–	551 aa	serine recombinase	serine recombinase-like protein	*Burkholderia* phage Bcep22	100	0	70.29	NP_944235.2
2	2081	1794	–	95 aa	hypothetical protein	hypothetical protein Bcep22_gp07	*Burkholderia* phage Bcep22	72	2×10^{-27}	65.22	YP_009173769.1
3	2493	2146	–	115 aa	hypothetical protein	hypothetical protein Bcep22_gp09	*Burkholderia* phage Bcep22	98	2×10^{-21}	40.35	NP_944237.1
4	2867	2490	–	125 aa	hypothetical protein	hypothetical protein	*Burkholderia multivorans*	100	3×10^{-84}	96.80	WP_217093966.1
5	3895	2864	–	343 aa	RecT-like protein	RecT-like protein	*Burkholderia* phage Bcep22	100	1×10^{-178}	74.16	NP_944238.1
6	4976	3945	–	343 aa	nuclease/RecB-like protein	nuclease/RecB-like protein	*Burkholderia* phage Bcepmigl	98	0	84.32	YP_007236753.1
7	5697	5104	–	197 aa	repressor	transcriptional regulator	*Burkholderia* phage Bcepmigl	100	7×10^{-81}	59.90	YP_007236754.1
8	5821	6165	+	114 aa	transcriptional regulator	transcriptional regulator	*Burkholderia* phage DC1	78	8×10^{-38}	66.29	YP_006589939.1
9	6335	6685	+	116 aa	hypothetical protein	hypothetical protein G167_gp75	*Burkholderia* phage Bcepmigl	96	4×10^{-67}	87.50	YP_007236756.1

10	6737	7546	+	269 aa	virion-associated protein [a]	hypothetical protein BcepIL02_gp11	*Burkholderia* phage Bcepil02	99	2×10^{-143}	73.98	YP_002922683.1
11	7642	8142	+	166 aa	single stranded DNA binding protein	single stranded DNA binding protein	*Burkholderia* phage DC1	100	4×10^{-82}	81.33	YP_006589943.1
12	8151	8369	+	72 aa	hypothetical protein	hypothetical protein B862_gp69	*Burkholderia* phage DC1	100	3×10^{-40}	88.89	YP_006589944.1
13	8366	8842	+	158 aa	hypothetical protein	hypothetical protein UAM5_00057	*Ralstonia* phage UAM5	99	2×10^{-68}	65.61	CAH053217 4.1
14	8839	9201	+	120 aa	hypothetical protein	hypothetical protein KMC44_gp61	*Ralstonia* phage Cimandef	98	1×10^{-59}	70.87	YP_010078217.1
15	9352	9807	+	151 aa	hypothetical protein	hypothetical protein B862_gp66	*Burkholderia* phage DC1	84	7×10^{-68}	85.94	YP_006589947.1
16	10,127	9801	–	108 aa	hypothetical protein	hypothetical protein	*Burkholderia multivorans*	100	2×10^{-75}	100	WP_217093 979.1
17	10,389	10,132	–	85 aa	hypothetical protein	hypothetical protein	*Burkholderia multivorans*	100	2×10^{-53}	100	WP_217093 980.1
18	10,744	10,974	+	76 aa	hypothetical protein	hypothetical protein B862_gp65	*Burkholderia* phage DC1	100	3×10^{-39}	84.21	YP_006589948.1
19	10,971	11,357	+	128 aa	helicase	TPA: MAG TPA: hypothetical protein	*Siphoviridae* sp.	61	6×10^{-18}	44.30	DAT31939.1
20	11,354	12,178	+	274 aa	eplication initiator protein	replication protein	*Burkholderia* phage Bcepmigl	39	2×10^{-48}	76.85	YP_007236768.1
21	12,175	12,975	+	266 aa	DnaC-like protein	DnaC-like protein	*Burkholderia* phage Bcepil02	99	4×10^{-150}	76.60	YP_002922693.1
22	13,057	13,182	+	41 aa	hypothetical protein	hypothetical protein G167_gp61	*Burkholderia* phage Bcepmigl	100	1×10^{-9}	56.10	YP_007236770.1
23	13,337	13,765	+	142 aa	hypothetical protein	hypothetical protein B862_gp60	*Burkholderia* phage DC1	98	5×10^{-51}	60.28	YP_006589953.1
24	13,771	14,106	+	111 aa	hypothetical protein	hypothetical protein BcepIL02_gp24	*Burkholderia* phage Bcepil02	85	1×10^{-16}	43.75	YP_002922696.1
25	14,166	14,609	+	147 aa	hypothetical protein	TPA: MAG TPA_asm: hypothetical protein	*Myoviridae* sp.	95	7×10^{-44}	49.29	DAL29776.1
26	14,652	15,041	+	129 aa	hypothetical protein	TPA: MAG TPA: hypothetical protein	*Myoviridae* sp.	95	1×10^{-9}	34.35	DAP81611.1 .1
27	15,044	15,325	+	93 aa	hypothetical protein	hypothetical protein B862_gp58	*Burkholderia* phage DC1	100	3×10^{-40}	70.83	YP_006589955.1
28	15,364	16,602	+	412 aa	hypothetical protein	hypothetical protein Bcep22_gp31	*Burkholderia* phage Bcep22	100	6×10^{-156}	62.42	NP_944260. 2
29	17,017	16,658	–	119 aa	hypothetical protein	hypothetical protein KMC50_gp40	*Ralstonia* phage Claudette	85	2×10^{-25}	49.02	YP_010078630.1
30	17,210	18,010	+	266 aa	terminase small subunit	terminase small subunit	*Burkholderia* phage DC1	93	8×10^{-161}	83.53	YP_006589958.1
31	18,090	18,338	+	82 aa	hypothetical protein	hypothetical protein B862_gp53	*Burkholderia* phage DC1	92	2×10^{-39}	82.89	YP_006589960.1
32	18,389	18,517	+	42 aa	hypothetical protein	hypothetical protein B862_gp49	*Burkholderia* phage DC1	97	2×10^{-17}	87.80	YP_006589964.1
33	18,562	18,840	+	92 aa	hypothetical protein	hypothetical protein	*Burkholderia multivorans*	100	1×10^{-59}	97.83	WP_217093 993.1
34	18,872	19,066	+	64 aa	hypothetical protein	hypothetical protein	*Burkholderia multivorans*	100	9×10^{-36}	96.88	WP_217093 994.1
35	19,059	20,366	+	435 aa	hypothetical protein	hypothetical protein phiE131_040	*Burkholderia* phage phiE131	47	9×10^{-23}	41.40	AYJ74306.1

36	20,356	20,766	+	136 aa	hypothetical protein	hypothetical protein HOT12_gp34	*Burkholderia* phage vB_BmuP_KL4	84	5×10^{-32}	68.10	YP_009800723.1
37	20,851	21,033	+	60 aa	hypothetical protein	hypothetical protein	*Burkholderia multivorans*	100	8×10^{-33}	100	WP_217093996.1
38	21,030	21,416	+	128 aa	hypothetical protein	TPA: MAG TPA: Protein of unknown function (DUF2591)	*Caudovirales* sp.	99	2×10^{-13}	36.76	DAH87964.1
39	21,413	21,700	+	95 aa	hypothetical protein	hypothetical protein	*Burkholderia multivorans*	100	9×10^{-63}	100	WP_217093998.1
40	21,697	22,035	+	112 aa	hypothetical protein	hypothetical protein Bcep22_gp48	*Burkholderia* phage Bcep22	99	2×10^{-65}	85.59	NP_944277.1
41	22,172	22,582	+	136 aa	DUF2778 domain-containing protein	TPA: MAG TPA: Protein of unknown function (DUF2778)	*Myoviridae* sp.	98	8×10^{-19}	39.57	DAO56318.1
42	22,579	22,860	+	93 aa	hypothetical protein	hypothetical protein	*Burkholderia multivorans*	100	7×10^{-57}	98.92	WP_217094000.1
43	22,948	24,549	+	533 aa	terminase large subunit	terminase large subunit	*Burkholderia* phage DC1	98	0	83.11	YP_006589971.1
44	24,560	24,991	+	143 aa	hypothetical protein	hypothetical protein BcepIL02_gp45	*Burkholderia* phage Bcepil02	99	2×10^{-82}	82.39	YP_002922717.1
45	25,013	27,310	+	765 aa	portal protein	phage portal protein	*Burkholderia* phage Bcepil02	95	0	77.53	YP_002922718.1
46	27,318	28,340	+	340 aa	virion-associated protein[a]	hypothetical protein Bcep22_gp52	*Burkholderia* phage Bcep22	98	3×10^{-110}	57.82	NP_944281.1
47	28,367	28,561	+	64 aa	carbon storage regulator	carbon storage regulator	*Burkholderia* phage DC1	100	1×10^{-30}	89.06	YP_006589976.1
48	28,660	29,754	+	364 aa	major capsid protein	major capsid protein	*Burkholderia* phage Bcepmigl	100	0	92.03	YP_007236797.1
49	29,821	30,288	+	155 aa	virion-associated protein	virion associated protein	*Burkholderia* phage Bcepmigl	100	2×10^{-77}	74.84	YP_007236798.1
50	30,346	30,942	+	198 aa	hypothetical protein	hypothetical protein B862_gp33	*Burkholderia* phage DC1	99	5×10^{-80}	63.41	YP_006589980.1
51	30,946	31,593	+	215 aa	virion-associated protein [a]	hypothetical protein B862_gp32	*Burkholderia* phage DC1	100	7×10^{-147}	92.09	YP_006589981.1
52	31,590	32,219	+	209 aa	virion-associated protein [a]	hypothetical protein G167_gp30	*Burkholderia* phage Bcepmigl	100	6×10^{-117}	77.14	YP_007236801.1
53	32,229	32,648	+	139 aa	virion-associated protein	major capsid protein	*Burkholderia* phage DC1	100	6×10^{-93}	94.24	YP_006589983.1
54	32,653	33,528	+	291 aa	hypothetical protein	hypothetical protein B862_gp29	*Burkholderia* phage DC1	97	9×10^{-147}	74.39	YP_006589984.1
55	33,510	33,788	+	92 aa	virion-associated protein	virion-associated phage protein	*Burkholderia* phage Bcepil02	100	2×10^{-53}	90.22	YP_002922729.1
56	33,790	34,740	+	316 aa	tail fiber protein	putative tail fiber protein	*Burkholderia* phage Bcepil02	100	4×10^{-177}	76.90	YP_002922730.1
57	34,744	35,814	+	356 aa	tail fiber protein	putative tail fiber protein	*Burkholderia* phage Bcepil02	100	2×10^{-145}	64.54	YP_002922731.1
58	35,811	36,323	+	170 aa	hypothetical protein	hypothetical protein BcepIL02_gp60	*Burkholderia* phage Bcepil02	98	7×10^{-39}	45.29	YP_002922732.1

59	36,484	37,530	+	348 aa	tail fiber protein	TPA: MAG TPA: Endo N acetylneuraminidase	*Siphoviridae* sp.	59	9×10^{-84}	63.59	DAM52127.1
60	37,532	38,221	+	229 aa	hypothetical protein	hypothetical protein	*Pseudomonas* phage Dolphis	100	6×10^{-18}	44.92	QNJ57341.1
61	38,276	40,018	+	580 aa	head closure protein	virion-associated phage protein	Burkholderia phage Bcepil02	100	0	90.00	YP_002922735.1
62	40,020	40,373	+	117 aa	hypothetical protein [a]	virion-associated phage protein	*Burkholderia* phage Bcepil02	97	2×10^{-62}	86.09	YP_002922736.1
63	40,424	40,864	+	146 aa	acetyltransferase	acetyltransferase	*Burkholderia* phage DC1	97	6×10^{-92}	89.51	YP_006589993.1
64	40,857	41,855	+	332 aa	virion-associated protein [a]	hypothetical protein B862_gp19	*Burkholderia* phage DC1	100	0	91.27	YP_006589994.1
65	41,867	42,589	+	240 aa	phosphoadenosine phosphosulfate reductase	phosphoadenosine phosphosulfate reductase	*Burkholderia* phage DC1	100	2×10^{-167}	94.17	YP_006589995.1
66	42,589	42,888	+	99 aa	hypothetical protein	hypothetical protein	*Burkholderia multivorans*	100	2×10^{-59}	100	WP_217094022.1
67	42,905	43,495	+	196 aa	virion-associated protein	virion-associated phage protein	*Burkholderia* phage Bcepil02	30	1×10^{-4}	49.21	YP_002922740.1
68	43,506	45,038	+	510 aa	virion-associated protein [a]	hypothetical protein B862_gp17	*Burkholderia* phage DC1	100	0	80.30	YP_006589996.1
69	45,123	58,670	+	4515 aa	DarB-like antirestriction protein	DarB-like antirestriction protein	*Burkholderia* phage Bcep22	100	0	79.33	NP_944303.1
70	58,940	58,701	–	79 aa	hypothetical protein	hypothetical protein BcepIL02_gp71	*Burkholderia* phage Bcepil02	97	1×10^{-46}	89.61	YP_002922743.1
71	59,287	58,991	–	98 aa	hypothetical protein	hypothetical protein G167_gp14	*Burkholderia* phage Bcepmigl	100	2×10^{-41}	67.35	YP_007236817.1
72	59,443	59,790	+	115 aa	LydA-like holin	LydA-like holin	uncultured *Caudovirales* phage	82	4×10^{-27}	54.74	CAB41215448.1
73	59,787	60,059	+	90 aa	holin	holin	*Burkholderia* phage vB_BceS_AH2	91	6×10^{-32}	68.29	YP_006561127.1
74	60,056	60,634	+	192 aa	lysozyme	hypothetical protein AXJ08_gp22	*Rhodoferax* phage P26218	94	7×10^{-57}	49.45	YP_009222572.1
75	60,631	61,140	+	169 aa	Rz	Rz-like phage lysis protein	*Burkholderia* phage Bcep22	95	7×10^{-65}	66.27	NP_944308.1
76	60,866	61,087	+	73 aa	Rz1	Rz1	*Burkholderia* phage DC1	100	9×10^{-16}	83.56	YP_006590003.1

[a] Putative function determined by mass spectrometry analysis.

Rho-independent termination sites were predicted using ARNold [336–338]. The 8 predicted sites are displayed in Table 3-6 and are located downstream of gp2 (hypothetical protein) and downstream of the serine tRNA, upstream of gp17 (hypothetical protein), downstream of gp22 (hypothetical protein), one within the coding region in the opposite direction of gp24

(hypothetical protein), two within the coding region in the opposite direction of gp69 (DarB-like antirestriction protein), and one immediately downstream of the lysis module (gp72-76).

Table 3-6: Predicted Rho-independent terminators in JC1.

Start	Program	Strand	Sequence	−ΔG
1753	Both	–	ATCGACTCCAACGGCACCCTCGCGGTGCCGTTTTTATTGCCC	−13.20
6258	Rnamotif	+	CCAGCTGTTGAGCCTCCCGTTTCAGGGAGGCTTTTTGCCCGTA	−15.70
10,407	Rnamotif	–	AGAGCGTCGTCGGCGGCCCGCACGGCCGCCaTTTTTTTCGATC	−16.00
13,228	Rnamotif	+	GGCGACTTTGGTGGGCGGCTCGTACAGCGCCCGTTTTTTTTCACC	−9.60
13,893	Rnamotif	–	CCGATGCGCACCGGCCGGATGTGGCTGATCCGGTTGTTGTATTCGCGG	−10.50
47,347	Rnamotif	–	TCGGCCGACACCTTGCGGCGCTCGGCCGTGAGcaTCTTGTTCCAGC	−12.10
51,986	Rnamotif	–	CCTCCTGAATCGCGCGCCAGATGGCGCGCTTCTGGTTCGGG	−15.60
61,154	Both	+	GGCTGAGACTTCCCCGGCGCGAGCCGGGGTTTTTTATGCCG	−16.40

Rho-independent terminators were identified using the ARNold [336–338] program and putative terminators with a ΔG value of −9 kcal/mol or less were retained. DNA predicted to form the loop in the RNA is in red, and DNA predicted to encode an RNA stem is blue.

DNA Replication, Repair, and Regulation Module

JC1 has at least 7 proteins involved in DNA replication, repair, and regulation spanning genes 5 through 21 (Table 3-5, Figure 3-4). Putative functions determined via BLASTp include RecT/RecB (gp 5/6), which may aid in phage recombination events, a transcriptional regulator (gp8), a single stranded DNA binding protein (gp11), a helicase (gp19), a replication initiator protein (gp20), and a DnaC-like helicase loader (gp21) (Table 3-5, Figure 3-4). An interesting hypothetical protein in this module is gp18, which is present in each Bcep22-like phage at the beginning of the gene cluster containing the replication initiator protein and the DnaC-like helicase loading protein. This protein has a predicted helix-turn-helix domain and likely binds to DNA (Table 3-7); though its function is unknown, the conserved sequence location and high percent identity (>77% to each homolog) suggests it may have an important role in DNA replication.

Table 3-7: The conserved domains found in the 76 gene products of JC1.

Gp	Hit Type	PSSM-ID	Interval	E-Value	Accession	Short Name	Superfamily
1	specific	238206	9–159	1.68×10^{-24}	cd00338	Ser_Recombinase	cl02788
5	superfamily	413988	31–245	2.47×10^{-48}	cl04285	RecT superfamily	-

6	superfamily	415607	14–168	6.92×10^{-17}	cl09232	YqaJ superfamily	-
7	specific	238045	11–63	1.31×10^{-5}	cd00093	HTH_XRE	cl22854
10	superfamily	413281	20–268	2.41×10^{-72}	cl02338	DUF2303 superfamily	-
14	superfamily	377777	34–98	6.08×10^{-8}	cl06229	DUF1364 superfamily	-
18	specific	404897	5–74	3.76×10^{-19}	pfam14090	HTH_39	cl16606
19	specific	214947	15–88	3.71×10^{-19}	smart00974	T5orf172	cl15257
20	superfamily	237940	106–141	2.12×10^{-3}	cl36477	PRK15313 superfamily	-
21	superfamily	422963	72–263	1.95×10^{-39}	cl38936	P-loop_NTPase superfamily	-
30	specific	397583	19–236	7.93×10^{-24}	pfam03592	Terminase_2	cl01513
38	superfamily	416328	2–120	1.32×10^{-21}	cl11584	DUF2591 superfamily	-
40	superfamily	404162	3–86	7.90×10^{-21}	cl16173	DUF4031 superfamily	-
41	specific	402478	1–125	6.70×10^{-48}	pfam10908	DUF2778	cl12489
43	superfamily	222858	51–252	3.53×10^{-09}	cl28557	17 superfamily	-
45	superfamily	293119	57–616	9.79×10^{-10}	cl24922	P22_portal superfamily	-
45	superfamily	135173	668–765	8.02×10^{-5}	cl31366	PRK04654 superfamily	-
47	specific	396934	1–44	7.10×10^{-8}	pfam02599	CsrA	cl00670
48	specific	404189	39–358	8.21×10^{-100}	pfam13252	DUF4043	cl22542
53	superfamily	412204	29–130	4.16×10^{-3}	cl00184	CAS_like superfamily	-
57	specific	404724	255–306	3.00×10^{-13}	pfam13884	Peptidase_S74	cl16452
59	specific	404724	248–304	2.58×10^{-12}	pfam13884	Peptidase_S74	cl16452
63	specific	224584	9–134	6.86×10^{-4}	COG1670	RimL	cl34333
65	specific	238846	10–181	5.36×10^{-24}	cd01713	PAPS_reductase	cl00292
68	superfamily	180240	299–400	9.02×10^{-7}	cl32090	PRK05759 superfamily	-
69	superfamily	226993	1810–2677	6.59×10^{-99}	cl18793	COG4646 superfamily	
69	specific	408627	4195–4401	1.56×10^{-36}	pfam18857	LPD38	cl40138
69	specific	408569	3170–3270	9.95×10^{-19}	pfam18798	LPD3	cl40093
69	specific	381594	80–192	7.10×10^{-14}	cd00254	LT-like	cl00222
69	specific	223897	1537–1783	3.77×10^{-11}	COG0827	YtxK	cl28092
69	superfamily	237171	1358–1500	3.31×10^{-7}	cl36163	PRK12678 superfamily	-
69	superfamily	223627	2412–2868	2.48×10^{-5}	cl33945	HepA superfamily	-
69	superfamily	235334	1071–1287	1.59×10^{-3}	cl35279	PRK05035 superfamily	-
72	specific	406481	24–103	3.77×10^{-16}	pfam16083	Phage_holin_3_3	cl24062
74	superfamily	226439	2–186	2.17×10^{-28}	cl34694	ZliS superfamily	-
75	superfamily	419854	54–163	2.39×10^{-10}	cl22701	Phage_lysis superfamily	-

JC1 follows a trend observed in Gram-negative phages where the recombination genes (gp5/6) are located between the repressor and the integrase genes (gp1/gp7) [339]. Interestingly, unlike Bcep22, BcepIL02, DC1, and BcepMigl, JC1 encodes a putative helicase protein (gp19) predicted both by BLASTp and conserved domain search results (Table 3-5, Table 3-7). Furthermore, it does not follow the typical organization of an initiator-helicase loader-helicase (ILH-type) replication module seen in other phage, where the helicase protein is downstream of

the replication initiator protein and the helicase loading protein [339]. Instead, the helicase protein is encoded upstream of the initiator protein, making it a helicase-initiator-helicase loader (HIL) replication module. This organization is also seen in the *B. multivorans* prophage discussed above, but whether this is a common module organization or unique to these phages is unknown and requires an in-depth evaluation of other phage genomes.

Virion Morphogenesis Module

The virion morphogenesis module takes up over half of the genome, is composed of at least 19 predicted proteins spanning from gp30 to gp69 and is encoded entirely on the positive strand (Figure 3-4). BLASTp, conserved domain search, and homology to other phages were used to putatively assign functions for these proteins and include a small and large terminase subunit (gp30 and gp43, respectively), a portal protein (gp45), a major capsid protein (gp48), three virion associated proteins (gp49, gp53, gp55, and gp67), three tail fiber proteins (gp56, gp57, gp59), a head closure protein (gp61), and a DarB-like antirestriction protein (gp69) (Table 3-5, Table 3-7). The end of this module is marked by two hypothetical genes on the reverse strand, and as discussed above, are highly conserved among the Bcep22-like phages.
Similar to Bcep22 and BcepIl02, the terminase small subunit is located a significant distance away from the terminase large subunit, contrasting what is seen in lambdoid phage and many other Bcc phage genomes [340–346]. BcepB1A is a *Myoviridae* phage that displays a degree of mosaicism to the *Lessievirus* phages and exhibits the larger distance between the two terminase subunits [347], suggesting this organization is not distinct to *Lessieviruses*. Conclusive with comparisons done by Gill et al. (2011), the terminase large subunit in JC1 is also related to the *terL* homologs in *Pseudomonas aeruginosa* phage F116 (YP_164303.1) and *Sinorhizobium* phage PBC5 (YP_010115347.1), and the putative portal protein, major capsid protein, and head

closure protein all have homology to *E. coli* phage 933W (NP_049512.1, NP_049514.1, NP_049522.1). These genomic similarities paired with JC1 being a terminally redundant circularly permuted genome suggests that phage in this group likely package their genomes via a headful mechanism.

The DarB-like antirestriction protein takes up a massive portion of the virion morphogenesis module (32.7%) and 22.1% of the whole phage genome. This protein is most similar to the DarB homolog in Bcep22 (gp75) and is also commonly found in many *Ralstonia* phages. *E. coli* phage P1 requires virion-associated proteins DarA and DarB to protect P1 DNA from restriction by the host type I restriction system [348], and as discussed previously likely provide a significant benefit to the Bcep22-like phages given the extra burden the size of these genes impose [332]. Interestingly, the P1 antirestriction system has been shown to require additional proteins, including DdrA, DdrB, Hdf, and Ulx [349]. No homologs of any of these other proteins have been identified in the *Lessieviruses* thus far, however there are a significant number of virion-associated proteins with no known function and therefore it is likely homologs of these genes exist.

Lysis Module

The lysis module is a collection of 5 genes (gp72–gp76); surprising given the lysis modules of the other four phages contain the typical SRRzRz1 lysis organization [332,333,350]. The module begins with two predicted holin genes and a lysozyme (gp72–gp74). The LydA-like holin (gp72) has a conserved Phage_holin_3_3 domain, and TMHMM predicts the protein to have two transmembrane domains, classifying it as a superfamily III, family 34 holin [351]. The stop codon of gp72 overlaps with the start codon of gp73, similar to how *lydA* and *lydB* are organized in coliphage P1 [352]. However, unlike P1 LydB, gp73 is predicted to have two

transmembrane domains. This is unusual as antiholins of class I and II holins typically display a dual-start motif or have been seen to be coded completely within the holin gene [353,354]. With that said, many *Streptococcus* phage encode a class I and class II holin (respectively) upstream of an endolysin, and it is likely the second holin gene acts as an antiholin [355]. The third gene in this module is a predicted lysozyme (gp74) with a conserved ZliS superfamily domain. These enzymes hydrolyze the β1,4-glycosidic bond in peptidoglycan, and gp72–gp74 are found in a similar organization as some Type X Secretion Systems (TXSS): two holins preceding a ZliS superfamily muramidase [167,356].

The top BLASTp hits for gp72–gp74 do not involve any *Burkholderia Podoviridae* phages. The LydA-like holin (gp72) is homologous to uncultured *Caudovirales* phages, and *Siphoviridae* phages from *Nitratiruptor*, *Psychrobacter*, and *Moraxella* species. Similarly, the second holin gene (gp73) is most related to *Siphoviridae* phage AH2 and *Myoviridae* phage PE067. Continuing the trend, the top BLASTp hit for the lysozyme (gp74) is to a *Rhodoferax* podovirus, and the rest of the top hits are to *Siphoviridae* phages. The overall identity is on the lower end, ranging between 50–65% over 80 to 95% of the query, and the evolutionary origin of these three genes is unknown.

The lysis module of JC1 is homologous to the two spanin subunits found in all the other *Lessievirus* phages. The Rz and Rz1 proteins (gp75 and gp76, respectively) also belong to the embedded class of Rz1 genes, where the entire coding sequence of Rz1 is found within the coding sequence of Rz [332,350]. Rz (gp75) is predicted to have an N-terminal transmembrane domain (TMD) and SignalP analysis of Rz1 (gp76) predicts a lipoprotein signal peptide (Sec/SPII) with a cleavage site between amino acids 19 and 20, resulting in a final processed protein of 54 amino acids [322,323].

The lysis module of JC1 differs in the mode of lysis from the rest of the phages in the *Lessieviruses* genus, an interesting feature considering how similar the genomes are to one another. The other *Lessieviruses* likely lyse cells using pinholins and SAR endolysins [332], while JC1 likely lyses cells using the canonical holin mechanism. Though Lynch et al. [333] has predicted gp68 in DC1 (homolog of gp70 in JC1) to be a putative antiholin based on the TMHMM prediction of a single transmembrane domain (also predicted in all the *Lessieviruses* homologues), it is likely this protein plays a different role after analysis of the JC1 lysis module. It has been suggested that pinholins are an intermediate stage in the evolution of holin-endolysin systems, with the canonical holins having a selective advantage [357]. Therefore, this mechanistic difference in lysis may potentially play a role in the larger host range exhibited by JC1, but further studies are needed to examine the lysis potential of these modules.

Moron Genes

The genome of JC1 harbours three interesting moron genes, a carbon storage regulator (CsrA), an N-acetyltransferase, and a phosphoadenosine phosphosulfate (PAPS) reductase (gp47, gp63, and gp65, respectively). All three of these genes are present in the *Lessieviruses*, in similar locations and with high percent identity between homologues. CsrA has been associated with a massive array of functions in bacteria, including but not limited to carbon metabolism, virulence, motility, and biofilm formation [358]. Gp63 has a conserved RimL domain, involved in acetylating the ribosomal L12 protein [359]. N-acetyltransferases have been proposed to be evolutionary precursors of the eukaryotic histone acetyltransferases [360], and therefore the N-acetyltransferase encoded by JC1 may play a role in modifying gene regulation. PAPS reductases are a class of sulfonucleotide reductases (SRs) that are involved in catalyzing the reduction of adenylated sulfate to sulfite, a crucial step in the cysteine biosynthesis pathway [361]. PAPS reductases are

found in pathogenic bacteria such as *E. coli*, *Salmonella typhimurium*, and *Yersinia pestis* and are not found in humans, making this class of protein interesting as potential targets for therapeutic intervention [361]. The JC1 PAPS reductase (gp65) likely plays a role in sulfate reduction and could play a role in increasing the pathogenicity of its host. Further experiments are needed to investigate the functions these moron genes play in the infection cycle of JC1 and the other *Lessieviruses*.

Analysis of JC1 Structural Proteins

We performed proteomic analysis on CsCl purified virions to identify any unknown virion-associated proteins and confirm predicted virion-associated proteins. Proteins determined to be virion-associated are listed in Table 3-8 and include the portal protein (gp45), the carbon storage regulator (CsrA) (gp47), the major capsid protein (gp48), the head closure protein (gp61), four virion-associated proteins (gp49, gp53, gp55, and gp67), six hypothetical proteins (gp10, gp46, gp51, gp52, gp64, and gp68), and the DarB-like antirestriction protein (gp69). As expected, the most abundant protein identified was the major capsid protein. The six hypothetical proteins have been assigned putative functions as virion-associated proteins in Table 3-5, though their functions beyond that are unknown.

Table 3-8: Proteins determined to be virion-associated by proteomic analysis of CsCl-purified JC1 virions.

Protein	Score	Coverage	Unique Peptides (#)	Putative Function
gp48	298.44	56.04	27	Major capsid protein
gp69	88.92	15.61	51	DarB-like antirestriction protein
gp49	82.92	50.32	6	Virion-associated protein
gp64	45.94	45.18	9	Hypothetical protein
gp53	30.63	58.99	5	Virion-associated protein
gp68	27.46	17.06	9	Hypothetical Protein
gp45	25.85	22.22	14	Portal protein
gp56	22.88	41.14	7	Tail fiber protein
gp52	19.47	46.41	8	Hypothetical protein
gp61	16.01	11.21	6	Virion-associated phage protein
gp10	13.4	21.56	5	Hypothetical protein

gp55	13.16	48.91	4	Virion-associated phage protein
gp51	12.97	25.58	5	Hypothetical protein
gp67	9.35	42.86	7	Virion-associated phage protein
gp46	4.14	13.82	4	Hypothetical protein
gp47	2.61	18.75	1	Carbon storage regulator

Interestingly, gp62 did not show up in the mass spectrometry data even though it is predicted to be virion associated. Mass spectrometry analysis done by Gill et al. (2011) did not identify gp68 in Bcep22 (a homolog of JC1 gp62) as virion-associated, but it was predicted to be virion-associated because the homolog was identified in BcepIl02 (gp64). Given that this protein was not identified by mass spectrometry for Bcep22 or JC1, it seems likely that this protein is not virion-associated for these two phages. Reasoning for the exclusion of this protein in Bcep22 and JC1 is purely speculative but could be associated with the number of tail fiber genes each phage encodes, as BcepIL02 has 4 tail fiber genes whereas JC1 and Bcep22 have three. Mass spectrometry analysis would need to be conducted on DC1 and BcepMigl for further insights. The carbon storage regulator protein (CsrA) was identified by mass spectrometry, but only one unique peptide was associated with it, and therefore though it is likely to be virion associated it cannot be definitively confirmed. No proteins were identified when the spectrometry data was screened against the UniProt *Burkholderia* database, suggesting this protein is not a result of bacterial protein contamination. Inclusion of CsrA in the actual virion is an interesting and exciting possibility, showing that it is not only a moron gene, but is providing an unknown benefit to the phage. Further experiments are necessary to explore the role of CsrA in infection, and if it is virion-associated in the other *Lessieviruses*.

An unexpected finding is that the hypothetical protein gp10 is virion associated. This protein has a conserved DUF2303 superfamily domain; homologs of this gene are in BcepIL02, BcepMigl, and DC1, but no homolog was found in Bcep22. The predicted structure of gp10

using Phyre2 shows similarity to a viral genome injection device from *Lactococcus* phage TP901-1 (90.4% confidence, 16% identity), a cytosolic disulfide reductase (DsbM) from *Pseudomonas aeruginosa* (49.3% confidence, 16% identity), and a *Citrobacter* restriction-modification controller protein (38.4% confidence, 20% identity). Given that gp10 is located in the replication and repair module, it is possible that this protein is associating with the DNA and not the actual structure of the virion. Gp10 could be similar in function to gp2 in T4 coliphage, associating with the ends of the DNA and protecting it from exonuclease activity [362,363].

Integration Site Characterization

The presence of lysogeny genes gp1 and gp7 led us to examine the potential of JC1 to form lysogens in Van1. Phage infection survivors that were superinfection resistant and had the presence of the JC1 genome verified using PCR were collected for further examination. Of the four previously characterized Bcc *Podoviridae* phages, one is obligately lytic and the others form unstable lysogens in the bacterial hosts tested [332,333,340]. Stability was tested and showed that lysogens maintained superinfection resistance and the presence of JC1 genome after three sequential platings, suggesting JC1 can stably lysogenize Van1. Genomic and plasmid DNA were isolated from four different JC1 lysogen isolates and wildtype Van1 and analyzed on an agarose gel. No significant differences were observed between the strains on the gels, suggesting JC1 likely is not taking the form of a phagemid (data not shown).

To identify the Van1 genome location where JC1 is integrating, we used a protocol from Williams et al. (2013). We determined that JC1 integrates into the 5′ end of the conserved gene *rimO* using an 18 bp *attP* overlapping region with 1 bp difference in the *attB* site (Figure 3-7). RimO belongs to the methylthiotransferase (MTTase) family of proteins and is involved in β-methylthiolation of residue D88 of the ribosomal S12 protein [364]. To further support these

findings, the prophage found in the four *B. multivorans* genomes discussed in the genomic characterization section is also located directly next to *rimO,* with part of its integrase gene overlapping with *rimO*. Since JC1 integration disrupts the sequence of *rimO* so early into the coding region, loss of function seemed likely. However, with closer examination of the region an ATG is found 15 bp upstream of the *attP* site in the JC1 genome that allows RimO in Van1 to remain in frame while only changing 6 of the first 10 amino acids, and no change to the overall length of the protein (Figure 3-8). It is possible that the amino acid changes or the phage DNA upstream of the start site could affect the expression or function of RimO, but highly conserved amino acids identified in the N-terminal region among the MTTase family are not affected by JC1 integration [364], and we predict RimO likely remains functional.

GTAGGGTTCGtatccctcggctgcccgaGAGATATCGG	*attL*
ATAGGTATAGtatccctcgggtgcccgaGAGATATCGG	virion
ATAGGTATAGtatccctcgggtgcccgaAAGCGCTCGT	*attR*

Figure 3-7: Sequence of JC1 *attP* overlap region in *Burkholderia cenocepacia* strain Van1. The 18 bp overlapping sequence present in *attL* and *attR* of the JC1 prophage and in the chromosome of the phage (virion) is lowercase. JC1 *attP* site is located 41 bp upstream of gp1, a predicted serine recombinase. The 1 bp difference between the *attB* site is underlined.

```
Van1        MSQSPKVGFVSLGCPKALVDSEQIITQLRAEGYEISGTYDGADLVVVNTCGFIDEAVQES      60
Lysogen     MSKKYSIGIVSLGCPKALVDSEQIITQLRAEGYEISGTYDGADLVVVNTCGFIDEAVQES      60
            **:. .:*:**************************************************

Van1        LDAIGEALTENGKVIVTGCLGAKSSASGSNLIEEVHPKVLAVTGPHAVGEVMQAVHSHLP      120
Lysogen     LDAIGEALTENGKVIVTGCLGAKSSASGSNLIEEVHPKVLAVTGPHAVGEVMQAVHSHLP      120
            ************************************************************

Van1        KPHDPFVDLVPAAGIKLTPRHYAYLKISEGCNHRCTFCIIPSMRGDLVSRPVAEVMLEAE      180
Lysogen     KPHDPFVDLVPAAGIKLTPRHYAYLKISEGCNHRCTFCIIPSMRGDLVSRPVAEVMLEAE      180
            ************************************************************

Van1        NLFKSGVKELLVISQDTSAYGVDVKYRTGFWNGKPIKTRMTDLVAALGELAAQYGAWVRL      240
Lysogen     NLFKSGVKELLVISQDTSAYGVDVKYRTGFWNGKPIKTRMTDLVAALGELAAQYGAWVRL      240
            ************************************************************

Van1        HYVYPYPSVDEVIPLMAEGPFKGHVLPYLDVPFQHAHPEVLKRMKRPANAEKVLERVQKW      300
Lysogen     HYVYPYPSVDEVIPLMAEGPFKGHVLPYLDVPFQHAHPEVLKRMKRPANAEKVLERVQKW      300
            ************************************************************

Van1        REICPDLTIRSTFIAGFPGETEEQFETLLDFVREAELDRVGCFAYSPVEGATANDLDGAL      360
Lysogen     REICPDLTIRSTFIAGFPGETEEQFETLLDFVREAELDRVGCFAYSPVEGATANDLDGAL      360
            ************************************************************

Van1        PDEVREERRARFMEVAEEVSANRMQRKVGKTLKVLIDEVGEEGGIGRTAADAPEIDGVVY      420
Lysogen     PDEVREERRARFMEVAEEVSANRMQRKVGKTLKVLIDEVGEEGGIGRTAADAPEIDGVVY      420
            ************************************************************

Van1        VEPAAKASKRYKVGDFVSVKITGADGHDLWGEV  453
Lysogen     VEPAAKASKRYKVGDFVSVKITGADGHDLWGEV  453
            *********************************
```

Figure 3-8: RimO protein sequence of Van1 versus JC1 lysogen. Asterisk (*) represents identical amino acids; semicolon (:) represents strongly similar properties between amino acids; period (.) represents weakly similar properties between amino acids.

Previous studies have found increased resistance when residues around D88 of the S12 ribosomal protein are mutated [365], but similar to previous studies examining *rimO* knockout mutants [364,366], we saw no difference in streptomycin resistance between the JC1 lysogen and wildtype Van1 (data not shown). Since we do not know if or how activity of RimO is affected by JC1 integration, this data only confirms that resistance to streptomycin is not altered by JC1 integration. This is the first account of stable integration identified for the Bcep22-like phages, and it is possible that other members of this phage group may integrate next to *rimO* in an appropriate host. As briefly noted above, Bcep22, BcepIL02, and DC1 have not had successful attempts to isolate stable lysogens in host strains *B. cenocepacia* PC184 and AU1054 [332,333]. This could be due to several reasons, including a non-functional recombinase or bacterial strain

incompatibility. Additionally, none of the other phages harbour the *attP* site that JC1 contains, and therefore their *attP* sites and integration locations may be different (or non-existent) than that of JC1.

Virulence Index of JC1

In addition to the qualitative observations done in this study we decided to provide a quantitative measure of JC1 virulence against its host strain. As mentioned by Storms et al. (2020), characterizing novel phage tends to focus on non-standardized methods when looking at phage virulence. Troubleshooting in the lab to get high titer JC1 stocks (~10^{10} PFU/mL) led us to discover JC1 propagates to a higher titer at 30 °C as opposed to 37 °C; an interesting discovery given the delay it takes for JC1 to form plaques at 30 °C as mentioned above. This discrepancy led us to look at the virulence index for JC1 at 30 °C and 37 °C (Figure 3-9). The most effective MOI at 30 °C was 1000, though a significant amount of outgrowth occurred at this MOI, leaving MOIs 100 and 10 being the most effective at the 48-h endpoint (Figure 3-9A). As expected, the least effective MOI at 30 °C was 0.001, almost matching the growth of the bacterial control. Surprisingly, the least effective MOI at 30 °C (MOI 0.001) reduces the most growth by the 48-h endpoint at 37 °C and the highest MOI of 1000 had the most outgrowth, almost reaching bacterial control levels at 48 h (Figure 3-9B).

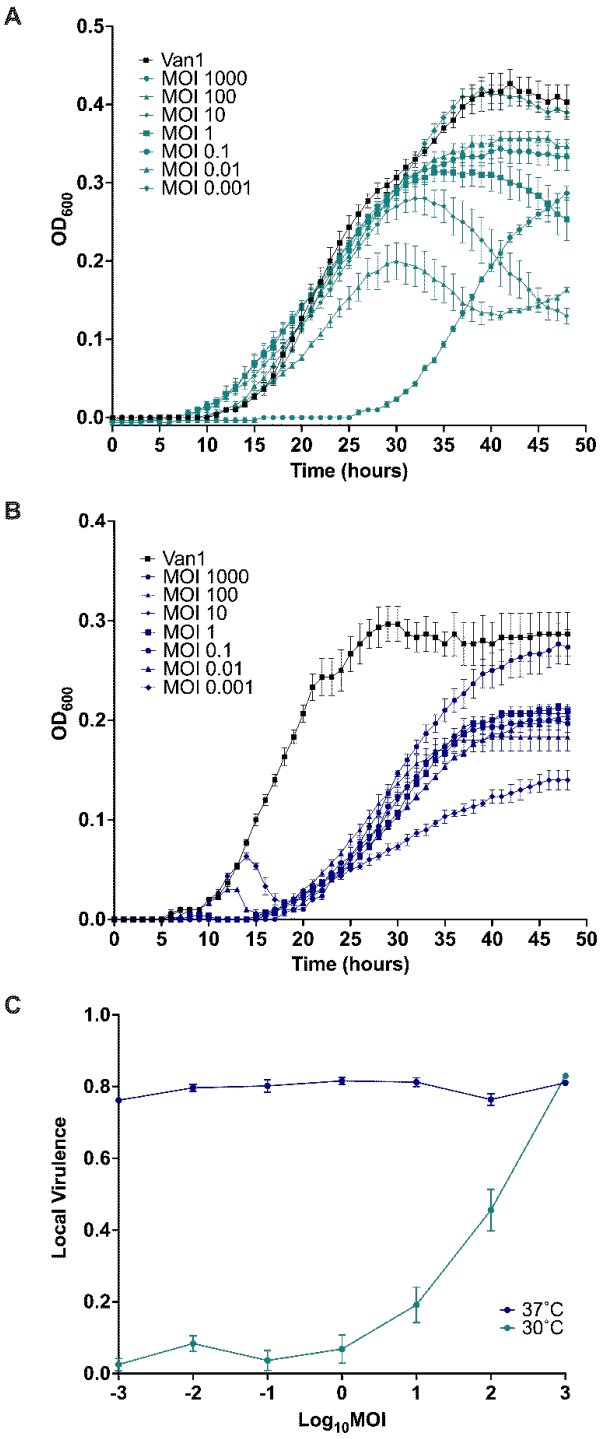

Figure 3-9: Virulence of JC1 against *Burkholderia cenocepacia* Van1 at (A) 30 °C versus (B) 37 °C. Kill curves were measured every hour for 48 h. (**C**) Virulence curves of JC1 at 30 °C and 37 °C were calculated by dividing the area under the curve for each MOI by the area under the curve of the bacterial control and subtracting that from 1. A virulence index of 0 to 1 signifies a complete absence of virulence to a theoretical maximum virulence, respectively. All error bars represent the standard error of the mean (SEM). Data from three biological replicates is shown.

Using the equations from Storms et al. (2020), the area under the curve for each MOI was calculated from time point 0 to the onset of stationary phase in the bacterial control. Time points 0–40 h and 0–30 h were used to calculate the local virulence for each MOI (log MOI −3 to 3) at 30 °C and 37 °C, respectively. JC1's local virulence at each MOI for both temperatures were plotted (Figure 3-9C) and the global virulence index is 0.21 and 0.8 at 30 °C and 37 °C, respectively. JC1 activity against Van1 seems mostly unaffected by MOI at 37 °C, maintaining a virulence above 0.75 for every MOI tested. JC1's global virulence index at 37 °C is more comparable to lytic *E. coli* phage T7 (0.84) than to lysogenic *E. coli* phage T5 (0.17) [367]. It is important to note that a different range of MOIs were used to test these phages (log MOI −7 to 0), and comparisons can only be made at similar MOIs. With that said, local virulence for T5 does not begin to match the level of virulence seen with JC1 at 37 °C until an MOI of 1 [367]. These similarities are the opposite when we look at virulence for 30 °C, where the curve and global virulence index is less virulent than T5 at comparable MOIs [367]. These results suggest that JC1 could be acting more lytic at 37 °C and more lysogenic at 30 °C. Furthermore, these results explain why JC1 reaches a higher titer when propagated at 30 °C, as a lower virulence is useful when propagating phage to high titer because the bacterial population is not reduced completely, and the phage have sufficient host cells to propagate on.

The cause of this surprising discrepancy in virulence at different temperatures is unknown but could potentially be due to a temperature sensitive switch between lytic and lysogenic lifestyle similar to podophage ØBp-AMP1 [368]. However, no bacterial lysis is seen when overlays of the JC1 lysogen are incubated at 30 °C or 37 °C (data not shown), suggesting a temperature switch may not be the cause of this discrepancy in virulence. Furthermore, infection efficiency and lysogen stability are not affected by a change in temperature (data not shown),

though this does not rule out the chance JC1 lysogenizes at a higher rate at 30 °C. It is also possible that the difference in virulence is an effect of the bacterial growth rate, as Van1 grows slower but to an overall higher density at 30 °C, and grows faster but to an overall lower density at 37 °C. Further experiments are required to determine the cause of this shift in virulence seen at 30 °C and 37 °C.

Lysogenic Conversion

One of the main reasons lytic phages are favoured for therapy is they cannot alter bacterial virulence with phage gene expression [369,370]. *Burkholderia* phages tend not to encode recognizable toxins or virulence factors but are known to encode proteins that can contribute to overall fitness [371]. Given the lack of obvious toxins/virulence factors, the significant number of hypothetical gene products with no predicted function, and the presence of moron genes involved in nutrient acquisition like *csrA*, an N-actyltransferase, and a PAPS reductase, we hypothesized JC1 may offer its host cell a growth advantage.

Examining the growth of the lysogen verses wildtype Van1 in three different rich mediums showed a difference in growth between the two strains (Figure 3-10A–C). The lysogen exhibited moderately increased growth after 48 h in MH and TSB liquid medias while exhibiting a slight decrease in growth in LB liquid media. A statistically significant difference in growth was observed between the lysogen and wildtype Van1 at 15–18 and 23–48 h when grown in LB ($p < 0.05$), at 30–33 h when grown in MH ($p < 0.05$), and at 19–24 h when grown in TSB ($p < 0.05$; $p < 0.01$; $p < 0.001$; $p < 0.0001$). To further examine the difference in growth we calculated the growth rate during log phase for each strain in each medium (Figure 3-10D–F); since the bacteria reach stationary phase at different time points in each media, the time points analyzed vary. A statistically significant difference in growth rate is observed between 25 and 30 h in MH

($p < 0.05$), further supporting the increase in growth exhibited by the lysogen at this time interval (Figure 3-10B,E). Overall, growth rate is not substantially affected in LB or TSB media, which is clear in the similar shapes of the curves for each strain in each media (Figure 3-10A,C,D,F). The largest difference in growth in LB and TSB begins when the bacterial growth is beginning to slow, resulting in lower growth rates that are closer together, even though the actual bacterial density is significantly different from one another (Figure 3-10A,C,D,F).

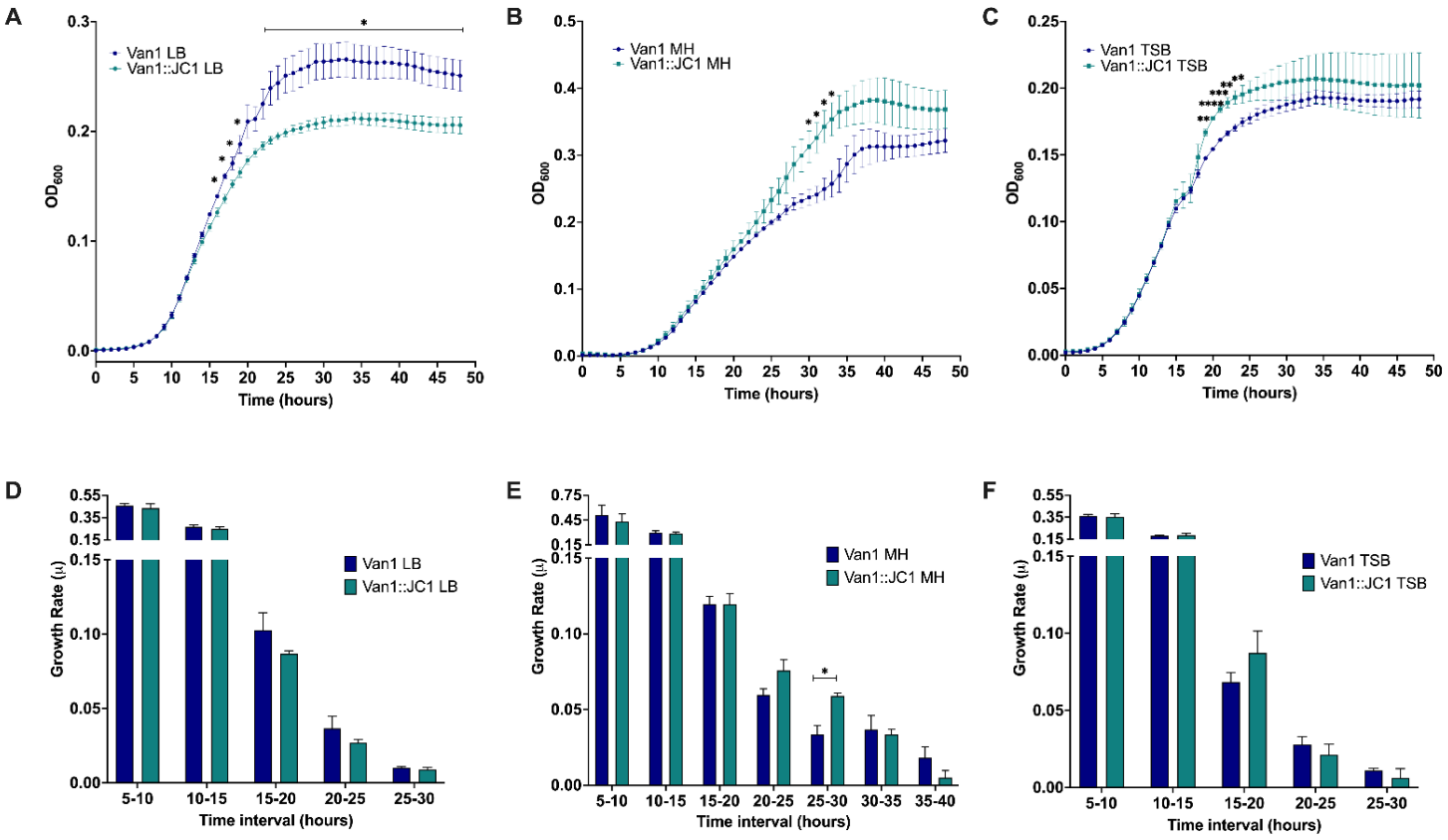

Figure 3-10: Growth comparison of Van1 versus Van1::JC1 lysogen. (**A**–**C**) Growth curve analysis of wildtype Van1 and Van1::JC1 lysogen in either Luria Bertani (LB), Muller Hinton (MH), or tryptic soy broth (TSB) liquid media. Overnight cultures were subcultured 1:100 in LB for 2 h and 45 min and further diluted 1:100 to a CFU/mL of approximately 1×10^6 in the desired medium and measured every hour for 48 h. (**D**–**F**) Growth rate of curves in (**A**–**C**) were calculated using growth rate equation $\log_{10}N - \log_{10}N_0 = (\mu/2.303)\ (t - t_0)$. Statistical analysis was performed using unpaired *t*-tests (* $p < 0.05$; ** $p < 0.01$; *** $p < 0.001$; **** $p < 0.0001$). All error bars represent the standard error of the mean (SEM). Data from three biological replicates is shown.

Lysogenic conversion is not well studied in *Burkholderia* species, and when done so typically examines change in virulence [344,369]. Two significant reasons for the paucity of studies in this area are that many of the characterized *Burkholderia* phages have been isolated from lysogens and therefore lack a wildtype strain for comparison [290,341,346,371–374], and/or attempts to create stable lysogens in other strains were unsuccessful [332,333]. A third reason is that most phage characterization studies are done with intent of using the phages for therapy and therefore favour the idea of removing lysogeny genes as opposed to studying lysogenic conversion [346,369]. To our knowledge, growth rate differences have not been studied in any *Burkholderia* lysogens but have been observed in *Stenotrophomonas maltophilia* lysogenized by bacteriophage DLP3 [375] and by ϕ24B integration in *E. coli* B strain MC1061 [376]. The differences observed between the growth of the Van1::JC1 lysogen and wildtype Van1 in each media demonstrates potential differences in energy utilization or nutrient acquisition.

Conclusions

Aside from encoding a repressor and an integrase, and being able to stably lysogenize its host bacterium, phage JC1 possesses several characteristics that would make it ideal for use in phage therapy. For one, JC1 has a considerably broad host range, being able to infect many member species of the Bcc. Phage JC1 also requires the inner core of the LPS for infection, so bacteria that mutate to evade infection by eliminating their O-antigen, outer core, and inner core will likely develop a fitness disadvantage, as observed in previously characterized LPS mutants that lack the inner core [145,146]. Another favorable factor is the high level of virulence JC1 exhibits against host strain Van1 at 37 °C, which is comparable to virulence exhibited by lytic *E. coli* phage T7 at similar MOIs [367]. If the decrease in virulence at 30 °C is caused by an increased rate of lysogeny, then deletion of the genes responsible for lysogeny should increase the virulence

index of JC1 at 30 °C and would make JC1 more suitable for use in therapy. Further experiments examining these potential alterations to make JC1 a suitable candidate for phage therapy against the Bcc will be an impactful contribution to the fight against AMR infections.

Acknowledgments

The authors thank Arlene Oatway and Kacie Norton from the University of Alberta Department of Biological Sciences Advanced Microscopy Facility for assistance with TEM. The authors thank members of the Dennis and Tracy Raivio's labs for thoughtful and helpful discussions.

Chapter 4

Conclusions and future directions

Projects In Progress

Isolation and characterization of P2-like phage Carl1

Assembly of the JC1 sequencing reads resulted in two complete contigs, one representing JC1 and one with very low coverage spanning 37,418 bp, now known as Carl1. The two phage were separated from each other by spotting multiple JC1 lysates previously prepared by Jamie Cole on *B. cenocepacia* strains C6433, K56-2, and Van1. Single plaques were isolated using a sterile Pasteur pipette and suspended in 500 µL of SM. Primers specific to the genomes of Carl1 (CF: AGCAGCAACCTGAACATC, CR: GTCGTTGATGGGCTTCTG) and JC1 (2F: CTGCTTCTTCGATAGTGGTG, 2R: TCGGATTCCTCCTTCTCG) were used to PCR each isolated plaque until a plaque was identified that had a PCR band for only one phage. PCR was also performed on the genomes of each strain to check if JC1 or Carl1 existed as a stable prophage, but each genome resulted in a negative PCR.

Annotation of Carl1 was performed using three different annotation software: GLIMMER using the Bacteria and Archaea setting [318], Prodigal [319], and GeneMarkS for phage [320]. Related phages were identified using BLASTn and predicted protein-coding genes and putative functions were identified using BLASTp. BLASTp was set to the Bacteria database (taxid:2) when no significant hits were found using the Viruses database (taxid:10239). Hits with an E-value of 1×10^{-3} or greater were not considered significant, and annotations were recorded as hypothetical. NCBI non-redundant protein sequence and nucleotide collection databases (update date: 8 May 2022) were used. Conserved domains were identified using Batch CD-Search against the CDD v3.19 58235 PSSMs database with default settings [321]. TMHMM 2.0 [322], and SignalP 6.0 [323], were used to analyze lysis proteins and predict lipoproteins, respectively. Aragorn (Galaxy Version 0.6) [324] was used to identify potential tRNA genes. Rho-independent

terminators were predicted using ARNold [336–338]. Whole genome alignments and comparisons were done using clinker v1.32 [328]. The complete genome sequence of Carl1 was deposited in GenBank with the accession number ON642070.

TEM analysis indicates Carl1 is a *Myoviridae* with an A1 Morphotype (Figure 4-1) [331]. Carl1 has a capsid diameter of 61nm and a tail length of 121 nm. Carl1 was difficult to propagate to high titer and therefore the TEM image is low quality. Carl1 should be reimaged following CsCl purification of a high titer stock. The inner core of the LPS has preliminarily been identified as the receptor for Carl1 (Table 4-1), as it is unable to infect the same mutants as JC1 [377]. Adsorption against Van1 treated with either periodate or proteinase K should be performed to confirm the LPS is the receptor.

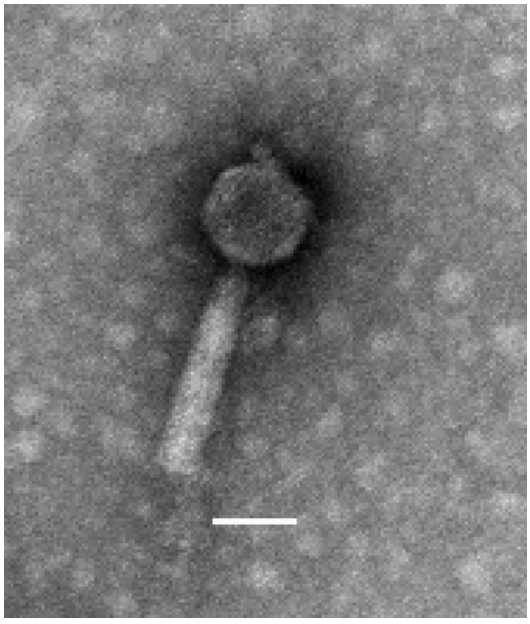

Figure 4-1: Transmission electron micrograph of Carl1. Lysate was stained with 4% uranyl acetate on a copper grid and viewed at 110,000× magnification with a transmission electron microscope. Measurements of 10 phage particles have an average capsid diameter of 61 nm and a tail length of 121 nm. Scale bars represent 50 nm.

Table 4-1: Carl1 receptor identification on *B. cenocepacia* K56-2 LPS mutants

Bacterial strain	Phenotype	Infection
K56-2	Wildtype LPS	+
SAL1	K56-2 *hldA*:: pSL5, Lacks inner and outer core	-
CCB1	K56-2 *waaC*::pGPΩTp, Lacks inner and outer core	-
XOA8	K56-2 *wabO*::pGPΩTp, Lacks inner and outer core	-
XOA7	K56-2 *waaL*::pGPΩTp, Lacks outer core	+
XOA15	K56-2 *wabR*::pGPΩTp, Lacks outer core	+
XOA17	K56-2 *wabS*::pGPΩTp, Lacks outer core	+
RSF19	K56-2 *wbxE*:: pRF201, Lacks O-antigen	+

The genome is 37, 418 bp with a G+C content of 64.6% (Figure 4-2) and is predicted to encode 50 proteins (Table 4-2). Analysis of the reads mapped to the assembled genome reveals Carl1 possesses 74 bp 5′ phosphoryl-terminal cohesive ends. The *cos* site is located downstream of the integrase gene (gp50), and the genome was oriented based on coliphage P2 (NC_001895). Of these 50 predicted proteins, many of them harbour conserved domains (Table 4-3), with only 17 being labelled hypothetical proteins with unknown function (Table 4-2). BLASTn analysis of Carl1 shows it has the most homology to *Myoviridae* phage KS5, a P2-like *Burkholderia cepacia* phage [346]. Carl1, along with many other P2-like *Burkholderia* phages have retained a significant degree of synteny to *E. coli* phage P2 [378,379] (Figure 4-3).

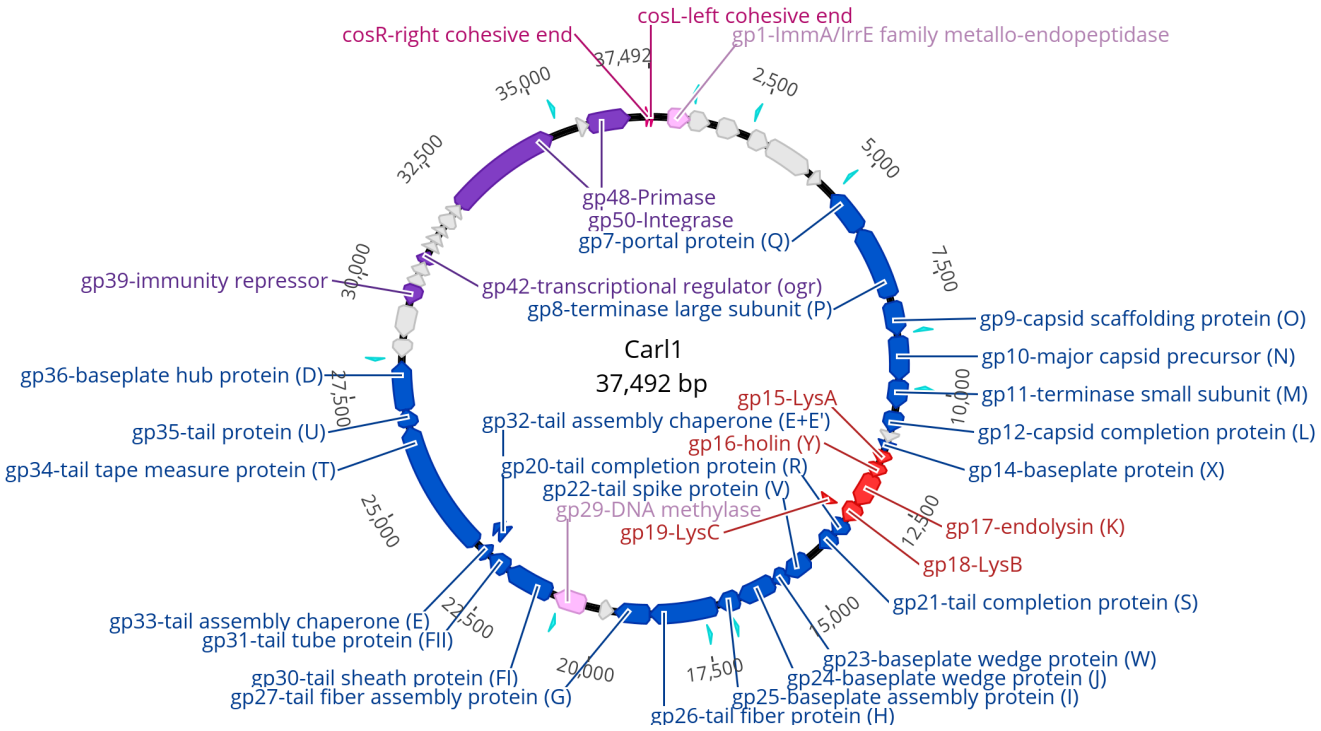

Figure 4-2: Circularized genomic map of Carl1. Scale (in bp) is shown on the outer periphery Assigned putative functions for each of the 50 predicted open reading frames are as follows: lysis (red), DNA replication and repair (purple), virion morphogenesis (blue), hypothetical (grey), moron genes (light pink), cos sites (pink). No tRNA genes were identified. Scale (in bp) is shown on the outer periphery. Carl1 has a GC content of 64.6%. Image created with Geneious Prime [380].

Table 4-2: Bacteriophage genome annotations for Carl1 obtained from BLASTp data.

Gene	Start	End	Strand	Length (aa)	Putative Function	BLASTp Hit	Species	Coverage (%)	E-Value	Identity (%)	Accession
1	422	937	+	171 aa	ImmA/IrrE family metallo-endopeptidase	hypothetical protein P2DC1_00041	*Peduovirus* P2	85	2×10^{-29}	42.21	CAG9593845.1
2	934	1449	+	171 aa	hypothetical protein	hypothetical protein	*Burkholderia multivorans*	100	3×10^{-96}	100	WP_155490662.1
3	1653	2189	+	178 aa	hypothetical protein	PAAR domain-containing protein	*Burkholderia phage* Menos	99	1×10^{-72}	73.18	YP_010109826.1
4	2456	2935	+	159 aa	hypothetical protein	hypothetical protein CPT_Menos_046	*Burkholderia phage* Menos	79	2×10^{-39}	56.25	UNY41820.1
5	2941	4089	+	382 aa	hypothetical protein	hypothetical protein CPT_Menos_047	*Burkholderia phage* Menos	96	0	68.75	UNY41821.1
6	4195	4494	+	99 aa	hypothetical protein	hypothetical protein	*Burkholderia cepacia* complex	89	2×10^{-46}	100	WP_081000735.1
7	5925	4873	–	350 aa	portal protein (Q)	portal protein	*Burkholderia* phage KS5	100	0	97.71	YP_004306410.1
8	7691	5925	–	588 aa	terminase large subunit (P)	terminase ATPase subunit family protein	*Burkholderia* phage KS5	100	0	98.98	YP_004306409.1
9	7841	8662	+	273 aa	capsid scaffolding protein (O)	GPO family capsid scaffolding protein	*Burkholderia* phage KS5	100	0	99.63	YP_004306408.1

10	8699	9724	+	341 aa	major capsid precursor (N)	major capsid protein, P2 family	*Burkholderia* phage KS5	96	0	99.39	YP_004306407.1
11	9721	10,407	+	228 aa	terminase small subunit (M)	terminase endonuclease subunit	*Burkholderia* phage KS5	100	6×10^{-160}	97.37	YP_004306406.1
12	10,511	10,987	+	158 aa	capsid completion protein (L)	head completion/stabilization protein	*Burkholderia* phage KS5	100	2×10^{-106}	97.47	YP_004306405.1
13	10,987	11,229	+	80 aa	hypothetical protein	gp37	*Burkholderia* phage KS5	100	7×10^{-29}	96.25	YP_004306404.1
14	11,229	11,441	+	70 aa	baseplate protein (X)	tail protein X	*Burkholderia* phage KS5	100	4×10^{-42}	98.57	YP_004306403.1
15	11,477	11,818	+	113 aa	LysA	holin family protein	*Burkholderia* phage KS5	100	2×10^{-70}	97.35	YP_004306402.1
16	11,818	12,138	+	106 aa	holin (Y)	holin family protein	*Burkholderia* phage KS5	83	9×10^{-33}	98.86	YP_004306401.1
17	12,131	12,931	+	266 aa	endolysin (K)	N-acetylmuramidase domain-containing protein	*Burkholderia* phage KS5	100	2×10^{-161}	91.35	YP_004306400.1
18	12,928	13,419	+	163 aa	LysB	gp32	*Burkholderia* phage KS5	100	7×10^{-77}	94.48	YP_004306398.1
19	13,178	13,372	+	64 aa	LysC	gp31	*Burkholderia* phage KS5	51	5×10^{-15}	100	YP_004306399.1
20	13,416	13,826	+	136 aa	tail completion protein (R)	tail protein	*Burkholderia phage* KS5	100	7×10^{-94}	96.32	YP_004306397.1
21	13,826	14,275	+	149 aa	tail completion protein (S)	virion morphogenesis protein	*Burkholderia phage* KS5	99	3×10^{-75}	90.54	YP_004306396.1
22	14,693	15,325	+	210 aa	tail spike protein (V)	baseplate assembly protein V	*Burkholderia phage* KS5	100	4×10^{-149}	99.05	YP_004306394.1
23	15,322	15,699	+	125 aa	baseplate protein (W)	GPW/gp25 family protein	*Burkholderia* phage KS5	92	1×10^{-63}	97.30	YP_004306393.1
24	15,696	16,601	+	301 aa	baseplate wedge protein (J)	baseplate J/gp47 family protein	*Burkholderia* phage AP3	100	0	93.02	YP_009785114.1
25	16,594	17,145	+	184 aa	baseplate wedge protein (I)	tail protein I	*Burkholderia* phage KS5	100	1×10^{-119}	91.30	YP_004306391.1
26	17,151	18,761	+	536 aa	tail fiber protein (H)	tail fiber protein	*Burkholderia* phage KS5	100	0	94.96	YP_004306390.1
27	18,771	19,607	+	278 aa	tail fiber assembly protein (G)	tail fiber assembly protein	*Burkholderia* phage KS5	92	4×10^{-175}	90.70	YP_004306389.1
28	19,956	19,654	-	101 aa	hypothetical protein	hypothetical protein	*Burkholderia multivorans*	100	7×10^{-70}	100	WP_223852571.1
29	20,368	21,117	+	249 aa	DNA methylase	site-specific DNA-methyltransferase	*Burkholderia* phage KS5	100	5×10^{-179}	96.79	YP_004306387.1
30	21,229	22,401	+	390 aa	tail sheath protein (F_I)	tail sheath protein	*Burkholderia* phage KS5	100	0	98.21	YP_004306386.1
31	22,431	22,940	+	169 aa	tail tube protein (F_{II})	major tail tube protein	*Burkholderia* phage KS5	100	3×10^{-120}	99.41	YP_004306385.1
32	22,973	23,403	+	143 aa	tail assembly chaperone (E+E')	gp17	*Burkholderia* phage KS5	100	4×10^{-95}	97.90	YP_004306383.1
33	22,973	23,284	+	103 aa	tail assembly chaperone (E)	tail assembly protein	*Burkholderia* phage KS5	100	2×10^{-64}	99.03	YP_004306384.1
34	23,400	26,651	+	1083 aa	tail tape measure protein (T)	gp17	*Burkholderia* phage KS5	82	0	86.82	YP_004306382.1
35	26,665	27,093	+	142 aa	tail tube initiator (U)	tail protein	*Burkholderia* phage KS5	100	2×10^{-99}	99.30	YP_004306381.1
36	27,090	28,235	+	381 aa	baseplate hub protein (D)	late control D family protein	*Burkholderia* phage KS5	99	0	98.68	YP_004306380.1
37	28,773	28,321	–	150 aa	hypothetical protein	TPA: MAG TPA: hypothetical protein	*Myoviridae* sp.	67	2×10^{-28}	50.50	DAY61748.1
38	29,572	28,826	–	248 aa	alpha/beta hydrolase	alpha/beta hydrolase	*Burkholderia* phage KS5	97	5×10^{-86}	64.61	YP_004306378.1

39	30,089	29,628	–	153 aa	immunity repressor	helix-turn-helix domain-containing protein	*Tigrvirus* phi52237	100	6×10^{-72}	80.39	YP_293722.1
40	30,122	30,409	+	95 aa	hypothetical protein	gp10	*Burkholderia* phage KS5	82	2×10^{-47}	97.44	YP_004306376.1
41	30,413	30,691	+	92 aa	hypothetical protein	gp9	*Burkholderia* phage KS5	100	6×10^{-62}	100	YP_004306375.1
42	30,701	30,949	+	82 aa	transcriptional regulator (ogr)	ogr/Delta-like zinc finger family protein	*Burkholderia* phage KS5	100	1×10^{-47}	89.02	YP_004306374.1
43	31,040	31,234	+	64 aa	hypothetical protein	gp7	*Burkholderia* phage KS5	100	3×10^{-36}	93.75	YP_004306373.1
44	31,239	31,442	+	67 aa	hypothetical protein	gp6	*Burkholderia* phage KS5	100	2×10^{-37}	98.51	YP_004306372.1
45	31,486	31,680	+	64 aa	hypothetical protein	hypothetical protein KNV21_gp42	*Burkholderia* phage Mana	100	6×10^{-24}	81.25	YP_010109814.1
46	31,685	32,044	+	119 aa	hypothetical protein	gp4	*Burkholderia* phage KS5	100	5×10^{-75}	93.28	YP_004306370.1
47	32,041	32,304	+	87 aa	hypothetical protein	gp3	*Burkholderia* phage KS5	87	4×10^{-33}	92.11	YP_004306369.1
48	32,307	35,099	+	930 aa	primase	toprim domain-containing protein	*Burkholderia* phage KS5	99	0	95.79	YP_004306368.1
49	35,779	36,009	+	76 aa	hypothetical protein	DUF4224 domain-containing protein	*Burkholderia* phage KL3	96	5×10^{-35}	82.19	YP_004306414.1
50	36,009	37,037	+	342 aa	tyrosine-type recombinase	tyrosine-type recombinase/integrase	*Burkholderia* phage KL3	100	0	96.78	YP_004306413.1

Table 4-3: The conserved domains found in the 50 gene products of Carl1.

Gp	Hit type	PSSM-ID	Interval	E-Value	Accession	Short name	Superfamily
1	superfamily	412729	42-169	1.15×10^{-22}	cl01076	Peptidase_M78 superfamily	–
3	specific	269829	4-82	2.51×10^{-32}	cd14744	PAAR_CT_2	cl21497
3	superfamily	413035	112-156	2.34×10^{-3}	cl01733	DUF2345 superfamily	–
5	superfamily	403171	136-348	1.15×10^{-56}	cl13337	DUF3396 superfamily	–
10	specific	398682	8-325	0	pfam05125	Phage_cap_P2	cl04947
13	superfamily	164914	2-79	1.18×10^{-8}	cl10430	PHA02417 superfamily	–
14	specific	283209	1-53	4.53×10^{-23}	pfam05489	Phage_tail_X	cl02088
15	superfamily	407159	2-110	2.88×10^{-24}	cl25205	Phage_holin_8 superfamil	–
16	specific	398877	20-84	3.8×10^{-7}	pfam05449	Phage_holin_3_7	cl05163
17	specific	403156	90-261	8.01×10^{-72}	pfam11860	Muraidase	cl13324
17	specific	225943	3-125	5.97×10^{-16}	COG3409	PGRP	cl34604
22	superfamily	418463	7-208	5.88×10^{-43}	cl17812	Phage_base_V superfamily	–
26	specific	400043	302-375	8.20×10^{-9}	pfam07484	Collar	cl26890
26	superfamily	222890	141-196	4.23×10^{-6}	cl33689	34 superfamily	–
26	superfamily	397817	197-301	1.52×10^{-5}	cl04319	Phage_T4_gp36 superfamily	–
30	specific	223931	4-242	8.99×10^{-34}	COG0863	YhdJ	cl17173
31	specific	164955	1-388	0	PHA02560	FI	cl01389
32	superfamily	412874	1-169	1.50×10^{-82}	cl01390	Phage_tube superfamily	–
36	specific	226030	1-136	4.20×10^{-65}	COG3499	COG3499	cl01391
37	superfamily	378982	32-147	7.22×10^{-17}	cl15130	tRNA_anti-like superfamily	–

39	specific	238045	5-61	4.06 x 10^{-8}	cd00093	HTH_XRE	cl22854
42	specific	398341	4-50	1.85 x 10^{-17}	pfam04606	Ogr_Delta	cl19592
48	superfamily	177362	1-930	0	cl26254	PHA02415 superfamily	–
49	specific	404807	4-48	1.01 x 10^{-15}	pfam13986	DUF4224	cl16521
50	superfamily	412227	181-335	1.53 x 10^{-38}	cl00213	DNA_BRE_C superfamily	–

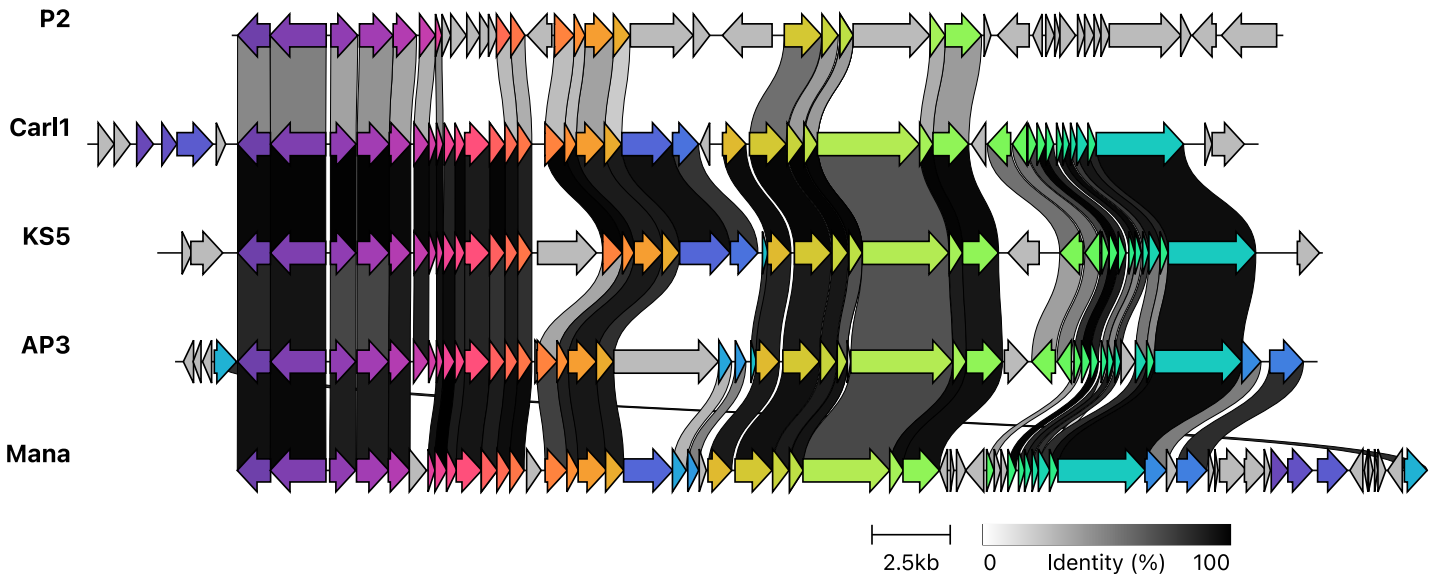

Figure 4-3: Clinker gene cluster comparison of Bcc P2-like phages and coliphage P2. Comparison of whole genomes for *Burkholderia* phage Carl1 against the other *Kisquinquevirus* phages KS5, AP3, and Mana and canonical coliphage P2. Percent amino acid identity is represented by greyscale links between genomes. Homologous proteins are assigned a unique color.

The 10 predicted Rho-independent termination sites are displayed in Table 4-3 and are located downstream of gp3 (primase), downstream of the gp14 (hypothetical protein), within but in the opposite direction gp23 (methylase), gp25 (tail fiber protein), gp27 (baseplate wedge protein), gp40 (small terminase subunit), gp42 (capsid scaffolding protein), and gp49 (hypothetical protein), downstream of gp44 (portal protein), and upstream of gp47 (hypothetical protein) in the opposite direction.

Table 4-4: Predicted Rho-independent terminators in Carl1. Rho-independent terminators were identified using the ARNold program and putative terminators with a ΔG value of -9 kcal/mol or less were retained, with some exceptions. DNA predicted to form the loop in the RNA is in red, and DNA predicted to encode an RNA stem is blue.

Start	Program	Strand	Sequence	-ΔG
2155	Rnamotif	–	ACGGAGCGGGGCCGCGCGGGCGGaTTTTTCCACAGG	-7.20
9187	Both	+	AGCGAACTGAAGCCCGCGATCGCGGGCTTTTTCGACGCA	-12.70
16545	Rnamotif	+	AGGCGCACGACTTCGCGCGCGAGCTGCGCGGGcTTTTCGGTCATG	-9.70
19998	Rnamotif	+	AAGCAGCAGCATCGCCGCTGGCGATTTTTCGAGAAT	-6.20
20621	Rnamotif	+	GCAGACTTCGCGCACGGCATCGGCCGTGCccTTTTTGCGCGCG	-13.70
27564	Rnamotif	+	GCGTCGTACGCCGGCAGGAACTGCCGTTTCAGTTCGGC	-8.90
28880	Rnamotif	+	TGCTGGCGGTCGCTGTCGGTGCGCGACAGCTTTTGCACCAGA	-12.50
32639	Both	+	GCAGACGACAAGCCGCCGGGCACTTCGGTGCCGGCGGCTTTTTTGCGTCTG	-18.10
35062	Rnamotif	+	GGGAGTCTTTTGTCCGGTTTCCTTTACCGACCGGGCgTTTTCGGAGTCA	-11.70
36480	Both	+	GAATCGGAAGAGGGAAGTCGTGTGACTTCCCTTTTCCCAGACG	-13.50

Future directions to characterize this phage should include extensive host range analysis on the 85 strains that JC1 was tested against and a one-step growth curve to determine important insights about infection cycle, such as burst size, latency period, and adsorption rate. Experiments to isolate a Carl1 lysogen should also be conducted and attempts to delete the lysogeny genes are recommended to make Carl1 more favourable for use in therapy.

Assembly of B. cenocepacia C6433 genome

B. cenocepacia strain C6433 is an epidemic strain isolated from Canadian CF patients [291] and has proven to be very useful in the lab. C6433 is particularly useful when it comes to phage research in our lab, as 8 out of our current 12 Bcc phages can infect this strain. The assembled genome of C6433 will be useful for future experiments examining host-phage relations. Furthermore, it will be a welcome contribution to Bcc genomic research, as these strains are quite complex consisting of multiple chromosomes and sometimes a plasmid [63,123,381]. Additionally, the impressive size of the Bcc, currently comprising 24 closely related species [77] could not have been deciphered without sequencing data of Bcc strains. In other words, as more sequencing data becomes available more species of the Bcc are discovered. An important limitation regarding sequencing data is that short next generation sequencing reads can show GC

biases, which causes uneven sequencing depth and can generate gaps in a draft genome [382–384]. This can prove to be problematic for assembling *Burkholderia* genomes because they have notoriously high GC content; that paired with their multi-chromosomal nature can make complete genomes difficult to assemble [123,385,386] especially if read coverage is affected.

Illumina paired-end DNA sequencing reads of the C6433 genome were assembled using SPAdes v3.13.0 32 resulting in 795 contigs. RagTag v2.1.0 [387] was used to perform homology-based assembly scaffolding against *B. cenocepacia* reference strains J2315 (NC_011000.1, NC_011001.1, NC_011002.1, NC_011003.1), 895 (NZ_CP015036.1, NZ_CP015037.1, NZ_CP015038.1), and VC2307 (NZ_CP019666.1, NZ_CP019664.1, NZ_CP019667.1, NZ_CP019665.1). These three strains were chosen because they were the top BLASTn hits against the partial assembly of C6433. Of the three strains, assembly against J2315 gave the best read coverage (though all three assemblies were >99%), and assembly against 895 reduced the total number of contigs to 107 (J2315 reduced them to 137 and VC2307 reduced them to 141) (Table 4-5). Based off these results, C6433 scaffolded against 895 was chosen as the best assembly.

Table 4-5: Ragtag scaffolded assemblies of *B. cenocepacia* C6433 against *B. cenocepacia* reference strains J2315, 895 and VC2307.

J2315	**Replicon**	**Avg fold**	**Length (bp)**	**Ref GC**	**Covered (%)**	**Read GC**
	Chr 1	22.7189	3,440,600	0.6720	99.2954	0.6512
	Chr 2	21.3163	3,139,555	0.6755	99.2474	0.6569
	Chr 3	19.6051	895,764	0.6744	99.2990	0.6564
	Plasmid	26.2649	61,503	0.6170	100.0000	0.6009
895	**Replicon**	**Avg fold**	**Length (bp)**	**Ref GC**	**Covered (%)**	**Read GC**
	Chr 1	22.1559	6650071	0.6733	99.2824	0.6531
	Chr 2	19.1278	1074343	0.6755	99.1770	0.6595
	Plasmid	26.2649	61503	0.6170	100.0000	0.6009
VC2307	**Replicon**	**Avg fold**	**Length (bp)**	**Ref GC**	**Covered (%)**	**Read GC**
	Chr 1	18.4943	869423	0.6794	99.1445	0.6629
	Chr 2	22.9336	5581278	0.6721	99.3232	0.6518
	Plasmid	19.1360	1074343	0.6775	99.1840	0.6595

The reads of C6433 have GC contents around 63-65% (Table 4-5), slightly lower than the 66-67% GC of most *B. cenocepacia* genomes. This draws attention to GC bias that may be occurring from Illumina sequencing of GC-rich sequences and indicates poor coverage may be an issue for regions of this genome [382–384]. To get a complete assembly of C6433 we need to obtain long sequencing reads, similar to how the *B. cenocepacia* strain K56-2 genome was assembled [381].

C6433 is predicted to encode 2 circular chromosomes of 6,650,071 bp and 1,074,343 bp, and a plasmid of 61,503 bp (Table 4-5). The smallest replicon sequence is likely accurate as it was predicted to exist in all three ragtag assemblies with 100% read coverage (Table 4-5). It has been labelled as a plasmid because it does not encode any rRNA or tRNA genes and is very similar (99.9% identity) to the plasmids of *B. contaminans* strains ZCC (CP042167.1) and XL73 (CP046610.1), though the C6433 plasmid is significantly smaller. Recently, *B. contaminans* has emerged as a hospital pathogen causing bacteremia in patients [111]. Since C6433 was an epidemic strain, it is therefore possible components in the plasmid may help strains carrying it establish infection in humans. PHASTER [388,389] did not identify any intact prophage in the genome but did identify 5 incomplete regions on chromosome 1 and 2 incomplete regions on chromosome 2. The fur gene sequence for C6433 has the highest percent identity to *B. cenocepacia* 895 (98.52% over 100% of the query) further supporting the best reference genome was chosen for C6433 scaffolding [300]. The draft genome assembly of C6433 has been deposited in GenBank with the accession numbers CP098497-CP098499 and was annotated using the NCBI prokaryotic genome annotation pipeline. According to the pipeline annotation there are at least 7,369 genes, with 7,309 protein coding genes, 55 tRNAs, 1 rRNA, 3 noncoding RNAs, and 1 tmRNA. There is a significant lack of identified rRNAs, as only one 5S subunit was identified on chromosome 1.

Typically, >3 rRNAs are present in *Burkholderia* genomes, and at least one 23S, 16S, and 5S subunit are found in all bacteria. Prokka [390] was used as another method to find rRNA genes, but only the same 5S subunit was identified. The lack of rRNA genes identified is likely caused by the gaps in the genome. C6433 probably encodes at least 3-18 rRNAs and more genes as well. Though this is a partial assembly of C6433, the amount of information obtained from assembling the genome is vast, and a great degree of research can be proposed looking into the many genes annotated for C6433.

Construction of pCD22

A well-established protocol for making unmarked "clean" *B. cenocepacia* mutants utilizes homologous recombination and a yeast endonuclease I-SceI [391]. This method has also been extended to create clean deletions in prophage, removing the integrase and causing them to be strictly lytic [369]. The methodology involves cloning upstream and downstream DNA sequences surrounding the gene of interest into a suicide vector (pGPI-SceI) that harbours an 18 bp recognition site for the I-SceI endonuclease. Homologous recombination of the suicide vector with either the upstream or downstream region into the bacterial genome is labelled as the single crossover and is selected for with trimethoprim. A second plasmid constitutively expressing the I-SceI endonuclease (pDAI-SceI) is then transformed into the single crossover strain. I-SceI will create a double stranded break at the cut site, and the bacteria will have to repair it using homologous recombination with either the upstream or downstream fragment in the suicide vector. This strain is known as the double crossover and is selected for with chloramphenicol resistance and trimethoprim sensitivity. Depending on the events of the crossovers, the surviving recombinants will be either wildtype or a clean deletion mutant.

This method was expanded for use in *B. cenocepacia* strains that harbour complex antibiotic resistance profiles [392] and the ori of pGPI-SceI was replaced with narrow-host-range oriR from pMB1, making it easier to work with (pAA1-MB1). Though the addition of a better ori has indeed made working with pAA1-MB1 easier, there are still a few drawbacks with this plasmid. Firstly, it still has a limited MCS, harbouring only 6 restriction cut sites (XbaI, KpnI, SphI, EcoRV, SmaI, EcoRI), and secondly there is no efficient technique to identify the successful ligation of your insert into the MCS of the plasmid. The second drawback is quite significant because for an unknown reason the transformation efficiency of the empty vector is very high, even with gel extracting the digested plasmid. This makes searching for a successful clone very difficult. For example, you could screen 20-30 transformants and only 1 would have your desired insert.

To make cloning with pAA1-MB1 more efficient the MCS was removed and replaced with the MCS of pBBr1Tp to create the new plasmid pCD22 (Figure 4-3). The MCS was removed from pAA1-MB1 by digestion with restriction enzymes XbaI and EcoRI (Thermo Scientific) and treatment with Mung Bean Nuclease (New England Biolabs) to blunt the ends and Shrimp Alkaline Phosphatase (rSAP) (New England Biolabs) to prevent re-ligation of linearized plasmid. The MCS was isolated from pBBr1Tp by digesting with restriction enzyme SspI, which creates blunt ends. The digestion was then run on a gel and the 704 bp product was gel extracted using a QIAquick Gel Extraction kit (Qiagen, Inc., Germantown, MD, USA). The two fragments were then blunt-end ligated with T4 DNA ligase (New England Biolabs) and transformed into chemically competent *E. coli* DH5α. The transformation was plated onto LB plates containing 100 µg/mL trimethoprim and 100 µg/mL of X-Gal. Blue colonies were selected and sent for Sanger sequencing using primers that flanked the old MCS of pAA1-MB1 (F 5'-

TTACTAAGCTGATCCGGTG-3’ and R 5’- GGGGAAACGCCTGGTATC-3’) to confirm sequence and orientation of the MCS.

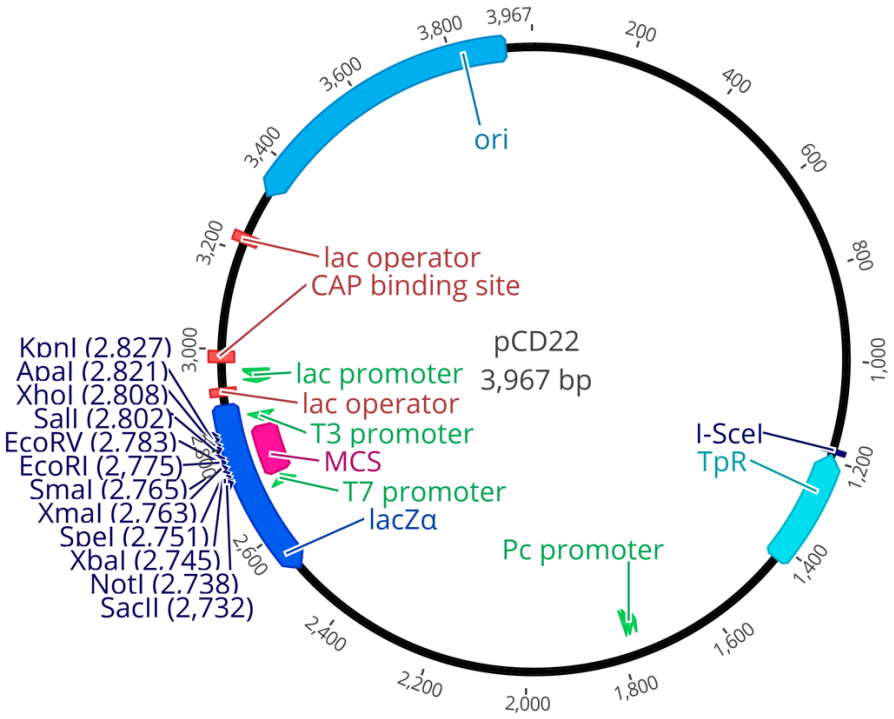

Figure 4-3: Plasmid map of pCD22. The MCS of pBBr1Tp was digested and ligated into the pGPI MCS digested with XbaI and EcoRI and treated with rSAP and Mung Bean Nuclease.

Conclusions

The rise of AMR has left antibiotics unable to successfully treat all bacterial infections [184], and alternative therapeutic options are needed for multi-drug resistant bacterial pathogens like members of the Bcc and *P. aeruginosa*. In addition to being nosocomial derived, these pathogens are significant contributors to premature lung degeneration and death in individuals with CF, and they can be incredibly difficult, if not impossible, to eradicate [35,64,119]. More than 60% of adult CF patients develop a chronic *P. aeruginosa* infection and being diagnosed with a Bcc lung infection can be devastating due to the unpredictable nature of these infections and clinically severe outcomes for CF patient [35,64,68]. Using phage as an alternative treatment option

for these kinds of infections is an incredibly promising avenue, and there is an increasing number of clinical reports and case series using phage therapy against multi-drug resistant infections in humans [393].

Research on the isolation and characterization of phages, as well as looking into combination treatments is crucial if we want to continue to see success in this field. Phage were discovered over a century ago by Frederick Twort in 1915 and by Felix d'Herelle in 1917 [394], and the effects of using phage in combination with antibiotics was being studied alongside the golden age of antibiotics [253,395]. Phage therapy research didn't gain much support or popularity in North America until the advent of the AMR crisis, and there remains a great deal of research that needs to be done on phages before they can be offered as an accessible treatment option [396]. There is much to be discovered about the interactions between phage, bacteria, and the human host, and the advantages and disadvantages of phage therapy must be considered [396]. The work in this thesis contributes to the field of using phage therapy as an alternative treatment option for multi-drug resistant bacterial pathogens *P. aeruginosa* and *B. cenocepacia*.

The synergistic relationship between phages E79 and phiKZ with the antibiotic aztreonam lysine (AzLys) was explored in chapter 2 [229]. E79, a phage that utilizes the LPS on the bacterial surface to adsorb to and inject its genomic material [250], exhibited increased lytic activity in the presence of the peptidoglycan inhibiting antibiotic. E79 exhibited increased plaque size, infection efficiency, and biofilm reduction. It also displayed accelerated time to lysis. The increased lytic activity is likely caused by a variety of factors including but not limited to increased adsorption to the enlarged cells, which correspondingly would have increased LPS, and accelerated time to lysis, which may be caused by reduced integrity of the cell wall allowing phage to lyse the bacteria quicker. PhiKZ was used to examine whether a phage might exhibit

reduced activity in the presence of AzLys if their receptor abundance decreases as opposed to increases, like the LPS. PhiKZ requires functional type 4 pili (T4P) to infect its host [277], and AzLys causes a significant decreases in the function of polar flagella and T4P motility structures. Though phiKZ exhibited reduced infection efficiency and smaller plaque sizes at some concentrations of AzLys, it unexpectedly displayed increased bacterial reduction at multiple MOIs in the presence of sub-inhibitory AzLys. Further examination similarly showed accelerated time to lysis, suggesting a potential mechanism for increased phage activity in the presence of AzLys may be increased time to lysis. This chapter also highlights the need for more studies looking into the mechanisms of phage antibiotic synergy, as finding positive synergy may be easier once we understand more about how phage can take advantage of the physiological changes to their host caused by antibiotics.

In chapter 3 a novel bacteriophage targeting the Bcc isolated from soil in Edmonton Alberta by an undergraduate in the Dennis lab, Jamie Cole, was genomically annotated and characterized. Experiments analyzing its host range, morphology, growth curve, receptor, virion-associated proteins, lifestyle, and virulence index showed that JC1 has a few desirable characteristics for use as a therapeutic. Firstly, it has an impressive host range, being able to infect many species of the Bcc, increasing the chances it may be able to infect clinical isolates from patients in need of alternative therapies. Second, it uses the inner core of the LPS to infect its host. *B. cenocepacia* has been shown to have a significant fitness disadvantage with severe truncation of the LPS [145,146], suggesting that JC1 can act not only as an antibacterial agent, but also as an antivirulence agent by targeting a significant contributor to bacteria virulence. Third, it is highly virulent against its host *in vitro* at a wide range of MOIs. The main caveat of JC1 is it is a lysogenic phage, and the lysogen displays growth differences compared to wildtype in different

nutritional medias. Therefore, before JC1 is used as a therapeutic, it should be genetically modified to remove the lysogeny genes to avoid any unknown, and potentially harmful, effects of lysogenizing its host.

Future Directions

Phage are the most abundant biological entity on earth and they are found ubiquitously through nature [397]. Finding phage is relatively easy, but finding phage that infect your desired bacteria, and possess ideal characteristics for use in therapy can be challenging. The Dennis lab to date has characterized a number of *B. cenocepacia* phages, where all but one phage contain lysogeny related genes in their genome, suggesting they are not obligately lytic, even if stable lysogeny cannot be confirmed for all phages [290,333,340,343,345,346,369,377,398]. We have had one successful case in our lab making a lysogenic phage obligately lytic by replacing the repressor gene in KS9 with a trimethoprim resistance cassette via homologous recombination [369]. The success of this was likely due to KS9 being stably integrated into its host's genome. A good majority of our *Burkholderia* phages form pseudolysogens, meaning they do not integrate into the bacterial genome of the hosts we have in our lab, but rather form circular phagemids with no partitioning system, eventually being lost over time (data not shown). This instability has proven to be a significant issue for isolating single crossovers into the phage genomes using the Flannagan et al (2008) method. It is possible there are hosts where our phages may stably integrate into the bacterial genome but finding said host would be difficult due to the narrow host range of most phages. It is also possible that the lysogeny related genes do not function properly, and the phage cannot integrate or maintain lysogeny for an extended period of time.

Due to unstable lysogeny of many of our phages, the development of a successful method for obtaining genetically modified phages is vital. There has been success in the literature using

the yeast gap repair system to construct synthetic phage genomes from PCR products and a yeast artificial chromosome (YAC) [399–402]. Utilizing this yeast-based phage-engineering methodology will nullify the issues occurring due to unstable lysogeny of our phages. If a successful method can be developed for our Bcc phages, then we can make all of our phages fully lytic, and therefore more desirable for use in therapy. The biggest hurdle will be whether or not our phage can successfully be rebooted from genomic DNA. If functional phage virions can be produced by electroporating the genomic phage DNA into either 10G *E. coli* cells or their natural host cell (rebooted), then the chances of this method being successful will be promising. The only other hurdle we may encounter is potential difficulty PCR amplifying 10kb fragments from the GC rich DNA of our phages (>60% GC), and whether this high GC content will display any issues recombining within yeast, who have a GC content around 38% and have been shown to display increased mutation rates and mitotic and meiotic recombination with GC rich DNA [403]. If problems arise with the high GC content in yeast, Gibson assembly could be an alternative method to assemble the phage genomes instead, as an updated protocol for Gibson-assembly of large DNA fragments with high GC contents has recently been published [404].

In addition to the removal of lysogeny genes, this method can also be used to increase the host range of our phages by removing hypothetical genes of unknown function to make room in the genome to add in additional tail fiber proteins. Tail fibers have successfully been modified using this method in *E. coli* and *Klebsiella* and directly affected the host range of the phages [399,402]. Typically the N-terminal regions of tail fibers in similar phages retain higher levels of homology owing to the structural role they play in attaching the fiber to the phage virion, while the C-termini vary from one another and play a role in binding to the host receptor [399,402]. This pattern in seen between the tail fibers of both the *Lessiviruses* and the *Kisquinqueviruses*, with

only the N-terminal regions having high sequence homology to one another. Exchanging and/or adding in additional tail fibers with these phages would be very interesting, especially if it could help broaden the host range of the other characterized *Lessieviruses* DC1, Bcep22, and BcepIL02, which have a significantly smaller host range than JC1 [332,333,377]. Extensive host range analyses have not been performed on the *Kisquinqueviruses*, but the current known host range for these phages differ from one another and could also provide interesting results [346]. Expanding the host range of our phages by adding additional tail fibers offers a bright outcome for phage therapy as we can expand the narrow host range of phage, one of the limitations associated with this therapy. Alternatively, adding a tail fiber from an uncharacterized phage to the genome a very well characterized phage could help phage therapy to be a more safe and accessible option to patients. This would mean that novel or lysogenic phage would not always need to be extensively characterized or genetically modified before being used in therapy. If a novel or lysogenic phage is found to infect a clinical isolate, the tail fiber of that phage could be added into a similar but very well characterized phage. Of course, in order for this to be an option we need a variety of extensively characterized phages for the multi-drug resistant bacteria in question.

Another way to increase the efficacy of phage therapy is by using phage cocktails and combination therapy with antibiotics because they can reduce the frequency of resistant mutants to the killing agents by targeting multiple surface structures (phage cocktails) or by killing the cells with different mechanisms of action (phage-antibiotic combination). The exploration of combination therapy with antibiotics and phage that require the inner core of the LPS for infections is noteworthy because the LPS of Gram-negative bacteria provide a significant degree of protection from the host immune system and are a physical barrier to many antibiotics [144].

Additionally, truncation of the LPS has been shown to result in significant fitness disadvantages of the bacterial cells, including increased sensitivity to antimicrobials [145,146]. Accelerated time to lysis caused by AzLys in *P. aeruginosa* allows for new phage virions to be released sooner, so they can infect new cells faster, accelerating the overall rate of killing [229]. The potential for treating a chronic *P. aeruginosa* infection with cell wall-inhibiting antibiotics and phage like E79 that utilize the LPS as their receptor is an incredibly promising area of research and should be examined further. Interestingly, the LPS seems to be a very popular phage receptor in Bcc phages isolated form the environment [335], and both phages JC1[377] and Carl1 (unpublished; ON642070.1) discussed in this thesis require the inner core of the LPS for infection. Given this phenomenon, exploring LPS dependent phage therapy in combination with cell wall-inhibiting antibiotics should also be explored in the Bcc as a potential alternative treatment option.

In the 2020 Annual Data Report from The Canadian Cystic Fibrosis Registry 7.5% of individuals infected with Bcc were infected with *B. gladioli*. Officially, this strain is not recognized as a Bcc species, but it is clearly emerging as an opportunistic pathogen colonizing the lungs of CF patients. JC1 has lytic activity against *B. gladioli* strains R1879 and R406 (unpublished data); it can lyse at high titer but cannot propagate to produce plaques. Further host range analysis of JC1 should be conducted on a large panel of *B. gladioli* strains, as JC1 has a very broad host range [377] and it is likely that JC1 can infect more *B. gladioli* strains. If the screen results in the same phenomenon being observed, where JC1 can lyse the strains at high titer but not propagate to produce plaques, then training JC1 by repeatedly passaging the phage on the *B. gladioli* strains it can infect could result in a strain of JC1 capable of propagating on *B. gladioli*. Sequencing of this evolved phage genome could also prove insightful in determining what caused the change in host range.

Alternatively, this lytic activity could be a result of depolymerase activity lysing the bacterial cell wall. Using InterProScan [405] to further analyze the predicted protein sequences of JC1 showed that gp57 and gp59 have predicted peptidase regions at the C-terminal end of the predicted proteins. These two proteins may have the ability to degrade LPS, and are likely required for infection of their host given that other phage proteins with this domain make up the tail spike of the phage and are involved in degrading the LPS so the phage can reach the cell surface [406–408]. It could also be interesting to purify these proteins and test if they display depolymerase activity on the phage host Van1, and if so, expand it to test an extensive host range. As discussed in the introduction, phage lysins that can destroy the cell wall of a target bacteria are a potential replacement for antibiotics because of their direct antibacterial action; similarly to phage lysins, phage depolymerases have potential for use as an alternative therapeutic, especially when it comes to biofilm reduction studies [409]. The fact that JC1 encodes two separate proteins with predicted peptidase regions may be playing a role in its wide host range as phageφK1-5 can infect two K-types of *E. coli* because it encodes two different enzymatic tail fiber proteins [410]. Overall, the depolymerase activity of JC1 and these two tail proteins should be analyzed further.

Final Remarks

The use of phage therapy is gaining recognition as a promising alternative to antibiotics, and rightfully so. There are many benefits to using phage, such as host-specificity, self-amplification, biofilm degradation, and low toxicity to humans [218]. There are also a few downsides to the use of phage therapy. For one, not all phage are useful as a therapeutic, some phage can display low virulence, or are lysogenic and/or encode toxins, virulence factors and antibiotic resistance genes that can help the pathogens we are trying to kill [218]. This highlights

the necessity of characterizing phage to assure successful treatment. The narrow host range, though a benefit to our microbiome which is now known to play a vital role in our health [411], is also an issue because we will never have a one-phage-fits-all for treating infections. Accurate identification of clinical isolates and subsequent screening against a panel of phages is the likely future of phage therapy, and often isolation of novel phages against a clinical isolate is required. Phage cocktails and tail fiber modifications can help to alleviate the complications with narrow host range, however patients that require immediate treatment likely will not have time to wait for their isolate to be screened against a panel of phage. Thirdly, phages can actively replicate, sometimes cause immune responses, and can potentially evolve during manufacturing or use. Nonetheless, protein-based therapeutics, chemical antibiotics, and whole vaccines also display these disadvantages and have been approved for use, so this hurdle should not stop phage therapy from being approved [218]. Alternatively, the use of lysins and depolymerases are similar to chemical antibiotics/protein-based therapeutics as the biologically active component of phage therapy has been removed. Though it is unlikely that phage therapy will replace the use of antibiotics in common infections, they offer monumental potential for treating chronic and antibiotic resistant infections.

Bibliography

1. Migula, W. Über ein neues System der Bakterien. *Arb Bakteriol Inst Karlsruhe* **1**, 235–238 (1894).
2. Palleroni, N. J. Prokaryote taxonomy of the 20th century and the impact of studies on the genus Pseudomonas: A personal view. *Microbiology* **149**, 1–7 (2003).
3. Cohn, F. Untersuchungen über Bakterien. *Beitr Biol Pflanz* **1**, 127–224 (1872).
4. Palleroni, N. J. The Pseudomonas Story. *Environ. Microbiol.* **12**, 1377–1383 (2010).
5. Migula, W. *System der Bakterien*. *Handbuch der morphologie Vol. 2* **2**, (Gustav Fischer, 1900).
6. Peix, A., Ramírez-Bahena, M. H. & Velázquez, E. Historical evolution and current status of the taxonomy of genus Pseudomonas. *Infect. Genet. Evol.* **9**, 1132–1147 (2009).
7. Palleroni, N. J., Kunisawa, R., Contopoulou, R. & Doudoroff, M. Nucleic acid homologies in the genus Pseudomonas. *Int. J. Syst. Bacteriol.* **23**, 333–339 (1973).
8. Gomila, M., Peña, A., Mulet, M., Lalucat, J. & García-Valdés, E. Phylogenomics and systematics in Pseudomonas. *Front. Microbiol.* **6**, 214 (2015).
9. Stanier, R. Y., Palleroni, N. J. & Doudoroff, M. The aerobic pseudomonads: a taxonomic study. *J. Gen. Microbiol.* **43**, 159–271 (1966).
10. Lalucat, J., Gomila, M., Mulet, M., Zaruma, A. & García-Valdés, E. Past, present and future of the boundaries of the Pseudomonas genus: Proposal of Stutzerimonas gen. Nov. *Syst. Appl. Microbiol.* **45**, 126289 (2022).
11. Diggle, S. P. & Whiteley, M. Microbe Profile: Pseudomonas aeruginosa: opportunistic pathogen and lab rat. *Microbiology* **166**, 30 (2020).
12. Villavicencio, R. T. The history of blue pus. *J. Am. Coll. Surg.* **187**, 212–216 (1998).

13. Haynes, W. C. Pseudomonas aeruginosa-its Characterization and Identification. *J Gen Microbiol* **5**, 939–950 (1951).

14. Hugh, R. & Leifson, E. The proposed Neotype Strains of Pseudomonas Aeruginosa (Schroeter 1872) Migula 1900. *Int. J. Syst. Evol. Microbiol.* **14**, 69–84 (1964).

15. Pachori, P., Gothalwal, R. & Gandhi, P. Emergence of antibiotic resistance Pseudomonas aeruginosa in intensive care unit; a critical review. *Genes and Diseases* **6**, 109–119 (2019).

16. Botzenhart, K. & Doring, G. Ecology and Epidemiology of Pseudomonas aeruginosa. in *Pseudomonas Aeruginosa as an Opportunistic Pathogen* (eds. Campa, M., Bendinelli, M., Friedman, H. & Eds) 1–18 (Plenum Press, 1993).

17. Hardalo, C. & Edberg, S. C. Pseudomonas aeruginosa: Assessment of Risk from Drinking Water. *Crit. Rev. Microbiol.* **23**, 47–75 (1997).

18. Blanc, D. S. *et al.* Hand soap contamination by Pseudomonas aeruginosa in a tertiary care hospital: no evidence of impact on patients. *J. Hosp. Infect.* **93**, 63–67 (2016).

19. Lister, P. D., Wolter, D. J. & Hanson, N. D. Antibacterial-Resistant Pseudomonas aeruginosa: Clinical Impact and Complex Regulation of Chromosomally Encoded Resistance Mechanisms. *Clin. Microbiol. Rev.* **22**, 582 (2009).

20. Kline, B. S. & Maschke, A. S. Three fatal cases of bacillus pyocyaneus infection. *J. Am. Med. Assoc.* **98**, 528–532 (1932).

21. Robb, H. *Aseptic surgical technique*. (1906).

22. Kerby, G. P. & Durham, N. C. Pseudomonas aeruginosa Bacteremia: Summary of Literature, with Report of a Case. *Am. J. Dis. Child.* **74**, 610–615 (1947).

23. Matsumoto, T., Wyte, S. R., Moseley, R. V., Hawley, R. J. & Lackey, G. R. Combat

Surgery in Communication Zone I. War Wound and Bacteriology (Preliminary Report). *Mil. Med.* **134**, 655–665 (1969).

24. Stillwell, M. & Caplan, E. S. The Septic Multiple-Trauma Patient. *Infect. Dis. Clin. North Am.* **3**, 155–183 (1989).

25. Rice, L. B. Federal Funding for the Study of Antimicrobial Resistance in Nosocomial Pathogens: No ESKAPE. *J. Infect. Dis.* **197**, 1079–1081 (2008).

26. Founou, R. C., Founou, L. L. & Essack, S. Y. Clinical and economic impact of antibiotic resistance in developing countries: A systematic review and meta-analysis. *PLoS One* **12**, (2017).

27. Mulani, M. S., Kamble, E. E., Kumkar, S. N., Tawre, M. S. & Pardesi, K. R. Emerging Strategies to Combat ESKAPE Pathogens in the Era of Antimicrobial Resistance: A Review. *Front. Microbiol.* **10**, 539 (2019).

28. Shrivastava, S. R., Shrivastava, P. S. & Ramasamy, J. World health organization releases global priority list of antibiotic-resistant bacteria to guide research, discovery, and development of new antibiotics. *J. Med. Soc.* **32**, 76 (2018).

29. World Health Organization. *WHO Publishes List of Bacteria for Which New Antibiotics are Urgently Needed*. (2017).

30. Gellatly, S. L. & Hancock, R. E. W. *Pseudomonas aeruginosa* : new insights into pathogenesis and host defenses. *Pathog. Dis.* **67**, 159–173 (2013).

31. Otter, J. A., Yezli, S. & French, G. L. The Role Played by Contaminated Surfaces in the Transmission of Nosocomial Pathogens. *Infect. Control Hosp. Epidemiol.* **2**, 687–699 (2011).

32. Williams, B. J., Dehnbostel, J. & Blackwell, T. S. Pseudomonas aeruginosa: Host defence

in lung diseases. *Respirology* **15**, 1037–1056 (2010).

33. Valentini, M., Gonzalez, D., Mavridou, D. A. & Filloux, A. Lifestyle transitions and adaptive pathogenesis of Pseudomonas aeruginosa. *Curr. Opin. Microbiol.* **41**, 15–20 (2018).

34. Chen, Q., Shen, Y. & Zheng, J. A review of cystic fibrosis: Basic and clinical aspects. *Anim. Model. Exp. Med.* **4**, 220 (2021).

35. Parkins, M. D., Somayaji, R. & Waters, V. J. Epidemiology, Biology, and Impact of Clonal Pseudomonas aeruginosa Infections in Cystic Fibrosis. *Clin. Microbiol. Rev.* **31**, (2018).

36. Cystic Fibrosis Canada. *The Canadian Cystic Fibrosis Registry 2019 Annual Data Report*. (2020).

37. Morrison, A. J. & Wenzel, R. P. Epidemiology of Infections Due to Pseudomonas aeruginosa. *Rev. Infect. Dis.* **6**, 627–642 (1984).

38. Campana, S. *et al.* Molecular epidemiology of Pseudomonas aeruginosa, Burkholderia cepacia complex and methicillin-resistant Staphylococcus aureus in a cystic fibrosis center. *J. Cyst. Fibros.* **3**, 159–163 (2004).

39. Wieland, K., Chhatwal, P. & Vonberg, R. P. Nosocomial outbreaks caused by Acinetobacter baumannii and Pseudomonas aeruginosa: Results of a systematic review. *Am. J. Infect. Control* **46**, 643–648 (2018).

40. Kramer, A., Schwebke, I. & Kampf, G. How long do nosocomial pathogens persist on inanimate surfaces? A systematic review. *BMC Infect. Dis.* **6**, 1–8 (2006).

41. Gilardi, G. L. Infrequently encountered Pseudomonas species causing infection in humans. *Ann. Intern. Med.* **77**, 211–215 (1972).

42. Campbell, R. & Greaves, M. P. Anatomy and community structure of the rhizosphere. in *The rhizosphere* (ed. Lynch, J. M.) 11–34 (John Wiley and Sons Ltd, 1990).

43. Rehm, B. H. A. Pseudomonas: Model Organism, Pathogen, Cell Factory. *Pseudomonas Model Org. Pathog. Cell Fact.* 1–402 (2008). doi:10.1002/9783527622009

44. Lugtenberg, B. J. J. & Dekkers, L. C. What makes Pseudomonas bacteria rhizosphere competent? *Environ. Microbiol.* **1**, 9–13 (1999).

45. Troxler, J., Azelvandre, P., Zala, M., Défago, G. & Haas, D. Conjugative Transfer of Chromosomal Genes between Fluorescent Pseudomonads in the Rhizosphere of Wheat. *Appl. Environ. Microbiol.* **63**, 213–219 (1997).

46. D'aes, J., De Maeyer, K., Pauwelyn, E. & Höfte, M. Biosurfactants in plant–Pseudomonas interactions and their importance to biocontrol. *Environ. Microbiol. Rep.* **2**, 359–372 (2010).

47. Castric, P. A. Glycine metabolism by Pseudomonas aeruginosa: hydrogen cyanide biosynthesis. *J. Bacteriol.* **130**, 826 (1977).

48. Jan, A. T., Azam, M., Ali, A. & Rizwanul Haq, Q. M. Novel approaches of beneficial Pseudomonas in mitigation of plant diseases – an appraisal. *J. plant Interact.* **6**, 195–205 (2011).

49. Bano, N. & Musarrat, J. Characterization of a New Pseudomonas aeruginosa Strain NJ-15 as a Potential Biocontrol Agent. *Curr. Microbiol. 2003 465* **46**, 0324–0328 (2003).

50. Yasmin, S. *et al.* Biocontrol of Bacterial Leaf Blight of rice and profiling of secondary metabolites produced by rhizospheric Pseudomonas aeruginosa BRp3. *Front. Microbiol.* **8**, 1895 (2017).

51. Islam, M. A., Nain, Z., Alam, M. K., Banu, N. A. & Islam, M. R. In vitro study of

biocontrol potential of rhizospheric pseudomonas aeruginosa against fusarium oxysporum f. Sp. cucumerinum. *Egypt. J. Biol. Pest Control* **28**, 1–11 (2018).

52. Minaxi & Saxena, J. Characterization of Pseudomonas aeruginosa RM-3 as a potential biocontrol agent. *Mycopathologia* **170**, 181–193 (2010).

53. Maier, R. M. & Soberón-Chávez, G. Pseudomonas aeruginosa rhamnolipids: biosynthesis and potential applications. *Appl. Microbiol. Biotechnol.* **54**, 625–633 (2000).

54. Soberón-Chávez, G., González-Valdez, A., Soto-Aceves, M. P. & Cocotl-Yañez, M. Rhamnolipids produced by Pseudomonas: from molecular genetics to the market. *Microb. Biotechnol.* **14**, 136–146 (2021).

55. Chong, H. & Li, Q. Microbial production of rhamnolipids: opportunities, challenges and strategies. *Microb. Cell Factories 2017 161* **16**, 1–12 (2017).

56. Burkholder, W. H. Sour skin, a bacterial rot of Onion bulbs. *Phytopathology* **40**, (1950).

57. Yabuuchi, E. *et al.* Proposal of Burkholderia gen. nov. and Transfer of Seven Species of the Genus Pseudomonas Homology Group II to the New Genus, with the Type Species Burkholderia cepacia (Palleroni and Holmes 1981) comb. nov. *Microbiol. Immunol.* **36**, 1251–1275 (1992).

58. Vandamme, P. *et al.* Occurrence of multiple genomovars of Burkholderia cepacia in cystic fibrosis patients and proposal of Burkholderia multivorans sp. nov. *Int. J. Syst. Bacteriol.* **47**, 1188–1200 (1997).

59. Ursing, J. B., Rossello-Mora, R. A., Garcia-Valdes, E. & Lalucat, J. Taxonomic note: A pragmatic approach to the nomenclature of phenotypically similar genomic groups. *Int. J. Syst. Bacteriol.* **45**, 604 (1995).

60. Gillis, M. *et al.* Polyphasic taxonomy in the genus Burkholderia leading to an emended

description of the genus and proposition of Burkholderia vietnamiensis sp. nov. for N2-fixing isolates from rice in Vietnam. *Int. J. Syst. Bacteriol.* **45**, 274–289 (1995).

61. Vandamme, P. *et al.* Burkholderia cenocepacia sp. nov.— a new twist to an old story. *Res. Microbiol.* **154**, 91–96 (2003).

62. Vandamme, P. *et al.* Identification and population structure of Burkholderia stabilis sp. nov. (formerly Burkholderia cepacia genomovar IV). *J. Clin. Microbiol.* **38**, 1042–1047 (2000).

63. Lessie, T. G., Hendrickson, W., Manning, B. D. & Devereux, R. Genomic complexity and plasticity of Burkholderia cepacia. *FEMS Microbiol. Lett.* **144**, 117–128 (1996).

64. Mahenthiralingam, E., Urban, T. A. & Goldberg, J. B. The multifarious, multireplicon Burkholderia cepacia complex. *Nat. Rev. Microbiol.* **3**, 144–156 (2005).

65. Govan, J. R. W., Hughes, J. E. & Vandamme, P. Burkholderia cepacia: medical, taxonomic and ecological issues. *J. Med. Microbiol.* **45**, 395–407 (1996).

66. Vermis, K., Vandamme, P. A. R. & Nelis, H. J. Burkholderia cepacia complex genomovars: utilization of carbon sources, susceptibility to antimicrobial agents and growth on selective media. *J. Appl. Microbiol.* **95**, 1191–1199 (2003).

67. Martina, P. *et al.* Burkholderia puraquae sp. nov., a novel species of the Burkholderia cepacia complex isolated from hospital settings and agricultural soils. *Int. J. Syst. Evol. Microbiol.* **68**, 14–20 (2018).

68. Scoffone, V. C. *et al.* Burkholderia cenocepacia infections in cystic fibrosis patients: Drug resistance and therapeutic approaches. *Frontiers in Microbiology* **8**, (2017).

69. Vandamme, P. *et al.* Burkholderia anthina sp. nov. and Burkholderia pyrrocinia, two additional Burkholderia cepacia complex bacteria, may confound results of new molecular

diagnostic tools. *FEMS Immunol. Med. Microbiol.* **33**, 143–149 (2002).

70. Vermis, K. *et al.* Proposal to accommodate Burkholderia cepacia genomovar VI as Burkholderia dolosa sp. nov. *Int. J. Syst. Evol. Microbiol.* **54**, 689–691 (2004).

71. Coenye, T. *et al.* Burkholderia ambifaria sp. nov., a novel member of the Burkholderia cepacia complex including biocontrol and cystic fibrosis-related isolates. *Int. J. Syst. Evol. Microbiol.* **51**, 1481–1490 (2001).

72. Vanlaere, E. *et al.* Taxon K, a complex within the Burkholderia cepacia complex, comprises at least two novel species, Burkholderia contaminans sp. nov. and Burkholderia lata sp. nov. *Int. J. Syst. Evol. Microbiol.* **59**, 102–111 (2009).

73. Vanlaera, E. *et al.* Burkholderia latens sp. nov., Burkholderia diffusa sp. nov., Burkholderia arboris sp. nov., Burkholderia seminalis sp. nov., and Burkholderia metallica sp. nov., novel species within the Burkholderia cepacia complex. *Int. J. Syst. Evol. Microbiol.* **58**, 1580–1590 (2008).

74. De Smet, B. *et al.* Burkholderia stagnalis sp. nov. and Burkholderia territorii sp. nov., two novel Burkholderia cepacia complex species from environmental and human sources. *Int. J. Syst. Evol. Microbiol.* **65**, 2265–2271 (2015).

75. Ong, K. S. *et al.* Burkholderia paludis sp. nov., an Antibiotic-Siderophore Producing Novel Burkholderia cepacia Complex Species, Isolated from Malaysian Tropical Peat Swamp Soil. *Front. Microbiol.* **7**, (2016).

76. Weber, C. F. & King, G. M. Volcanic soils as sources of novel CO-oxidizing Paraburkholderia and Burkholderia: Paraburkholderia hiiakae sp. nov., Paraburkholderia metrosideri sp. nov., Paraburkholderia paradisi sp. nov., Paraburkholderia peleae sp. nov., and Burkholderia alpina sp. nov. a member of the Burkholderia cepacia complex. *Front.*

Microbiol. **8**, 207 (2017).

77. Bach, E. *et al.* Detection of misidentifications of species from the Burkholderia cepacia complex and description of a new member, the soil bacterium Burkholderia catarinensis sp. nov. *Pathog. Dis.* **75**, (2017).

78. Morales-Ruíz, L. M. *et al.* Burkholderia orbicola sp. nov., a novel species within the Burkholderia cepacia complex. *Arch. Microbiol.* **204**, 1–9 (2022).

79. Lin, Q. H., Lv, Y. Y., Gao, Z. H. & Qiu, L. H. Pararobbsia silviterrae gen. nov., sp. nov., isolated from forest soil and reclassification of Burkholderia alpina as Pararobbsia alpina comb. nov. *Int. J. Syst. Evol. Microbiol.* **70**, 1412–1420 (2020).

80. Vandamme, P. & Peeters, C. Time to revisit polyphasic taxonomy. *Antonie van Leeuwenhoek, Int. J. Gen. Mol. Microbiol.* **106**, 57–65 (2014).

81. Laraya-Cuasay, L. R., Lipstein, M. & Huang, N. N. Pseudomonas cepacia in the respiratory flora of patients with cystic fibrosis (CF). *Pediatr. Res. 1977 114* **11**, 502–502 (1977).

82. Isles, A. *et al.* Pseudomonas cepacia infection in cystic fibrosis: An emerging problem. *J. Pediatr.* **104**, 206–210 (1984).

83. Thomassen, M. J., Demko, C. A., Doershuk, C. F., Stern, R. C. & Klinger, J. D. Pseudomonas cepacia: Decrease in Colonization in Patients with Cystic Fibrosis 1 3. *Am. Rev. Respir. Dis.* **134**, 669–671 (1986).

84. Hardy, K. A., McGowan, K. L., Fisher, M. C. & Schidlow, D. V. Pseudomonas cepacia in the hospitalsetting: Lack of transmission between cystic fibrosis patients. *J. Pediatr.* **109**, 51–54 (1986).

85. Simmonds, E. J., Conway, S. P., Ghoneim, A. T. M., Ross, H. & Littlewood, J. M.

Pseudomonas cepacia: a new pathogen in patients with cystic fibrosis referred to a large centre in the United Kingdom. *Arch. Dis. Child.* **65**, 874–877 (1990).

86. LiPuma, J. J., Dasen, S. E., Stull, T. L., Nielson, D. W. & Stern, R. C. Person-to-person transmission of Pseudomonas cepacia between patients with cystic fibrosis. *Lancet (London, England)* **336**, 1094–1096 (1990).

87. Govan, J. R. W. *et al.* Evidence for transmission of Pseudomonas cepacia by social contact in cystic fibrosis. *Lancet (London, England)* **342**, 15–19 (1993).

88. Lewis, E. R. G. & Torres, A. G. The art of persistence—the secrets to Burkholderia chronic infections. *Pathog. Dis.* **74**, 70 (2016).

89. Hauser, N. & Orsini, J. Cepacia Syndrome in a Non-Cystic Fibrosis Patient. *Case Rep. Infect. Dis.* **2015**, 1–4 (2015).

90. Grimwood, K., Kidd, T. J. & Tweed, M. Successful treatment of cepacia syndrome. *J. Cyst. Fibros.* **8**, 291–293 (2009).

91. Gilchrist, F. J., Webb, A. K., Bright-Thomas, R. J. & Jones, A. M. Successful treatment of cepacia syndrome with a combination of intravenous cyclosporin, antibiotics and oral corticosteroids. *J. Cyst. Fibros.* **11**, 458–460 (2012).

92. Weidmann, A., Webb, A. K., Dodd, M. E. & Jones, A. M. Successful treatment of cepacia syndrome with combination nebulised and intravenous antibiotic therapy. *J. Cyst. Fibros.* **7**, 409–411 (2008).

93. Branstetter, J. W., Yarbrough, A. & Poole, C. Management of Cepacia Syndrome With a Combination of Intravenous and Inhaled Antimicrobials in a Non-Cystic Fibrosis Pediatric Patient. *J. Pediatr. Pharmacol. Ther.* **25**, 730–734 (2020).

94. Goodlet, K. J. *et al.* Successful Lung Re-transplant in a Patient with Cepacia Syndrome

due to Burkholderia ambifaria. *J. Cyst. Fibros.* **18**, e1–e4 (2019).

95. Nash, E. F. *et al.* Survival of Burkholderia cepacia sepsis following lung transplantation in recipients with cystic fibrosis. *Transpl. Infect. Dis.* **12**, 551–554 (2010).

96. Kazachkov, M., Lager, J., Lipuma, J. & Barker, P. M. Survival following Burkholderia cepacia sepsis in a patient with cystic fibrosis treated with corticosteroids. *Pediatr. Pulmonol.* **32**, 338–340 (2001).

97. Drevinek, P. & Mahenthiralingam, E. Burkholderia cenocepacia in cystic fibrosis: epidemiology and molecular mechanisms of virulence. *Clin. Microbiol. Infect.* **16**, 821–830 (2010).

98. Marciano, B. E. *et al.* Common Severe Infections in Chronic Granulomatous Disease. *Clin. Infect. Dis. An Off. Publ. Infect. Dis. Soc. Am.* **60**, 1176 (2015).

99. Manglani, R., Sherman, E., Shengelia, A. & Epelbaum, O. Of onions and men: Report of cavitary community acquired pneumonia due to Burkholderia cepacia complex in an immunocompetent patient and review of the literature. *Monaldi Arch. Chest Dis.* **90**, 557–560 (2020).

100. Taplin, D., Bassett, D. C. J. & Mertz, P. M. Foot lesions associated with Pseudomonas cepacia. *Lancet* **298**, 568–571 (1971).

101. Chiu, L. Q. & Wang, W. A case of unusual Gram-negative bacilli septic arthritis in an immunocompetent patient. *Singapore Med. J.* **54**, (2013).

102. Hamilton, J. *et al.* Successful treatment of Pseudomonas cepacia endocarditis with trimethoprim-sulfamethoxazole. *Antimicrob. Agents Chemother.* **4**, 551–554 (1973).

103. Dellalana, L. E. *et al.* A Unique Case of Burkholderia cepacia Prosthetic Mitral Valve Endocarditis and Literature Review. *Infect. Dis. Clin. Pract. (Baltim. Md).* **27**, 123–125

(2019).

104. Sabir, N. *et al.* Native valve dual pathogen endocarditis caused by Burkholderia cepacia and Aspergillus flavus - a case report. *JMM case reports* **5**, (2018).

105. Khan, M., Lalani, F. K., Ikram, A., Zaman, G. & Ahmed, P. Dual infection by Burkholderia cepacia and Pseudomonas putida in an infective endocarditis case. *J. Coll. Physicians Surg. Pakistan* **27**, 367–369 (2017).

106. Ghazal, S. S., Al-Mudaimeegh, K., Al Fakihi, E. M. & Asery, A. T. Outbreak of Burkholderia cepacia bacteremia in immunocompetent children caused by contaminated nebulized sulbutamol in Saudi Arabia. *Am. J. Infect. Control* **34**, 394–398 (2006).

107. Saratziotis, A., Zanotti, C., Baldovin, M., Prosenikliev, V. & Emanuelli, E. Burkholderia Cepacia Causes Frontal Mucopyocele with Anterior Cranial Fossa Extension: A Novel Case Report. *Iran. J. Otorhinolaryngol.* **33**, 327–332 (2021).

108. Stettler, G. R., Preslaski, C., Lawless, R., Cohen, M. & Platnick, B. Burkholderia Cepacia Infection in an Immunocompetent Patient Following Pancreaticoduodenectomy. *Am. Surg.* (2020). doi:10.1177/0003134820971625

109. Saran, S., Azim, A. & Gurjar, M. Multidrug-resistant Burkholderia cepacia bacteremia in an immunocompetent adult diagnosed with dengue and scrub coinfection: A rare case report. *Int. J. Crit. Illn. Inj. Sci.* **8**, 173–175 (2018).

110. Ranjan, R., Chowdhary, P. & Kamra, A. Community Acquired Burkholderia cepacia Bacteraemia Presenting as MODS in an Immunocompetent Individual: An Unusual Case. *J. Clin. Diagn. Res.* **11**, DD01–DD02 (2017).

111. Murugesan, M. *et al.* Diagnostic methods and identification challenges experienced in a Burkholderia contaminans outbreak occurred in a tertiary care centre. *Indian J. Med.*

Microbiol. **39**, 192–195 (2021).

112. Ishtiaq, R. *et al.* Ceftazidime-Resistant Burkholderia Cepacia: An Unusual Case in a Pregnant Patient. *Cureus* **9**, (2017).

113. Batura, D., Boakes, E., Hashemzehi, T. & Khanna, P. Burkholderia cenocepacia urosepsis with a perinephric haematoma in an immunocompetent patient with ureteral calculus obstruction. *https://doi.org/10.12968/hmed.2020.0648* **82**, (2021).

114. Rasmussen, M. & Oldberg, K. Febrile urinary tract infection in an immunocompetent male caused by Burkholderia multivorans- evidence of transmission in a home hot tub. *IDCases* **17**, (2019).

115. Miryala, R., Marathe, N., Mallepally, A. R., Das, K. & Mohapatra, B. Iatrogenic postoperative spondylodiscitis attributed to Burkholderia cepacia infection in an immunocompetent patient. *Surg. Neurol. Int.* **12**, (2021).

116. Hammoud, M., Fares, Y., Atoui, R. & Dabboucy, B. Burkholderia cepacia as a cause of pyogenic spondylodiscitis in immunocompetent patients: a single-institution case series and literature review. *J. spine Surg. (Hong Kong)* **5**, 372–377 (2019).

117. Zhai, Y., DeSear, K. E., Cherabuddi, K., Morris, J. G. & Jeong, K. C. Draft Genome Sequence of a Burkholderia cepacia Complex Strain Isolated from a Human Intra-abdominal Abscess. *Microbiol. Resour. Announc.* **10**, (2021).

118. Sun, L. *et al.* The emergence of a highly transmissible lineage of cbl+ Pseudomonas (Burkholderia) cepacia causing CF centre epidemics in North America and Britain. *Nat. Med.* **1**, 661–666 (1995).

119. Cystic Fibrosis Canada. *The Canadian Cystic Fibrosis Registry 2020 Annual Data Report*. (2022).

120. Matsui, H. *et al.* Evidence for periciliary liquid layer depletion, not abnormal ion composition, in the pathogenesis of cystic fibrosis airways disease. *Cell* **95**, 1005–1015 (1998).

121. Robinson, M. & Bye, P. T. B. Mucociliary clearance in cystic fibrosis. *Pediatr. Pulmonol.* **33**, 293–306 (2002).

122. Coenye, T. *et al.* Burkholderia cepacia genomovar VI, a new member of the Burkholderia cepacia complex isolated from cystic fibrosis patients. *Int. J. Syst. Evol. Microbiol.* **51**, 271–279 (2001).

123. Holden, M. T. G. *et al.* The genome of Burkholderia cenocepacia J2315, an epidemic pathogen of cystic fibrosis patients. *J. Bacteriol.* **91**, 261–277 (2009).

124. Speert, D. P., Henry, D., Vandamme, P., Corey, M. & Mahenthiralingam, E. Epidemiology of Burkholderia cepacia Complex in Patients with Cystic Fibrosis, Canada. *Emerg. Infect. Dis.* **8**, 181 (2002).

125. Zlosnik, J. E. A. *et al.* Epidemiology of burkholderia infections in people with cystic fibrosis in Canada between 2000 and 2017. *Ann. Am. Thorac. Soc.* **17**, 1549–1557 (2020).

126. Dentini, P. *et al.* Burkholderia cepacia complex in cystic fibrosis in a Brazilian reference center. *Med. Microbiol. Immunol.* **206**, 447–461 (2017).

127. LiPuma, J. J. The Changing Microbial Epidemiology in Cystic Fibrosis. *Clin. Microbiol. Rev.* **23**, 299 (2010).

128. Kenna, D. T. D. *et al.* Prevalence of Burkholderia species, including members of Burkholderia cepacia complex, among UK cystic and non-cystic fibrosis patients. *J. Med. Microbiol.* **66**, 490–501 (2017).

129. Jones, A. M. *et al.* Burkholderia cenocepacia and Burkholderia multivorans: influence on

survival in cystic fibrosis. *Thorax* **59**, 948 (2004).

130. Zlosnik, J. E. A. *et al.* Burkholderia species infections in patients with cystic fibrosis in British Columbia, Canada. 30 years' experience. *Ann. Am. Thorac. Soc.* **12**, 70–78 (2015).

131. LiPuma, J. J., Spilker, T., Coenye, T. & Gonzalez, C. F. An epidemic Burkholderia cepacia complex strain identified in soil. *Lancet (London, England)* **359**, 2002–2003 (2002).

132. Peeters, C., Depoorter, E., Praet, J. & Vandamme, P. Extensive cultivation of soil and water samples yields various pathogens in patients with cystic fibrosis but not Burkholderia multivorans. *J. Cyst. Fibros.* **15**, 769–775 (2016).

133. Tavares, M., Kozak, M., Balola, A. & Sá-Correia, I. Burkholderia cepacia complex bacteria: A feared contamination risk in water-based pharmaceutical products. *Clin. Microbiol. Rev.* **33**, (2020).

134. Lupo, A., Isis, E., Perreten, V. & Endimiani, A. Raw meat contaminated with epidemic clones of Burkholderia multivorans found in cystic fibrosis patients. *J. Cyst. Fibros.* **14**, 150–152 (2015).

135. Chiarini, L., Bevivino, A., Dalmastri, C., Tabacchioni, S. & Visca, P. Burkholderia cepacia complex species: health hazards and biotechnological potential. *Trends Microbiol.* **14**, 277–286 (2006).

136. Parke, J. L. & Gurian-Sherman, D. Diversity of the burkholderia cepacia complex and implications for risk assessment of biological control strains. *Annu. Rev. Phytopathol.* **39**, 225–258 (2001).

137. Boucher, R. C. Cystic fibrosis: a disease of vulnerability to airway surface dehydration. *Trends Mol. Med.* **13**, 231–240 (2007).

138. O'Sullivan, B. P. & Freedman, S. D. Cystic fibrosis. *Lancet* **373**, 1891–1904 (2009).

139. Casadevall, A. & Pirofski, L. A. Virulence factors and their mechanisms of action: the view from a damage-response framework. *J. Water Health* **7 Suppl 1**, (2009).

140. Granato, E. T., Harrison, F., Kümmerli, R. & Ross-Gillespie, A. Do bacterial 'virulence factors' always increase virulence? A meta-analysis of pyoverdine production in Pseudomonas aeruginosa as a test case. *Front. Microbiol.* **7**, 1952 (2016).

141. Pfeiffer, R. Untersuchungen über das Choleragift. *Zeitschrift für Hyg. und Infekt.* **11**, 393–411 (1892).

142. Cavaillon, J. M. Exotoxins and endotoxins: Inducers of inflammatory cytokines. *Toxicon* **149**, 45–53 (2018).

143. Whitfield, C. & Stephen Trent, M. Biosynthesis and Export of Bacterial Lipopolysaccharides*. *http://dx.doi.org.login.ezproxy.library.ualberta.ca/10.1146/annurev-biochem-060713-035600* **83**, 99–128 (2014).

144. Maldonado, R. F., Sá-Correia, I. & Valvano, M. A. Lipopolysaccharide modification in Gram-negative bacteria during chronic infection. *FEMS Microbiol. Rev.* **40**, 480 (2016).

145. Ortega, X. *et al.* Biosynthesis and structure of the Burkholderia cenocepacia K56-2 lipopolysaccharide core oligosaccharide: Truncation of the core oligosaccharide leads to increased binding and sensitvity to polymyxin B. *J. Biol. Chem.* **284**, 21738–21751 (2009).

146. Loutet, S. A., Flannagan, R. S., Kooi, C., Sokol, P. A. & Valvano, M. A. A complete lipopolysaccharide inner core oligosaccharide is required for resistance of Burkholderia cenocepacia to antimicrobial peptides and bacterial survival in vivo. *J. Bacteriol.* **188**,

2073–2080 (2006).

147. Walport, M. J. Complement. First of two parts. *N. Engl. J. Med.* **344**, 1058–66 (2001).

148. Chadha, J., Harjai, K. & Chhibber, S. Revisiting the virulence hallmarks of Pseudomonas aeruginosa: a chronicle through the perspective of quorum sensing. *Environ. Microbiol.* (2021). doi:10.1111/1462-2920.15784

149. Josenhans, C. & Suerbaum, S. The role of motility as a virulence factor in bacteria. *Int. J. Med. Microbiol.* **291**, 605–614 (2002).

150. Soutourina, O. A. & Bertin, P. N. Regulation cascade of flagellar expression in Gram-negative bacteria. *FEMS Microbiol. Rev.* **27**, 505–523 (2003).

151. Wilson, J. W. *et al.* Mechanisms of bacterial pathogenicity. *Postgrad. Med. J.* **78**, 216–224 (2002).

152. Craig, L., Pique, M. E. & Tainer, J. A. Type IV pilus structure and bacterial pathogenicity. *Nat. Rev. Microbiol.* **2**, 363–378 (2004).

153. Tomich, M. & Mohr, C. D. Adherence and autoaggregation phenotypes of a Burkholderia cenocepacia cable pilus mutant. *FEMS Microbiol. Lett.* **228**, 287–297 (2003).

154. Lemichez, E. & Barbieri, J. T. General Aspects and Recent Advances on Bacterial Protein Toxins. *Cold Spring Harb. Perspect. Med.* **3**, (2013).

155. Cox, G. M., Mukherjee, J., Cole, G. T., Casadevall, A. & Perfect, J. R. Urease as a virulence factor in experimental cryptococcosis. *Infect. Immun.* **68**, 443–448 (2000).

156. Francis, J., Macturk, H. M., Madinaveitia, J. & Snow, G. A. Mycobactin, a growth factor for Mycobacterium johnei. I. Isolation from Mycobacterium phlei. *Biochem. J.* **55**, 596–607 (1953).

157. Holden, V. I. & Bachman, M. A. Diverging roles of bacterial siderophores during

infection. *Metallomics* **7**, 986–995 (2015).

158. Costerton, J. W., Geesey, G. G. & Cheng, K. J. How bacteria stick. *Sci. Am.* **238**, 86–95 (1978).

159. Antunes, L. C. M. & Ferreira, R. B. R. Biofilms and bacterial virulence. *Rev. Res. Med. Microbiol.* **22**, 12–16 (2011).

160. Schulze, A., Mitterer, F., Pombo, J. P. & Schild, S. Biofilms by bacterial human pathogens: Clinical relevance - development, composition and regulation - therapeutical strategies. *Microb. Cell* **8**, 28 (2021).

161. Fux, C. A., Costerton, J. W., Stewart, P. S. & Stoodley, P. Survival strategies of infectious biofilms. *Trends Microbiol.* **13**, 34–40 (2005).

162. Hall-Stoodley, L. & Stoodley, P. Evolving concepts in biofilm infections. *Cell. Microbiol.* **11**, 1034–1043 (2009).

163. Penesyan, A., Paulsen, I. T., Gillings, M. R., Kjelleberg, S. & Manefield, M. J. Secondary Effects of Antibiotics on Microbial Biofilms. *Front. Microbiol.* **11**, 2109 (2020).

164. Hoffman, L. R. *et al.* Aminoglycoside antibiotics induce bacterial biofilm formation. *Nature* **436**, 1171–1175 (2005).

165. Green, E. R. & Mecsas, J. Bacterial Secretion Systems – An overview. *Microbiol. Spectr.* **4**, (2016).

166. Depluverez, S., Devos, S. & Devreese, B. The Role of Bacterial Secretion Systems in the Virulence of Gram-Negative Airway Pathogens Associated with Cystic Fibrosis. *Front. Microbiol.* **7**, 1336 (2016).

167. Palmer, T., Finney, A. J., Saha, C. K., Atkinson, G. C. & Sargent, F. A holin/peptidoglycan hydrolase-dependent protein secretion system. *Mol. Microbiol.* **115**,

345–355 (2021).

168. Grossman, A. S., Mauer, T. J., Forest, K. T. & Goodrich-Blair, H. A Widespread Bacterial Secretion System with Diverse Substrates. *MBio* **12**, (2021).

169. Lasica, A. M., Ksiazek, M., Madej, M. & Potempa, J. The Type IX Secretion System (T9SS): Highlights and Recent Insights into Its Structure and Function. *Front. Cell. Infect. Microbiol.* **7**, 215 (2017).

170. Vance, R. E., Isberg, R. R. & Portnoy, D. A. Patterns of pathogenesis: discrimination of pathogenic and non-pathogenic microbes by the innate immune system. *Cell Host Microbe* **6**, 10 (2009).

171. Rutherford, S. T. & Bassler, B. L. Bacterial Quorum Sensing: Its Role in Virulence and Possibilities for Its Control. *Cold Spring Harb. Perspect. Med.* **2**, (2012).

172. Ng, W. L. & Bassler, B. L. Bacterial Quorum-Sensing Network Architectures. *Annu. Rev. Genet.* **43**, 197 (2009).

173. Pena, R. T. *et al.* Relationship between quorum sensing and secretion systems. *Front. Microbiol.* **10**, 1100 (2019).

174. Tateda, K. *et al.* The Pseudomonas aeruginosa autoinducer N-3-oxododecanoyl homoserine lactone accelerates apoptosis in macrophages and neutrophils. *Infect. Immun.* **71**, 5785–5793 (2003).

175. Wu, H., Song, Z., Givskov, M. & Høiby, N. Effects of quorum-sensing on immunoglobulin G responses in a rat model of chronic lung infection with Pseudomonas aeruginosa. *Microbes Infect.* **6**, 34–37 (2004).

176. Chun, C. K., Ozer, E. A., Welsh, M. J., Zabner, J. & Greenberg, E. P. Inactivation of a Pseudomonas aeruginosa quorum-sensing signal by human airway epithelia. *Proc. Natl.*

Acad. Sci. U. S. A. **101**, 3587–3590 (2004).

177. Paul, D., Gopal, J., Kumar, M. & Manikandan, M. Nature to the natural rescue: Silencing microbial chats. *Chem. Biol. Interact.* **280**, 86–98 (2018).

178. Beier, D. & Gross, R. Regulation of bacterial virulence by two-component systems. *Curr. Opin. Microbiol.* **9**, 143–152 (2006).

179. Tiwari, S. *et al.* Two-component signal transduction systems of pathogenic bacteria as targets for antimicrobial therapy: An overview. *Front. Microbiol.* **8**, 1878 (2017).

180. Ferber, S. & Karnath, H.-O. Papyrus of Ebers and Smith. *J. Neurol. Neurosurg. Psychiatry* **67**, 578–578 (1999).

181. Gelpi, A., Gilbertson, A. & Tucker, J. D. Magic bullet: Paul Ehrlich, Salvarsan and the birth of venereology. *Sex. Transm. Infect.* **91**, 68–69 (2015).

182. Hutchings, M., Truman, A. & Wilkinson, B. Antibiotics: past, present and future. *Curr. Opin. Microbiol.* **51**, 72–80 (2019).

183. Ventola, C. L. The Antibiotic Resistance Crisis: Part 1: Causes and Threats. *Pharm. Ther.* **40**, 277 (2015).

184. O'Neill, J. *Tackling Drug-resistant Infections Globally: Final Report And Recommendations*. (2016).

185. Council of Canadian Academies. *When Antibiotics Fail*. (2019).

186. Murray, C. J. *et al.* Global burden of bacterial antimicrobial resistance in 2019: a systematic analysis. *Lancet* **399**, 629–655 (2022).

187. McMurry, L., Petrucci, R. E. & Levy, S. B. Active efflux of tetracycline encoded by four genetically different tetracycline resistance determinants in Escherichia coli. *Proc. Natl. Acad. Sci. U. S. A.* **77**, 3974–3977 (1980).

188. Blanco, P. *et al.* Bacterial Multidrug Efflux Pumps: Much More Than Antibiotic Resistance Determinants. *Microorganisms* **4**, (2016).

189. George, A. M. & Levy, S. B. Amplifiable resistance to tetracycline, chloramphenicol, and other antibiotics in Escherichia coli: involvement of a non-plasmid-determined efflux of tetracycline. *J. Bacteriol.* **155**, 531 (1983).

190. Hirakata, Y. *et al.* Multidrug Efflux Systems Play an Important Role in the Invasiveness of Pseudomonas aeruginosa. *J. Exp. Med.* **196**, 109 (2002).

191. Evans, K. *et al.* Influence of the MexAB-OprM Multidrug Efflux System on Quorum Sensing in Pseudomonas aeruginosa. *J. Bacteriol.* **180**, 5443 (1998).

192. Cox, G. & Wright, G. D. Intrinsic antibiotic resistance: Mechanisms, origins, challenges and solutions. *Int. J. Med. Microbiol.* **303**, 287–292 (2013).

193. Vaara, M. Agents that increase the permeability of the outer membrane. *Microbiol. Rev.* **56**, 395–411 (1992).

194. Obst, S., Kastowsky, M. & Bradaczek, H. Molecular dynamics simulations of six different fully hydrated monomeric conformers of Escherichia coli re-lipopolysaccharide in the presence and absence of Ca2+. *Biophys. J.* **72**, 1031–1046 (1997).

195. Decad, G. M. & Nikaido, H. Outer membrane of gram negative bacteria. XII. Molecular sieving function of cell wall. *J. Bacteriol.* **128**, 325–336 (1976).

196. Nikaido, H., Rosenberg, E. Y. & Foulds, J. Porin channels in Escherichia coli: Studies with β-lactams in intact cells. *J. Bacteriol.* **153**, 232–240 (1983).

197. Cowan, S. *et al.* Crystal structures explain functional properties of two E. coli porins. *nature.com* (1992).

198. Blair, J. M. A., Webber, M. A., Baylay, A. J., Ogbolu, D. O. & Piddock, L. J. V.

Molecular mechanisms of antibiotic resistance. *Nat. Rev. Microbiol. 2014 131* **13**, 42–51 (2014).

199. Rhodes, K. A. & Schweizer, H. P. Antibiotic Resistance in Burkholderia Species. *Drug Resist. Updat.* **28**, 82 (2016).

200. Beceiro, A. *et al.* Phosphoethanolamine modification of lipid A in colistin-resistant variants of Acinetobacter baumannii mediated by the pmrAB two-component regulatory system. *Antimicrob. Agents Chemother.* **55**, 3370–3379 (2011).

201. Wilson, D. N., Hauryliuk, V., Atkinson, G. C. & O'Neill, A. J. Target protection as a key antibiotic resistance mechanism. *Nat. Rev. Microbiol. 2020 1811* **18**, 637–648 (2020).

202. Vetting, M. W. *et al.* Structure of QnrB1, a plasmid-mediated fluoroquinolone resistance factor. *J. Biol. Chem.* **286**, 25265–25273 (2011).

203. Tran, J. H., Jacoby, G. A. & Hooper, D. C. Interaction of the Plasmid-Encoded Quinolone Resistance Protein QnrA with Escherichia coli Topoisomerase IV. *Antimicrob. Agents Chemother.* **49**, 3050 (2005).

204. Tran, J. H., Jacoby, G. A. & Hooper, D. C. Interaction of the Plasmid-Encoded Quinolone Resistance Protein Qnr with Escherichia coli DNA Gyrase. *Antimicrob. Agents Chemother.* **49**, 118 (2005).

205. Vega, N. M. & Gore, J. Collective antibiotic resistance: mechanisms and implications. *Curr. Opin. Microbiol.* **21**, 28–34 (2014).

206. Peterson, E. & Kaur, P. Antibiotic resistance mechanisms in bacteria: Relationships between resistance determinants of antibiotic producers, environmental bacteria, and clinical pathogens. *Front. Microbiol.* **9**, 2928 (2018).

207. Sabnis, A., Ledger, E. V. K., Pader, V. & Edwards, A. M. Antibiotic interceptors:

Creating safe spaces for bacteria. *PLOS Pathog.* **14**, e1006924 (2018).

208. Herrmann, M., Nkuiya, B. & Dussault, A. R. Innovation and antibiotic use within antibiotic classes: Market incentives and economic instruments. *Resour. Energy Econ.* **35**, 582–598 (2013).

209. da Cunha, B. R., Fonseca, L. P. & Calado, C. R. C. Antibiotic Discovery: Where Have We Come from, Where Do We Go? *Antibiot. 2019, Vol. 8, Page 45* **8**, 45 (2019).

210. Wang, Z. *et al.* A naturally inspired antibiotic to target multidrug-resistant pathogens. *Nat. 2022 6017894* **601**, 606–611 (2022).

211. Opal, S. M. Non-antibiotic treatments for bacterial diseases in an era of progressive antibiotic resistance. *Crit. Care* **20**, 1–3 (2016).

212. Liu, Y. Y. *et al.* Emergence of plasmid-mediated colistin resistance mechanism MCR-1 in animals and human beings in China: a microbiological and molecular biological study. *Lancet Infect. Dis.* **16**, 161–168 (2016).

213. Hinchliffe, S., Butcher, A. & Rahman, M. M. The AMR problem: demanding economies, biological margins, and co-producing alternative strategies. *Palgrave Commun. 2018 41* **4**, 1–12 (2018).

214. Kumar, M. *et al.* Futuristic Non-antibiotic Therapies to Combat Antibiotic Resistance: A Review. *Front. Microbiol.* **12**, 16 (2021).

215. Pacios, O. *et al.* Strategies to Combat Multidrug-Resistant and Persistent Infectious Diseases. *Antibiotics* **9**, (2020).

216. Czaplewski, L. *et al.* Alternatives to antibiotics—a pipeline portfolio review. *Lancet Infect. Dis.* **16**, 239–251 (2016).

217. Fischetti, V. A. Phage lysins: Novel alternative to antibiotics. *Phage Ther. A Pract.*

Approach 317–334 (2019). doi:10.1007/978-3-030-26736-0_12

218. Loc-Carrillo, C. & Abedon, S. T. Pros and cons of phage therapy. *Bacteriophage* **1**, 111–114 (2011).

219. Semler, D. D., Lynch, K. H. & Dennis, J. J. The Promise of Bacteriophage Therapy for Burkholderia cepacia Complex Respiratory Infections. *Front. Cell. Infect. Microbiol.* **1**, 27 (2012).

220. Wang, G., Zarodkiewicz, P. & Valvano, M. A. Current Advances in Burkholderia Vaccines Development. *Cells* **9**, (2020).

221. Gordillo Altamirano, F. L. & Barr, J. J. Phage therapy in the postantibiotic era. *Clinical Microbiology Reviews* **32**, (2019).

222. Abedon, S. T., Kuhl, S. J., Blasdel, B. G. & Kutter, E. M. Phage treatment of human infections. *Bacteriophage* **1**, 66–85 (2011).

223. Shen, Y. & Loessner, M. J. Beyond antibacterials – exploring bacteriophages as antivirulence agents. *Curr. Opin. Biotechnol.* **68**, 166–173 (2021).

224. Comeau, A. M., Tétart, F., Trojet, S. N., Prère, M. F. & Krisch, H. M. Phage-antibiotic synergy (PAS): β-lactam and quinolone antibiotics stimulate virulent phage growth. *PLoS One* **2**, (2007).

225. Kamal, F. & Dennis, J. J. Burkholderia cepacia complex phage-antibiotic synergy (PAS): Antibiotics stimulate lytic phage activity. *Appl. Environ. Microbiol.* **81**, 1132–1138 (2015).

226. Ryan, E. M., Alkawareek, M. Y., Donnelly, R. F. & Gilmore, B. F. Synergistic phage-antibiotic combinations for the control of Escherichia coli biofilms in vitro. *FEMS Immunol. Med. Microbiol.* **65**, 395–398 (2012).

227. Chaudhry, W. N. *et al.* Synergy and order effects of antibiotics and phages in killing pseudomonas aeruginosa biofilms. *PLoS One* **12**, (2017).

228. Kim, M. *et al.* Phage-Antibiotic Synergy via Delayed Lysis. *Appl. Environ. Microbiol.* **84**, (2018).

229. Davis, C. M., McCutcheon, J. G. & Dennis, J. J. Aztreonam Lysine Increases the Activity of Phages E79 and phiKZ against Pseudomonas aeruginosa PA01. *Microorganisms* **9**, 152 (2021).

230. Torres-Barceló, C. & Hochberg, M. E. Evolutionary Rationale for Phages as Complements of Antibiotics. *Trends Microbiol.* **24**, 249–256 (2016).

231. Anonymous Editorial. Wanted: A reward for antibiotic development. *Nat. Biotechnol.* **36**, 555 (2018).

232. Trend, S., Chang, B. J., O'Dea, M., Stick, S. M. & Kicic, A. Use of a primary epithelial cell screening tool to investigate phage therapy in cystic fibrosis. *Front. Pharmacol.* **9**, (2018).

233. Holloway, B. W. Genetic Recombination in Pseudomonas aeruginosa. *Microbiology* **13**, 572–581 (1955).

234. Holloway, B. W., Egan, J. B. & Monk, M. Lysogeny in Pseudomonas aeruginosa. *Aust. J. Exp. Biol. Med. Sci.* **38**, 321–329 (1960).

235. Slayter, H. S., Holloway, B. W. & Hall, C. E. The structure of Pseudomonas aeruginosa phages B3, E79, and F116. *J. Ultrasructure Res.* **11**, 274–281 (1964).

236. Krylov, V. N. & Zhazykov, I. Z. Pseudomonas bacteriophage phiKZ--possible model for studying the genetic control of morphogenesis]. *Genetika* **14**, 678–85 (1978).

237. Kropinski, A. M., Mazzocco, A., Waddell, T. E., Lingohr, E. & Johnson, R. P.

Enumeration of bacteriophages by double agar overlay plaque assay. *Methods Mol. Biol.* **501**, 69–76 (2009).

238. McCutcheon, J., Peters, D. & Dennis, J. Identification and Characterization of Type IV Pili as the Cellular Receptor of Broad Host Range Stenotrophomonas maltophilia Bacteriophages DLP1 and DLP2. *Viruses* **10**, 338 (2018).

239. Hutchinson, D., Barclay, M., Prescott, W. A. & Brown, J. Inhaled aztreonam lysine: an evidence-based review. *Expert Opin. Pharmacother.* **14**, 2115–2124 (2013).

240. Wiegand, I., Hilpert, K. & Hancock, R. E. W. Agar and broth dilution methods to determine the minimal inhibitory concentration (MIC) of antimicrobial substances. *Nat. Protoc.* **3**, 163–175 (2008).

241. Schneider, C. A., Rasband, W. S. & Eliceiri, K. W. NIH Image to ImageJ: 25 years of image analysis. *Nat. Methods* **9**, 671–675 (2012).

242. Carlson, K., Kutter, E., Sulakvelidze, A. & Editors. Bacteriophages: Biology and Applications. in *Working with Bacteriophages: Common Techniques and Methodological Approaches* 437–494 (CRC Press, 2005).

243. Turnbull, L. & Whitchurch, C. B. Motility Assay: Twitching Motility. in 73–86 (Humana Press, New York, NY, 2014). doi:10.1007/978-1-4939-0473-0_9

244. Ha, D.-G., Kuchma, S. L. & O'Toole, G. A. Plate-Based Assay for Swimming Motility in Pseudomonas aeruginosa. in 59–65 (Humana Press, New York, NY, 2014). doi:10.1007/978-1-4939-0473-0_7

245. Bray, D. F., Bagu, J. & Koegler, P. Comparison of hexamethyldisilazane (HMDS), Peldri II, and critical-point drying methods for scanning electron microscopy of biological specimens. *Microsc. Res. Tech.* **26**, 489–95 (1993).

246. Yamagami, H. & Endo, H. Loss of lysis inhibition in filamentous Escherichia coli infected with wild-type bacteriophage T4. *J. Virol.* **3**, 343–9 (1969).

247. Santos, S. B. *et al.* The use of antibiotics to improve phage detection and enumeration by the double-layer agar technique. *BMC Microbiol.* **9**, 148 (2009).

248. Knezevic, P., Curcin, S., Aleksic, V., Petrusic, M. & Vlaski, L. Phage-antibiotic synergism: A possible approach to combatting Pseudomonas aeruginosa. *Res. Microbiol.* **164**, 55–60 (2013).

249. Hadas, H., Einav, M., Fishov, I. & Zaritsky, A. Bacteriophage T4 Development Depends on the Physiology of its Host Escherichia Coli. *Microbiology* **143**, 179–185 (1997).

250. Jarrell, K. & Kropinski, A. M. *Identification of the Cell Wall Receptor for Bacteriophage E79 in Pseudomonas aeruginosa Strain PAO*. *JOURNAL OF VIROLoGY* (1977).

251. Kaur, S., Harjai, K. & Chhibber, S. Methicillin-resistant Staphylococcus aureus phage plaque size enhancement using sublethal concentrations of antibiotics. *Appl. Environ. Microbiol.* **78**, 8227–8233 (2012).

252. Abedon, S. T., Herschler, T. D. & Stopar, D. Bacteriophage Latent-Period Evolution as a Response to Resource Availability. *Appl. Environ. Microbiol.* **67**, 4233–4241 (2001).

253. Krueger, A. P., Col-In, T., Smith, P. N. & Mcguire, C. D. Observations On The Effect Of Penicillin On The Reaction Between Phage And Staphylococci. *J. Gen. Physiol.* 477–488 (1948).

254. Price, W. H. Bacteriophage formation without bacterial growth; the effect of iodoacetate, fluoride, gramicidin, and azide on the formation of bacteriophage. *J. Gen. Physiol.* **31**, 135–139 (1947).

255. Price, W. H. Bacteriophage formation without bacterial growth; the effect of niacin and

yeast extract on phage formation and bacterial growth in the presence of penicillin. *J. Gen. Physiol.* **31**, 127–133 (1947).

256. Price, W. H. Bacteriophage formation without bacterial growth; formation of staphylococcus phage in the presence of bacteria inhibited by penicillin. *J. Gen. Physiol.* **31**, 119–126 (1947).

257. Akturk, E. *et al.* Synergistic action of phage and antibiotics: Parameters to enhance the killing efficacy against mono and dual-species biofilms. *Antibiotics* **8**, (2019).

258. Chang, R. Y. K. *et al.* Bacteriophage PEV20 and Ciprofloxacin Combination Treatment Enhances Removal of Pseudomonas aeruginosa Biofilm Isolated from Cystic Fibrosis and Wound Patients. *AAPS J.* **21**, (2019).

259. Coulter, L. B., McLean, R. J. C., Rohde, R. E. & Aron, G. M. Effect of bacteriophage infection in combination with tobramycin on the emergence of resistance in Escherichia coli and Pseudomonas aeruginosa biofilms. *Viruses* **6**, 3778–3786 (2014).

260. Henriksen, K. *et al.* P. Aeruginosa flow-cell biofilms are enhanced by repeated phage treatments but can be eradicated by phage–ciprofloxacin combination —monitoring the phage–P. Aeruginosa biofilms interactions. *Pathog. Dis.* **77**, (2019).

261. Moulton-Brown, C. E. & Friman, V. P. Rapid evolution of generalized resistance mechanisms can constrain the efficacy of phage–antibiotic treatments. *Evol. Appl.* **11**, 1630–1641 (2018).

262. Nouraldin, A. A. M., Baddour, M. M., Harfoush, R. A. H. & Essa, S. A. M. Bacteriophage-antibiotic synergism to control planktonic and biofilm producing clinical isolates of Pseudomonas aeruginosa. *Alexandria J. Med.* **52**, 99–105 (2016).

263. Tkhilaishvili, T., Winkler, T., Müller, M., Perka, C. & Trampuz, A. Bacteriophages as

Adjuvant to Antibiotics for the Treatment of Periprosthetic Joint Infection Caused by Multidrug-Resistant Pseudomonas aeruginosa. *Antimicrob. Agents Chemother.* **64**, (2020).

264. Tkhilaishvili, T., Wang, L., Perka, C., Trampuz, A. & Gonzalez Moreno, M. Using Bacteriophages as a Trojan Horse to the Killing of Dual-Species Biofilm Formed by Pseudomonas aeruginosa and Methicillin Resistant Staphylococcus aureus. *Front. Microbiol.* **11**, (2020).

265. Uchiyama, J. *et al.* Piperacillin and ceftazidime produce the strongest synergistic phage–antibiotic effect in Pseudomonas aeruginosa. *Arch. Virol.* **163**, 1941–1948 (2018).

266. Donlan, R. M. Biofilms: microbial life on surfaces. *Emerg. Infect. Dis.* **8**, 881–90 (2002).

267. Braga, P. C., Sasso, M. D. & Sala, M. T. Sub-MIC concentrations of cefodizime interfere with various factors affecting bacterial virulence. *J. Antimicrob. Chemother.* **45**, 15–25 (2000).

268. de Andrade, J. P. L. *et al.* Sub-Inhibitory Concentration of Piperacillin–Tazobactam May be Related to Virulence Properties of Filamentous Escherichia coli. *Curr. Microbiol.* **72**, 19–28 (2016).

269. Drago, L. *et al.* Activity of levofloxacin and ciprofloxacin against urinary pathogens. *J. Antimicrob. Chemother.* **48**, 37–45 (2001).

270. Fonseca, A. P., Extremina, C., Fonseca, A. F. & Sousa, J. C. Effect of subinhibitory concentration of piperacillin/ tazobactam on Pseudomonas aeruginosa. *J. Med. Microbiol.* **53**, 903–910 (2004).

271. Fonseca, A. P. & Sousa, J. C. Effect of antibiotic-induced morphological changes on surface properties, motility and adhesion of nosocomial Pseudomonas aeruginosa strains under different physiological states. *J. Appl. Microbiol.* **103**, 1828–1837 (2007).

272. Wolter, J. M. & McCormack, J. G. The effect of subinhibitory concentrations of antibiotics on adherence of Pseudomonas aeruginosa to cystic fibrosis (CF) and non-CF-affected tracheal epithelial cells. *J. Infect.* **37**, 217–23 (1998).

273. Bradley, D. E. A function of Pseudomonas aeruginosa PAO polar pili: twitching motility. *Can. J. Microbiol.* **26**, 146–54 (1980).

274. Burrows, L. L. *Pseudomonas aeruginosa* Twitching Motility: Type IV Pili in Action. *Annu. Rev. Microbiol.* **66**, 493–520 (2012).

275. Campodónico, V. L. *et al.* Evaluation of flagella and flagellin of Pseudomonas aeruginosa as vaccines. *Infect. Immun.* **78**, 746–55 (2010).

276. Liu, Z. *et al.* Antibiotics at subinhibitory concentrations improve the quorum sensing behavior of Chromobacterium violaceum. *FEMS Microbiol. Lett.* **341**, 37–44 (2013).

277. Danis-Wlodarczyk, K. *et al.* A proposed integrated approach for the preclinical evaluation of phage therapy in Pseudomonas infections. *Sci. Rep.* **6**, (2016).

278. Sousa, A. M. & Olí Via Pereira, M. Pseudomonas aeruginosa Diversification during Infection Development in Cystic Fibrosis Lungs—A Review. *Pathogens* **3**, 680–703 (2014).

279. Chhibber, S., Kaur, T. & Sandeep Kaur, S. Co-Therapy Using Lytic Bacteriophage and Linezolid: Effective Treatment in Eliminating Methicillin Resistant Staphylococcus aureus (MRSA) from Diabetic Foot Infections. *PLoS One* **8**, e56022 (2013).

280. Jo, A., Ding, T. & Ahn, J. Synergistic antimicrobial activity of bacteriophages and antibiotics against Staphylococcus aureus. *Food Sci. Biotechnol.* **25**, 935–940 (2016).

281. Jo, A., Kim, J., Ding, T. & Ahn, J. Role of phage-antibiotic combination in reducing antibiotic resistance in Staphylococcus aureus. *Food Sci. Biotechnol.* **25**, 1211–1215

(2016).

282. Kirby, A. E. Synergistic Action of Gentamicin and Bacteriophage in a Continuous Culture Population of Staphylococcus aureus. *PLoS One* **7**, (2012).

283. Lin, Y. *et al.* Inhalable combination powder formulations of phage and ciprofloxacin for P. aeruginosa respiratory infections. *Eur. J. Pharm. Biopharm.* **142**, 543–552 (2019).

284. Lin, Y. *et al.* Synergy of nebulized phage PEV20 and ciprofloxacin combination against Pseudomonas aeruginosa. *Int. J. Pharm.* **551**, 158–165 (2018).

285. Shlezinger, M., Coppenhagen-Glazer, S., Gelman, D., Beyth, N. & Hazan, R. Eradication of Vancomycin-Resistant Enterococci by Combining Phage and Vancomycin. *Viruses* **11**, (2019).

286. Torres-Barceló, C. *et al.* A Window of Opportunity to Control the Bacterial Pathogen Pseudomonas aeruginosa Combining Antibiotics and Phages. *PLoS One* **9**, e106628 (2014).

287. Verma, V., Harjai, K. & Chhibber, S. Restricting ciprofloxacin-induced resistant variant formation in biofilm of Klebsiella pneumoniae B5055 by complementary bacteriophage treatment. *J. Antimicrob. Chemother.* **64**, 1212–1218 (2009).

288. Chan, B. K. *et al.* Phage selection restores antibiotic sensitivity in MDR Pseudomonas aeruginosa. *Sci. Rep.* **6**, 1–8 (2016).

289. Zhang, Q. G. & Buckling, A. Phages limit the evolution of bacterial antibiotic resistance in experimental microcosms. *Evol. Appl.* **5**, 575–582 (2012).

290. Seed, K. D. & Dennis, J. J. Isolation and characterization of bacteriophages of the Burkholderia cepacia complex. *FEMS Microbiol. Lett.* **251**, 273–280 (2005).

291. Mahenthiralingam, E. *et al.* Diagnostically and Experimentally Useful Panel of Strains

from the Burkholderia cepacia Complex. *J. Clin. Microbiol.* **38**, 910–913 (2000).

292. Gonzalez, C. F., Pettit, E. A., Valadez, V. A. & Provin, E. M. Mobilization, Cloning, and Sequence Determination of a Plasmid-Encoded Polygalacturonase from a Phytopathogenic Burkholderia (Pseudomonas) cepacia. *http://dx.doi.org/10.1094/MPMI.1997.10.7.840* **10**, 840–851 (1997).

293. McKenney, D., Brown, K. E. & Allison, D. G. Influence of Pseudomonas aeruginosa exoproducts on virulence factor production in Burkholderia cepacia: evidence of interspecies communication. *J. Bacteriol.* **177**, 6989 (1995).

294. Cheng, H. P. & Lessie, T. G. Multiple replicons constituting the genome of Pseudomonas cepacia 17616. *J. Bacteriol.* **176**, 4034–4042 (1994).

295. Gaffney, T. D. & Lessie, T. G. Insertion-sequence-dependent rearrangements of Pseudomonas cepacia plasmid pTGL1. *J. Bacteriol.* **169**, 224–230 (1987).

296. Chu, K. K., Davidson, D. J., Halsey, T. K., Chung, J. W. & Speert, D. P. Differential persistence among genomovars of the Burkholderia cepacia complex in a murine model of pulmonary infection. *Infect. Immun.* **70**, 2715–2720 (2002).

297. Whiteford, M. L. *et al.* Outcome of Burkholderia (Pseudomonas) cepacia colonisation in children with cystic fibrosis following a hospital outbreak. *Thorax* **50**, 1194–1198 (1995).

298. Mahenthiralingam, E., Campbell, M. E., Henry, D. A. & Speert, D. P. Epidemiology of Burkholderia cepacia infection in patients with cystic fibrosis: analysis by randomly amplified polymorphic DNA fingerprinting. *J. Clin. Microbiol.* **34**, 2914–2920 (1996).

299. Revets, H. *et al.* Burkholderia (Pseudomonas) cepacia and cystic fibrosis: the epidemiology in Belgium. *Acta Clin. Belg.* **51**, 222–230 (1996).

300. Lynch, K. H. & Dennis, J. J. Development of a species-specific fur gene-based method for

identification of the Burkholderia cepacia complex. *J. Clin. Microbiol.* **46**, 447–455 (2008).

301. McKevitt, A. I., Bajaksouzian, S., Klinger, J. D. & Woods, D. E. Purification and characterization of an extracellular protease from Pseudomonas cepacia. *Infect. Immun.* **57**, 771 (1989).

302. Mahenthiralingam, E., Simpson, D. A. & Speert, D. P. Identification and characterization of a novel DNA marker associated with epidemic Burkholderia cepacia strains recovered from patients with cystic fibrosis. *J. Clin. Microbiol.* **35**, 808 (1997).

303. Conway, B. A. D., Chu, K. K., Bylund, J., Altman, E. & Speert, D. P. Production of exopolysaccharide by Burkholderia cenocepacia results in altered cell-surface interactions and altered bacterial clearance in mice. *J. Infect. Dis.* **190**, 957–966 (2004).

304. Hutchison, M. L., Poxton, I. R. & Govan, J. R. W. Burkholderia cepacia Produces a Hemolysin That Is Capable of Inducing Apoptosis and Degranulation of Mammalian Phagocytes. *Infect. Immun.* **66**, 2033 (1998).

305. Lewenza, S., Conway, B., Greenberg, E. P. & Sokol, P. A. Quorum Sensing in Burkholderia cepacia: Identification of the LuxRI Homologs CepRI. *J. Bacteriol.* **181**, 748 (1999).

306. Balandreau, J. *et al.* Burkholderia cepacia genomovar III is a common plant-associated bacterium. *Appl. Environ. Microbiol.* **67**, 982–985 (2001).

307. LiPuma, J. J. *et al.* Ribotype analysis of Pseudomonas cepacia from cystic fibrosis treatment centers. *J. Pediatr.* **113**, 859–862 (1988).

308. Walsh, T. A. & Ballou, D. P. Halogenated protocatechuates as substrates for protocatechuate dioxygenase from Pseudomonas cepacia. *J. Biol. Chem.* **258**, 14413–

14421 (1983).

309. Burns, J. L. *et al.* Invasion of respiratory epithelial cells by Burkholderia (Pseudomonas) cepacia. *Infect. Immun.* **64**, 4054–4059 (1996).

310. Larsen, G. Y., Stull, T. L. & Burns, J. L. Marked phenotypic variability in Pseudomonas cepacia isolated from a patient with cystic fibrosis. *J. Clin. Microbiol.* **31**, 788 (1993).

311. Yeager, C. M., Bottomley, P. J., Arp, D. J. & Hyman, M. R. Inactivation of toluene 2-monooxygenase in Burkholderia cepacia G4 by alkynes. *Appl. Environ. Microbiol.* **65**, 632–639 (1999).

312. Coenye, T., Vandamme, P., LiPuma, J. J., Govan, J. R. W. & Mahenthiralingam, E. Updated Version of the Burkholderia cepacia Complex Experimental Strain Panel. *J. Clin. Microbiol.* **41**, 2797 (2003).

313. Mahenthiralingam, E., Baldwin, A. & Dowson, C. G. Burkholderia cepacia complex bacteria: opportunistic pathogens with important natural biology. *J. Appl. Microbiol.* **104**, 1539–1551 (2008).

314. Palleroni, N. J., Ballard, R. W., Ralston, E. & Doudoroff, M. Deoxyribonucleic acid homologies among some Pseudomonas species. *J. Bacteriol.* **110**, 1–11 (1972).

315. Yabannavar, A. V. & Zylstra, G. J. Cloning and characterization of the genes for p-nitrobenzoate degradation from Pseudomonas pickettii YH105. *Appl. Environ. Microbiol.* **61**, 4284–4290 (1995).

316. Bolger, A. M., Lohse, M. & Usadel, B. Trimmomatic: a flexible trimmer for Illumina sequence data. *Bioinformatics* **30**, 2114–2120 (2014).

317. Bankevich, A. *et al.* SPAdes: A new genome assembly algorithm and its applications to single-cell sequencing. *J. Comput. Biol.* **19**, 455–477 (2012).

318. Delcher, A. L., Bratke, K. A., Powers, E. C. & Salzberg, S. L. Identifying bacterial genes and endosymbiont DNA with Glimmer. *Bioinformatics* **23**, 673–679 (2007).

319. Hyatt, D. *et al.* Prodigal: Prokaryotic gene recognition and translation initiation site identification. *BMC Bioinformatics* **11**, 1–11 (2010).

320. Besemer, J., Lomsadze, A. & Borodovsky, M. GeneMarkS: a self-training method for prediction of gene starts in microbial genomes. Implications for finding sequence motifs in regulatory regions. *Nucleic Acids Res.* **29**, 2607 (2001).

321. Lu, S. *et al.* CDD/SPARCLE: the conserved domain database in 2020. *Nucleic Acids Res.* **48**, D265–D268 (2020).

322. Krogh, A., Larsson, B., Von Heijne, G. & Sonnhammer, E. L. L. Predicting transmembrane protein topology with a hidden Markov model: application to complete genomes. *J. Mol. Biol.* **305**, 567–580 (2001).

323. Teufel, F. *et al.* SignalP 6.0 predicts all five types of signal peptides using protein language models. *Nat. Biotechnol. 2022* 1–3 (2022). doi:10.1038/s41587-021-01156-3

324. Laslett, D. & Canback, B. ARAGORN, a program to detect tRNA genes and tmRNA genes in nucleotide sequences. *Nucleic Acids Res.* **32**, 11–16 (2004).

325. Edgar, R. C. MUSCLE: multiple sequence alignment with high accuracy and high throughput. *Nucleic Acids Res.* **32**, 1792–1797 (2004).

326. Katoh, K. & Standley, D. M. MAFFT Multiple Sequence Alignment Software Version 7: Improvements in Performance and Usability. *Mol. Biol. Evol.* **30**, 772–780 (2013).

327. Darling, A. E., Mau, B. & Perna, N. T. progressiveMauve: Multiple Genome Alignment with Gene Gain, Loss and Rearrangement. *PLoS One* **5**, (2010).

328. Gilchrist, C. L. M. & Chooi, Y. H. clinker & clustermap.js: automatic generation of gene

cluster comparison figures. *Bioinformatics* **37**, 2473–2475 (2021).

329. Kiljunen, S. *et al.* Identification of the Lipopolysaccharide Core of Yersinia pestis and Yersinia pseudotuberculosis as the Receptor for Bacteriophage φA1122. *J. Bacteriol.* **193**, 4963 (2011).

330. Williams, R. *et al.* Determination of the attP and attB sites of phage ϕCD27 from Clostridium difficile NCTC 12727. *J. Med. Microbiol.* **62**, 1439–1443 (2013).

331. Ackermann, H.-W. Frequency of morphological phage descriptions in the year 2000 Brief Review. *Arch Virol* **146**, 843–857 (2001).

332. Gill, J. J. *et al.* Genomes and characterization of phages Bcep22 and BcepIL02, founders of a novel phage type in Burkholderia cenocepacia. *J. Bacteriol.* **193**, 5300–5313 (2011).

333. Lynch, K. H., Stothard, P. & Dennis, J. J. Characterization of DC1, a broad-host-range Bcep22-like podovirus. *Appl. Environ. Microbiol.* **78**, 889–891 (2012).

334. Ragupathi, N. K. D. & Veeraraghavan, B. Accurate identification and epidemiological characterization of Burkholderia cepacia complex : an update. *Ann. Clin. Microbiol. Antimicrob.* **18**, (2019).

335. Lauman, P. & Dennis, J. J. Advances in Phage Therapy: Targeting the Burkholderia cepacia Complex. *Viruses 2021, Vol. 13, Page 1331* **13**, 1331 (2021).

336. Gautheret, D. & Lambert, A. Direct RNA motif definition and identification from multiple sequence alignments using secondary structure profiles. *J. Mol. Biol.* **313**, 1003–1011 (2001).

337. Macke, T. J. *et al.* RNAMotif, an RNA secondary structure definition and search algorithm. *Nucleic Acids Res.* **29**, 4724–4735 (2001).

338. Lesnik, E. A. *et al.* Prediction of rho-independent transcriptional terminators in

Escherichia coli. *Nucleic Acids Res.* **29**, 3583 (2001).

339. Weigel, C. & Seitz, H. Bacteriophage replication modules. *FEMS Microbiol. Rev.* **30**, 321–381 (2006).

340. Lynch, K. H., Abdu, A. H., Schobert, M. & Dennis, J. J. Genomic characterization of JG068, a novel virulent podovirus active against Burkholderia cenocepacia. *BMC Genomics* **14**, 574 (2013).

341. Summer, E. J. *et al.* Burkholderia cenocepacia phage BcepMu and a family of Mu-like phages encoding potential pathogenesis factors. *J. Mol. Biol.* **340**, 49–65 (2004).

342. Casjens, S. R. Diversity among the tailed-bacteriophages that infect the Enterobacteriaceae. *Res. Microbiol.* **159**, 340 (2008).

343. Goudie, A. D. *et al.* Genomic sequence and activity of KS10, a transposable phage of the Burkholderia cepacia complex. *BMC Genomics* **9**, 1–14 (2008).

344. Roszniowski, B. *et al.* The temperate Burkholderia phage AP3 of the Peduovirinae shows efficient antimicrobial activity against B. cenocepacia of the IIIA lineage. *Appl. Microbiol. Biotechnol.* **101**, 1203–1216 (2017).

345. Lynch, K. H., Liang, Y., Eberl, L., Wishart, D. S. & Dennis, J. J. Identification and characterization of ϕH111-1. *Bacteriophage* **3**, e26649 (2013).

346. Lynch, K. H., Stothard, P. & Dennis, J. J. Genomic analysis and relatedness of P2-like phages of the Burkholderia cepacia complex. *BMC Genomics* **11**, 599 (2010).

347. Summer, E. J. *et al.* Divergence and Mosaicism among Virulent Soil Phages of the Burkholderia cepacia Complex. *J. Bacteriol.* **188**, 255 (2006).

348. Iida, S., Streiff, M. B., Bickle, T. A. & Arber, W. Two DNA antirestriction systems of bacteriophage P1, darA, and darB: characterization of darA- phages. *Virology* **157**, 156–

166 (1987).

349. Piya, D., Vara, L., Russell, W. K., Young, R. & Gill, J. J. The multicomponent antirestriction system of phage P1 is linked to capsid morphogenesis. *Mol. Microbiol.* **105**, 399 (2017).

350. Summer, E. J. *et al.* Rz/Rz1 lysis gene equivalents in phages of Gram-negative hosts. *J. Mol. Biol.* **373**, 1098–1112 (2007).

351. Reddy, B. L. & Saier, M. H. Topological and Phylogenetic Analyses of Bacterial Holin Families and Superfamilies. *Biochim. Biophys. Acta* **1828**, 2654 (2013).

352. Schmidt, C., Velleman, M. & Arber, W. Three functions of bacteriophage P1 involved in cell lysis. *J. Bacteriol.* **178**, 1099 (1996).

353. Wang, I. N., Smith, D. L. & Young, R. Holins: the protein clocks of bacteriophage infections. *Annu. Rev. Microbiol.* **54**, 799–825 (2000).

354. Vukov, N., Moll, I., Bläsi, U., Scherer, S. & Loessner, M. J. Functional regulation of the Listeria monocytogenes bacteriophage A118 holin by an intragenic inhibitor lacking the first transmembrane domain. *Mol. Microbiol.* **48**, 173–186 (2003).

355. Sheehan, M. M., Stanley, E., Fitzgerald, G. F. & Van Sinderen, D. Identification and Characterization of a Lysis Module Present in a Large Proportion of Bacteriophages Infecting Streptococcus thermophilus. *Appl. Environ. Microbiol.* **65**, 569 (1999).

356. Vermassen, A. *et al.* Cell Wall Hydrolases in Bacteria: Insight on the Diversity of Cell Wall Amidases, Glycosidases and Peptidases Toward Peptidoglycan. *Front. Microbiol.* **10**, 331 (2019).

357. Park, T., Struck, D. K., Dankenbring, C. A. & Young, R. The Pinholin of Lambdoid Phage 21: Control of Lysis by Membrane Depolarization. *J. Bacteriol.* **189**, 9135 (2007).

358. Pourciau, C., Lai, Y. J., Gorelik, M., Babitzke, P. & Romeo, T. Diverse Mechanisms and Circuitry for Global Regulation by the RNA-Binding Protein CsrA. *Front. Microbiol.* **11**, 2709 (2020).

359. Tanaka, S., Matsushita, Y., Yoshikawa, A. & Isono, K. Cloning and molecular characterization of the gene rimL which encodes an enzyme acetylating ribosomal protein L12 of Escherichia coli K12. *Mol. Gen. Genet.* **217**, 289–293 (1989).

360. Vetting, M. W., Magnet, S., Nieves, E., Roderick, S. L. & Blanchard, J. S. A Bacterial Acetyltransferase Capable of Regioselective N-Acetylation of Antibiotics and Histones. *Chem. Biol.* **11**, 565–573 (2004).

361. Chartron, J., Shiau, C., Stout, C. D. & Carroll, K. S. 3′-Phosphoadenosine-5′-phosphosulfate Reductase in Complex with Thioredoxin: A Structural Snapshot in the Catalytic Cycle. *Biochemistry* **46**, 3942 (2007).

362. Silverstein, J. L. & Goldberg, E. B. T4 DNA injection. I. Growth cycle of a gene 2 mutant. *Virology* **72**, 195–211 (1976).

363. Silverstein, J. L. & Goldberg, E. B. T4 DNA injection. II. Protection of entering DNA from host exonuclease V. *Virology* **72**, 212–223 (1976).

364. Anton, B. P. *et al.* RimO, a MiaB-like enzyme, methylthiolates the universally conserved Asp88 residue of ribosomal protein S12 in Escherichia coli. *Proc. Natl. Acad. Sci. U. S. A.* **105**, 1826–1831 (2008).

365. Kurland, C. ., Hughes, D. & Ehrenberg, M. Escherichia coli and Salmonella: Cellular and Molecular Biology. 979–1004 (1996).

366. Carr, J. F., Hamburg, D. M., Gregory, S. T., Limbach, P. A. & Dahlberg, A. E. Effects of Streptomycin Resistance Mutations on Posttranslational Modification of Ribosomal

Protein S12. *J. Bacteriol.* **188**, 2020 (2006).

367. Storms, Z. J., Teel, M. R., Mercurio, K. & Sauvageau, D. The Virulence Index: A Metric for Quantitative Analysis of Phage Virulence. *https://home.liebertpub.com/phage* **1**, 27–36 (2020).

368. Shan, J. *et al.* Temperature dependent bacteriophages of a tropical bacterial pathogen. *Front. Microbiol.* **5**, (2014).

369. Lynch, K. H., Seed, K. D., Stothard, P. & Dennis, J. J. Inactivation of Burkholderia cepacia Complex Phage KS9 gp41 Identifies the Phage Repressor and Generates Lytic Virions. *J. Virol.* **84**, 1276–1288 (2010).

370. Boyd, E. F. & Brüssow, H. Common themes among bacteriophage-encoded virulence factors and diversity among the bacteriophages involved. *Trends Microbiol.* **10**, 521–529 (2002).

371. Summer, E. J., Gill, J. J., Upton, C., Gonzalez, C. F. & Young, R. Role of phages in the pathogenesis of Burkholderia or "Where are the toxin genes in Burkholderia phages?" *Curr. Opin. Microbiol.* **10**, 410 (2007).

372. Nzula, S., Vandamme, P. & Govan, J. R. W. Sensitivity of the Burkholderia cepacia complex and Pseudomonas aeruginosa to transducing bacteriophages. *FEMS Immunol. Med. Microbiol.* **28**, 307–312 (2000).

373. Langley, R., Kenna, D. T., Vandamme, P., Ure, R. & Govan, J. R. W. Lysogeny and bacteriophage host range within the Burkholderia cepacia complex. *J. Med. Microbiol.* **52**, 483–490 (2003).

374. Hens, D. K., Ghosh, A. N. & Kumar, R. A new small temperate DNA phage BcP15 isolated from Burkholderia cepacia DR11. *Arch Virol* **150**, 2421–2428 (2005).

375. Peters, D. L., McCutcheon, J. G. & Dennis, J. J. Characterization of Novel Broad-Host-Range Bacteriophage DLP3 Specific to Stenotrophomonas maltophilia as a Potential Therapeutic Agent. *Front. Microbiol.* **11**, 1358 (2020).

376. Holt, G. S. *et al.* Shigatoxin encoding Bacteriophage ϕ24B modulates bacterial metabolism to raise antimicrobial tolerance. *Sci. Rep.* **7**, (2017).

377. Davis, C. M., Ruest, M. K., Cole, J. H. & Dennis, J. J. The Isolation and Characterization of a Broad Host Range Bcep22-like Podovirus JC1. *Viruses 2022, Vol. 14, Page 938* **14**, 938 (2022).

378. Bertani, G. Studies on lysogenesis. I. The mode of phage liberation by lysogenic Escherichia coli. *J. Bacteriol.* **62**, 293–300 (1951).

379. Christie, G. E. & Calendar, R. Bacteriophage P2. *Bacteriophage* **6**, e1145782 (2016).

380. Kearse, M. *et al.* Geneious Basic: An integrated and extendable desktop software platform for the organization and analysis of sequence data. *Bioinformatics* **28**, 1647–1649 (2012).

381. García-Romero, I. & Valvano, M. A. Complete Genome Sequence of Burkholderia cenocepacia K56-2, an Opportunistic Pathogen . *Microbiol. Resour. Announc.* **9**, (2020).

382. Chen, Y. C., Liu, T., Yu, C. H., Chiang, T. Y. & Hwang, C. C. Effects of GC Bias in Next-Generation-Sequencing Data on De Novo Genome Assembly. *PLoS One* **8**, (2013).

383. Dohm, J. C., Lottaz, C., Borodina, T. & Himmelbauer, H. Substantial biases in ultra-short read data sets from high-throughput DNA sequencing. *Nucleic Acids Res.* **36**, 105 (2008).

384. Sohn, J.-I. & Nam, J.-W. The present and future of de novo whole-genome assembly. *Brief. Bioinform.* **19**, 23–40 (2018).

385. Lee, A. H. Y. *et al.* Phenotypic diversity and genotypic flexibility of Burkholderia cenocepacia during long-Term chronic infection of cystic fibrosis lungs. *Genome Res.* **27**,

650–662 (2017).

386. Bochkareva, O. O., Moroz, E. V., Davydov, I. I. & Gelfand, M. S. Genome rearrangements and selection in multi-chromosome bacteria Burkholderia spp. *BMC Genomics* **19**, 965 (2018).

387. Alonge, M. *et al.* RaGOO: Fast and accurate reference-guided scaffolding of draft genomes. *Genome Biol.* **20**, 1–17 (2019).

388. Zhou, Y., Liang, Y., Lynch, K. H., Dennis, J. J. & Wishart, D. S. PHAST: a fast phage search tool. *Nucleic Acids Res.* **39**, (2011).

389. Arndt, D. *et al.* PHASTER: a better, faster version of the PHAST phage search tool. *Nucleic Acids Res.* **44**, W16–W21 (2016).

390. Seemann, T. Prokka: rapid prokaryotic genome annotation. *Bioinformatics* **30**, 2068–2069 (2014).

391. Flannagan, R. S., Linn, T. & Valvano, M. A. A system for the construction of targeted unmarked gene deletions in the genus Burkholderia. *Environ. Microbiol.* **10**, 1652–1660 (2008).

392. Abdu, A., Juarez-Lara, G. & Dennis, J. J. Development of an Sce-I mutagenesis system for Burkholderia cepacia complex strains. *J. Microbiol. Methods* **146**, 16–21 (2018).

393. Suh, G. A. *et al.* Considerations for the Use of Phage Therapy in Clinical Practice. *Antimicrob. Agents Chemother.* **66**, (2022).

394. Taylor, M. W. The Discovery of Bacteriophage and the d'Herelle Controversy. *Viruses Man A Hist. Interact.* 53–61 (2014). doi:10.1007/978-3-319-07758-1_4

395. Davies, J. Where have All the Antibiotics Gone? *Can. J. Infect. Dis. Med. Microbiol.* **17**, 287 (2006).

396. Lin, D. M., Koskella, B. & Lin, H. C. Phage therapy: An alternative to antibiotics in the age of multi-drug resistance. *World J. Gastrointest. Pharmacol. Ther.* **8**, 162 (2017).

397. Clokie, M. R. J., Millard, A. D., Letarov, A. V. & Heaphy, S. Phages in nature. *Bacteriophage* **1**, 31–45 (2011).

398. Lynch, K. H., Stothard, P. & Dennis, J. J. Comparative analysis of two phenotypically-similar but genomically-distinct Burkholderia cenocepacia-specific bacteriophages. *BMC Genomics* **13**, 223 (2012).

399. Ando, H., Lemire, S., Pires, D. P. & Lu, T. K. Engineering Modular Viral Scaffolds for Targeted Bacterial Population Editing. *Cell Syst.* **1**, 187–196 (2015).

400. Pires, D. P. *et al.* Designing P. aeruginosa synthetic phages with reduced genomes. *Sci. Rep.* **11**, 1–10 (2021).

401. Jaschke, P. R., Lieberman, E. K., Rodriguez, J., Sierra, A. & Endy, D. A fully decompressed synthetic bacteriophage øX174 genome assembled and archived in yeast. *Virology* **434**, 278–284 (2012).

402. Latka, A. *et al.* Engineering the modular receptor-binding proteins of klebsiella phages switches their capsule serotype specificity. *MBio* **12**, (2021).

403. Kiktev, D. A., Sheng, Z., Lobachev, K. S. & Petes, T. D. GC content elevates mutation and recombination rates in the yeast Saccharomyces cerevisiae. *Proc. Natl. Acad. Sci. U. S. A.* **115**, E7109–E7118 (2018).

404. Li, L., Jiang, W. & Lu, Y. A Modified Gibson Assembly Method for Cloning Large DNA Fragments with High GC Contents. *Methods Mol. Biol.* **1671**, 203–209 (2018).

405. Blum, M. *et al.* The InterPro protein families and domains database: 20 years on. *Nucleic Acids Res.* **49**, D344–D354 (2021).

406. Li, Z., Park, Y. & Marcotte, E. M. A Bacteriophage Tailspike Domain Promotes Self-Cleavage of a Human Membrane-Bound Transcription Factor, the Myelin Regulatory Factor MYRF. *PLoS Biol.* **11**, 1001624 (2013).

407. Xiang, Y. *et al.* Crystallographic Insights Into the Autocatalytic Assembly Mechanism of a Bacteriophage Tail Spike. *Mol. Cell* **34**, 375 (2009).

408. Knecht, L. E., Veljkovic, M. & Fieseler, L. Diversity and Function of Phage Encoded Depolymerases. *Front. Microbiol.* **10**, 2949 (2020).

409. Pires, D. P., Oliveira, H., Melo, L. D. R., Sillankorva, S. & Azeredo, J. Bacteriophage-encoded depolymerases: their diversity and biotechnological applications. *Appl. Microbiol. Biotechnol.* **100**, 2141–2151 (2016).

410. Scholl, D., Rogers, S., Adhya, S. & Merril, C. R. Bacteriophage K1-5 Encodes Two Different Tail Fiber Proteins, Allowing It To Infect and Replicate on both K1 and K5 Strains of Escherichia coli . *J. Virol.* **75**, 2509–2515 (2001).

411. Valdes, A. M., Walter, J., Segal, E. & Spector, T. D. Role of the gut microbiota in nutrition and health. *BMJ* **361**, 36–44 (2018).